Silicate Based Hydrogels for Tissue Engineering and Drug Delivery Applications

by

Sadaf Samimi Gharaie

B.Sc., Azad University, 2011
M.Sc., Azad University, Iran, 2014

A Dissertation Submitted in Partial Fulfillment
of the Requirements for the Degree of

DOCTOR OF PHILOSOPHY

in the Department of Mechanical Engineering

Silicate Based Hydrogels for Tissue Engineering and Drug Delivery Applications

by

Sadaf Samimi Gharaie
B.Sc., Azad University, 2011
M.Sc., Azad University, Iran, 2014

Supervisory Committee

Dr. Mohsen Akbari, **Supervisor**
Department of Mechanical Engineering

Dr. Andrew Rowe, **Departmental Member**
Department of Mechanical Engineering

Dr. Cornelia Bohne, **Outside Member**
Department of Chemistry

Abstract

This dissertation presents the fabrication of a silicate-based nanocomposite hydrogel with outstanding shear-thinning properties, viscoelastic behaviour, and water retention capacity. Due to their adaptable mechanical properties, bioavailability, and water retention capacity, these nanocomposite hydrogels have been extensively used for biomedical applications. Laponite nanoparticles are among the most utilized silicate-based minerals. These clay nanoparticles are composed of platelets that are positively charged on the edges and negatively charged on the surface. The high aspect ratio of the polyanionic surface of the Laponite nanoparticles can absorb and trap ionic functional groups with non-covalent interactions.

These silicate-based nanocomposite hydrogels are produced by dispersing Laponite nanoparticles in deionized water, forming a homogenous colloid. The uniform dispersion of these nanoparticles in aqueous solutions forms a “house of cards” structure, which eliminates particle aggregation and improves their surface interaction with ionic compounds. The fabrication process is followed by the addition of the stable colloid to various organic and inorganic mixtures including, chitosan, alginate, graphene oxide, and gelatin. The chemical, physical, and mechanical properties of these nanocomposites are experimentally evaluated.

Silicate-based nanocomposite hydrogels offer unique rheological characteristics, which facilitate the injection process while preserving the mechanical integrity of the construct following extrusion. The injectability of these nanocomposites was assessed by evaluating their shear-thinning properties through multiple rheological analyses. As per the definition of shear-thinning, the viscosity of nanocomposites is directly affected by the

applied shear stress; the viscosity of these compositions decreases under shear stress and reverts to the original viscosity after removal of the force. Accordingly, nanocomposite hydrogels with shear-thinning properties can be utilized for extrusion-based 3D printing and for depositing drugs in localized tissue without the jeopardy of being washed away by circulating blood.

In addition, the large number of surface interactions and cationic exchange capacity of Laponite nanoparticles improve electrostatic interactions between the nanocomposite components and a wide range of ionic compounds. Accordingly, these chemical properties facilitate the incorporation of stimuli-responsive materials into the polymeric structure of the nanocomposite, allowing for the utilization of these hydrogels in on-demand drug delivery applications. These properties of the silicate-based nanocomposite hydrogels are investigated through swelling and release studies, Fourier transforms infrared spectroscopy (FTIR), and zeta potential measurements. The results of these experiments indicate that the non-covalent electrostatic interactions and chemical properties of these hydrogels improve the solubility and loading efficiency of therapeutic agents.

Silicate-based nanocomposite hydrogels may also be utilized for developing electrical conductive bioinks for extrusion-based three-dimensional (3D) printing. Adjusting the viscosity and shear-thinning properties of the hydrogel plays a significant role in the printability of a bioink. For instance, a highly viscous bioink disrupts extrusion, while a bioink with a low viscosity results in the formation of droplets instead of the desired cylindrical filaments. Optimized formulations of the nanocomposite hydrogels are investigated by conducting various mechanical property measurements. Consequently, the

unique chemical and rheological properties of the proposed hydrogels make them superior candidates for drug delivery and tissue engineering applications.

Table of Contents

List of Tables

List of Figures

Acknowledgments

Hereby, I acknowledge the roles of several individuals who supported me in completing my Ph.D. research. First of all, I would like to express my sincere gratitude toward my supervisor Dr. Mohsen Akbari for his continuous support and guidance, and for motivating me to grow as a research scientist during the years of my Ph.D. program.

I would like to acknowledge my committee members Dr. Cornelia Bohne and Dr. Andrew Rowe for their encouragement and insightful comments. Their willingness to resolve problems and contribution to various discussions, helped me shape this project. I would like to express my special gratitude to Dr. Stephanie Willerth, Dr. Cornelia Bohne, and Dr. Alexandra Brolo from the department of Biomedical Engineering and Chemistry for providing access to their laboratory facilities.

These acknowledgements would not be complete without mentioning my research lab colleagues Bardia Khunjush, Tavia Walsh, Brent Godau, Erik Pagan, and Dr. Amir Seyfoori. I would like to recognize the importance of productive collaborations and exchanging ideas and express my special gratitude for their continuous support, great sense of humour, and constructive feedbacks. I cannot forget to thank my friends for their emotional support and for encouraging me at all stages of writing this dissertation and my colleagues Bardia Khunjush and Tavia Walsh for reviewing this work.

Finally, my deepest appreciation belongs to my dearest parents for their love and endless support which helped me in the completion of this dissertation.

Dedication

To my beloved parents Nahid Tashakori and Nojan Samimi

It would have never been possible without your unlimited love and lifetime support

1. Introduction

This dissertation presents the fabrication and characterization of silicate-based nanocomposite hydrogels for drug delivery and tissue engineering applications. Section 1.1 of this chapter describes the motivations underpinning this work. The introduction is followed by descriptions of different hydrogels, crosslinking methods, and the benefits of using hydrogels for drug delivery and tissue engineering are described in Section 1.2. The classifications of hydrogel and silicate-based clay nanoparticles are provided in Sections 1.3 and 1.4, respectively. The biomedical properties of silicate-based nanocomposite hydrogels are discussed in terms of drug delivery and tissue engineering applications in Section 1.5. Finally, the research objectives and the structure of the dissertation are described in Sections 1.6 and 1.7, respectively.

1.1.Research Motivations

Silicate-based nanocomposite hydrogels have unique rheological properties, such as *in situ* mechanical stiffness and substantial shear-thinning behaviour. The shear-thinning properties of these hydrogels are among the most fundamental characteristics of injectable hydrogels. Such injectable hydrogels can be utilized for localized deposition of therapeutic agents and in the development of bioinks for extrusion-based 3D printing. *In situ* mechanical stiffness prevents premature drug leakage and degradation by providing a stable hydrogel in the body while enhancing the steady absorption of therapeutic agents by the surrounding tissue by providing a sustainable therapeutic release. Additionally, the shear-thinning properties of these hydrogels maintain the cylindrical geometry of stacked layers of filaments after extrusion from a 3D printing nozzle for tissue engineering applications.

Furthermore, silicate-based nanoparticles have a large surface area and ionic compounds, which allows for more surface interaction with ionic compounds. In addition, the viscoelastic behaviour and shear-thinning properties of these nanoparticles remain the same upon mixture with specific formulations of various hydrogels. These properties give silicate-based nanoparticles the ability to combine with and modify the properties of many different hydrogels, each of which will yield a nanocomposite hydrogel with distinct properties.

In addition to their unique chemical and rheological properties, when introduced into the body, silicate-based nanocomposite hydrogels are broken down into non-toxic minerals compounds. Due to these properties, silicate-based nanocomposite hydrogels can be aptly employed for drug delivery and tissue engineering applications.

1.2.Literature Review

1.2.1. Hydrogels for Biomedical Applications

1.2.1.1.Hydrogel Definitions

A hydrogel is a 3D network of hydrophilic polymer chains that can swell, but not dissolve, in water [1]. The high swelling ratio of hydrogels arises from the hydrophilic nature of the polymer chains. Additionally, the simple crosslinking reaction of one or more of the polymer chains preserves the macromolecular structure from dissolving in water [2]. When a hydrogel is initially exposed to water, the most polar hydrophilic groups interact with water molecules, followed by swelling via hydration of polar groups and the exposure of hydrophilic groups to water. Within these hydrophilic polymer chains, hydrogels retain a significant portion of water. After absorbing the water to both hydrophilic and hydrophobic sites, the osmotic driving force leads to further water absorption and

hypothetically, infinite dilution. Additional swelling can be halted by chemical or physical crosslinking of the hydrogel, where the hydrogel reaches equilibrium swelling level when saturated with water. Further exposure of the hydrogel to water may result in disintegration and dissolution of the chain network at a rate dependent on the crosslinking method of the composition [3].

1.2.1.2.Benefits of Hydrogels for Biomedical Applications

Hydrogels consist of 3D polymer networks, which have been increasingly studied for drug delivery and tissue engineering applications. These biomaterials are appealing for biomedical applications due to the exceptional physical and chemical properties such as swelling ability, flexibility, softness, and biocompatibility. The high elasticity of hydrogels has attracted considerable attention in the past 50 years and allows for imitating the extracellular matrix (ECM) and the formation of various 3D structures for tissue engineering applications [4]. Chemical modification of the polymeric chains and control of the chemical composition of the hydrogel network allows for customization of the hydrogel for various biomedical applications including regenerative medicine, drug/gene delivery, and cancer research. Furthermore, the incorporation of additional binding sites and stimulus-responsive biomaterials into the hydrogel polymeric network has two advantages, including, improved cellular attachment and facilitation of drug and growth factor loading into the bio-carriers[5]. For instance, the addition of stimuli-responsive materials to hydrogels allows for drug release in response to local pH and temperature variations [6]. In addition, the high water content of hydrogels allows for the cultivation of living cells, while the adjustable pore size of the polymer networks controls the overall permeation of nutrients [7]. Besides, their softness and viscoelastic properties provide

adequate support and mechanical integrity for preserving cell viability and proliferation [8]. The mechanical stiffness and physical characteristics of hydrogels can be controlled by adjusting the crosslinking density and incorporating a wide variety of polymer chains and nanoparticles into the 3D hydrogel network [9]. Furthermore, the mechanical stiffness and degradation rate of a hydrogel can be modified by adjusting the degree of crosslinking and the addition of synthetic biomaterial components [8].

1.2.1.3.Crosslinking Methods

Hydrogel networks are formed through crosslinking bonds including covalent bonds, hydrogen bonding, van der Waals interactions and physical entanglement of hydrophobic interactions [1,3,10]. This crosslinking causes a noticeable elastic force to oppose the expansion of polymer networks [11]. By linking polymer chains together, mechanical properties are consolidated and entangled chains of microstructure are fortified. In addition, crosslinking is an efficient method for controlling the stiffness of the swollen hydrogels by increasing both the Young's Modulus and the ultimate strength of the hydrogel [11-12]. Various crosslinking techniques have been used to synthesize hydrogels, such as physical and chemical interactions. Physically crosslinked hydrogels can be synthesized through changes in environmental factors such as temperature and pH [13]. Furthermore, these biomaterials can be formed through crystallization, hydrophobic modification, ionic interactions, and hydrogen bonds [8]. These electrostatic interactions prevent the expansion and dissolution of the hydrogel polymeric networks in aqueous environments. This class of physically crosslinked hydrogels has gained increased attention in the area of regenerative medicine due to the inherently non-toxic fabrication method, where they are formed in aqueous solutions in the absence of cytotoxic materials

(e.g. chemical cross-linkers). However, physically crosslinked polymer chains lack mechanical properties that support their structural integrity when in aqueous solutions for long periods of time, and when in contact with environmental stimuli such as pH and temperature [5]. In comparison, chemically crosslinked hydrogels, involve grafting multiple monomers to the backbone of a polymer through covalent bonding, which results a stable structure in aqueous environments. This method of crosslinking forms hydrogels with higher mechanical integrity through enzymatic, chemical, energy irradiation, and radical polymerization reactions [14]. However, the toxicity of crosslinking reagents in biological environments limits the use of this class of hydrogels.

1.2.2. Classification of Hydrogels for Biomedical Applications

1.2.2.1.Naturally Derived Hydrogels

Hydrogels can be classified according to their origins either from natural or synthetic biomaterials. Naturally derived hydrogels are obtained from two main groups: proteins and polysaccharides [2]. A majority of natural hydrogels exhibit bioactivity, non-toxicity, biocompatibility, lack of inflammatory response, and a lower cost in comparison to their synthetic counterparts [15]. Furthermore, a high water content of this class of hydrogels improves their cell-interactive properties, which is appealing for biological applications [5]. However, low mechanical strength, batch variations due to the natural sources, and lack of control over their degradation are the most significant draw-backs of natural origin hydrogels [16]. By contrast, synthetic hydrogels exhibit high reproducibility and amenable physical characteristics for biological applications. However, their lack of biocompatibility and cytotoxicity remains a significant issue for many synthetic hydrogels [2].

1.2.2.2.Synthetic Hydrogels

Synthetic hydrogels are produced by chemical polymerization reactions of purely synthetic polymers [16]. This class of hydrogels is preferred when a long service life, high gel strength, and thermal stability are required [2]. Additionally, polymeric networks of synthetic hydrogels can be modified to provide controlled degradation rates, swelling ratio, and structural integrity. The characteristic of a well-defined polymeric network of synthetic hydrogels is appropriately suited to develop carriers for on-demand therapeutic delivery applications. However, these hydrogels may contain cytotoxic residues from initiators or crosslinking agents, which can interfere with cell-specific bioactivities [6]. Therefore, a new class of semisynthetic/nanocomposite hydrogels has been developed to overcome the individual limitations of natural and synthetic hydrogels by combining the advantages of these hydrogels minus the individual drawbacks [17]. Hybrid or nanocomposite hydrogels are known for their ability to enhance the mechanical strength and biological stability of natural hydrogels while preserving their biocompatibility [18].

1.2.2.3.Nanocomposite Hydrogels

Hybrid or nanocomposite hydrogels are produced by combining the advantages of natural and synthetic polymers, and there has been an increasing demand for using nanocomposite hydrogels for biomedical applications [19]. This combination increases the number of functional groups, enhances the mechanical strength and biocompatibility of the manufacture hydrogels [2]. Two common approaches exist for combining natural and synthetics polymers and nanoparticles in the preparation of nanocomposite hydrogels. The first fabrication method is initiated by grafting one polymer to another, followed by a crosslinking process, while the second technique involves crosslinking the mixture of two

polymers simultaneously [20]. In addition, minerals can be incorporated into polymeric blends to improve the mechanical, chemical, electrical and biological properties of the nanocomposite hydrogels [19]. These mineral-containing hydrogels were observed to have great potential for mimicking the *in vivo* tissue microenvironments and the elasticity of native tissue, with low cytotoxicity and high reproducibility [16]. The addition of organic (carbon-based) and inorganic (metallic and salt-based) materials allows for multiple functionalities in one composition [21]. Inorganic silicate-based nanomaterials have gained attention during the past 10 years due to their outstanding water absorbance, elasticity, and cationic exchange [19]. Among the wide variety of organic and inorganic materials, silicate-based nanomaterials have been the primary focus of this research.

1.2.3. Silicate-based Hydrogels for Biomedical Applications

1.2.3.1.Naturally Derived Clay Minerals

Phyllosilicates or silicate sheets have gained greater research attention than other minerals during the last decade. The phyllosilicates include minerals such as the micas, vermiculite, talc, serpentine, chlorite, and clay minerals [22]. The interconnections of six hexagonally symmetric member rings of SiO_4^{-4} (silicate) tetrahedra forms the unit structure of the phyllosilicates [23]. The tetrahedral rings are connected through three oxygens to form $Si_2O_5^{-2}$ [24]. Individual sheets of silicate can also be coupled through the coordination of oxygen complexes by covalent bonding from one side and ionic or van der Waals bonding from the other side [24]. Oxygen networks are therefore playing an important role in determining the shape and extension of silicate sheets. The natural formation of phyllosilicates followed by electrostatic interactions between the hydroxyl ions of the member rings and various cations (including Al^{3+}, Ca^{2+} Fe^{2+}, Mg^{2+}, Cu^{2+}, Li^{+}, Na^{+},

K^+) produces a positive charge on the surface silicate sheets [25]. Due to the affinity of negatively charged member rings and the silicate sheets' capacity for preserving positively charged biological substances, silicate-based materials have benefits for drug delivery and tissue engineering applications. Among all silicate-based materials, the clay minerals are known for their high aspect ratio and substantial cationic exchange capacity. The cationic exchange capacity of clay minerals resolves the charge imbalance of the isomorphic substitution of silicate sheets [26]. For instance, a remaining negative charge from the substitution of Al^{3+} with Si^{4+} in tetrahedral units and $Mg^{2+}$and Fe^{2+} with Al^{3+} in octahedral units is balanced by the cationic exchange of Ca^{2+}, Li^+, Na^+, K^+. Clay-based minerals can be divided into 1:1 and 1:2 layer clays based on the 3D orientation of the tetrahedral and octahedral units [27]. In fact, the 1:1 layer clays are produced by the direct interaction of the oxygen and hydroxyl groups of the tetrahedral, and the octahedral units, respectively. On the other hand, 1:2 layer clays consist of an octahedral layer sandwiched by two tetrahedral layers with oxygen atoms of tetrahedral units facing the adjacent oxygen counterpart from another tetrahedral unit. Therefore, 1:2 layer clays have high swelling capacity due to their steric hindrance and charge repulsion between two abutting tetrahedral units [28]. Consequently, a wide variety of clay minerals have been employed to enhance the mechanical strength, elasticity, and biological properties of hydrogels due to their unique properties [21]. Clay minerals can be classified as natural or synthetic based on their level of surface modifications. The naturally occurring clays (e.g. smectites, fibrous silicates, hectorite, montmorillonite, and saponite) are non-modified inorganic cationic exchangers [29]. The physical and chemical properties of natural clays can be rectified to enhance the bioavailability of silicate sheets [30]. Various modification techniques have

been proposed to provide more control over the aspect ratio, porosity, and hydrophilic affinity. The thermal modification, acid activation, and chemical intercalation with ionic compounds are among the most common modification techniques of natural clay minerals [31].

1.2.3.2. Synthetic Clay Minerals

Synthetic clay minerals such as Laponite, hydrotalcite, kaolinite, pyrophyllite, fluoromica, smectite, fluorohectorite, chlorite, and sepiolite have arisen as the next generation of smart silicate-based biomaterials for biomedical applications due to their modified surface interactions [29,32]. When in the form of clay nanoparticles, surface modification can be approached through physical adsorption and chemical [33]. Physical adsorption can enhance the surface interactions while preserving the structure of the clay nanoparticles. Alternatively, chemical grafting provides a stronger attachment between clay minerals and the attached molecules [34]. The physical, chemical and mechanical properties of the synthetic clay minerals are influenced by the structure and morphology of starting materials. Laponite ($Na^{+}_{0.6}[(Mg_{5.5}Li_{0.3})Si_8O_{20}(OH)_4]^{-}_{0.7}$) is a well-known synthetic clay mineral which has been reported as the most non-toxic and bioactive silicate-based material [35]. Laponite consists of basic or complex salts of silicic acids, has a plate-shaped structure of 20-30 nm in diameter and 1 nm in height [36]. The aspect ratio of Laponite is 100 times greater than natural clay minerals, and its chemical reactivity, as well as bioactivity, is attributed to the high surface area of the Laponite platelets. Electrostatic and van der Waals interactions between Laponite nanoparticles form a “house of cards” stable morphology in aqueous solutions [37]. Another reason for the popularity of using Laponite in biomedical applications is its solubility in aqueous solutions and its

degradation into non-toxic minerals common to the body [38]. This dissociation of Laponite into non-toxic substances Mg^{2+} and $Si(OH)_4$improves the cell adhesion by increasing the affinity of the silicate platelets to absorb integrin proteins and stimulate collagen type I synthesis, respectively [39]. Accordingly, Laponite shows high cytocompatibility and substantial cell adhesion due to protein adsorption on silicate platelets [36]. Hydride or nanocomposite hydrogels with Laponite have been successfully used for controlling cell spreading and producing injectable therapeutic carriers, and antimicrobial films [36,39-40].

1.2.3.3.Clay Nanocomposites

Laponite, an example of a synthetic clay mineral, has been observed to improve the physical and mechanical properties of polymeric hydrogels. The addition of Laponite produces nanocomposite hydrogels with beneficial viscoelastic behaviour and shear-thinning properties [41]. The unique properties of these nanoparticles are attributed to their high aspect ratio and their cationic exchange capacity. The ionic surface of Laponite nanoparticles can absorb and trap the ionic functional groups of organic and inorganic materials [42]. However, non-covalent interactions between these nanoparticles and polymer chains are reversible and result in non-Newtonian behaviour (shear-thinning properties) when under shear stress [43]. The property of shear-thinning is an essential characteristic for injectable drug carriers and bioinks used in extrusion-based 3D printing [36]. Laponite also has a strong affinity for absorbing both positively and negatively charged polymers. Accordingly, self-assembly is the most common method of producing a Laponite-hydrogel nanocomposite [19]. The favourable influence of combining Laponite

nanoparticles and hydrogels has been studied in several drug delivery and tissue engineering studies [36,39-40].

1.2.4. Applications of Silicate-based Biomaterials in Biomedical Engineering

1.2.4.1.Drug Delivery

The administration of drugs into the human body poses various challenges, including the location of the pathological condition and the incorporation of the drug in the blood circulation before reaching the targeting organ [44]. Therefore, optimizing drug efficiency and minimizing the collateral side effects remains a challenge [45]. However, precisely timed drug administration and controlled drug release kinetics have been observed to greatly enhance drug delivery efficiency [46]. Porous texture, morphology, and functionalization of drug carriers are known to play a key role in adjusting the permeability, aspect ratio, and drug-membrane binding strength [44].

Silicate-based clay nanoparticles, such as Laponite nanoparticles and montmorillonite, have been widely used as pharmaceutical carriers for injectable drug deposition and allow for consistent release over a long period. Laponite is a naturally occurring cationic exchanger with a drug loading mechanism involving ionic exchanges between the nanoparticles and basic drugs in aqueous solutions [47]. These electrostatic interactions and the high swelling capacity are essential characteristics for extending release time, targeting specific sites in the human body, and delivering therapeutic agents efficiently. The chemical composition and manufacturing conditions of Laponite play key roles in the dispersion stability of these nanoparticles, which eventually affects the solubility and bioavailability of drugs. Dispersion stability of Laponite nanoparticles significantly decreases in physiological conditions due to the high concentrations of salts

and polyelectrolytes. However, the addition of hydrogels with dispersed Laponite enhances the colloidal stability of the nanoparticles [48]. While the high surface ratio of these nanoparticles improves the bioavailability of drugs. Therefore, the effective combination of Laponite nanoparticles and hydrogels improves the mechanical integrity and viscoelastic behaviour of the final composition [2]. Besides, ionic crosslinking between Laponite and hydrogels have been shown to provide sustainable drug release and high loading efficiency to create a predictable release profile [38].

1.2.4.1.1. Silicate-based Injectable Drug Depots

Various formulations of drug carriers have been introduced for *in vivo* and *in vitro* drug deposition applications[45]. *In situ* mechanical stiffness and shear-thinning properties of hydrogels are essential tools for developing biomaterials for depositing drugs in localized tissue. The encapsulation of a drug in these types of hydrogels eliminates premature drug leakage or degradation in physiological environments and promotes gradual drug release in surrounding tissue [49]. Furthermore, the *in situ* formation and shear-thinning properties of hydrogels prevent encapsulated drugs from being washed away due to blood circulation and are essential characteristics for localized drug delivery application [50]. Improved i*n situ* mechanical hydrogel stiffness can be achieved by employing shear-thinning nanocomposites, stimuli-responsive biomaterials, and various crosslinking agents [51]. Following injection, this increase in the mechanical integrity of the drug carriers further shields the localized drug. Injectable drug deposition has several advantages over traditional drug administration techniques; primary benefits include minimally invasive treatment, ease of handling, and minimization of drug side effects. Such negative effects of high drug dosages can be reduced by providing a controlled release

system, thus decreasing the requirement for high doses. This beneficial technique maintains an efficient dosage of drugs in the specific location while protecting the encapsulated drugs from premature degradation [50].

A wide variety of nanocomposite hydrogels with shear-thinning properties have been employed for developing biocarriers for injectable drug deposition applications. Nanocomposite hydrogels have high water retention capacities and favourable surface interactions with ionic compounds, which are essentials for improving drug solubility and encapsulation efficiency [52]. Recently, Silicate-based nanocomposite has research interest in the area of injectable drug carriers development, due to their unique shear-thinning properties [45]. Furthermore, the high surface area and straight/narrow channels of the silicate-based hydrogels allow for greater control over drug diffusion over specific time frames [52]. Surface modification, chemical composition, particle size, tunable biological properties, and the stimuli-responsive nature of the silicate-based hydrogels can be modified to adjust the release kinetic [51].

1.2.4.2.Tissue Engineering and Regenerative Medicine Applications

Tissue engineering is a promising approach that integrates biology with engineering to restore, maintain, and improve tissue functions [53]. Tissue engineering involves assembling functional constructs to produce biological substitutes and biosensors for a greater understanding of cellular responses to various biological threat agents [54]. In addition, this technology can be used for pursuing tissue-specific regeneration for drug screening and remedying the shortage of organs required for transplantation procedures. The functional engineered tissues can be fabricated by high-density seeding of stem cells onto a 3D nanoporous scaffold [55]. These natural and/or synthetic scaffold biomaterials

can recapitulate the viscoelasticity and morphology of the ECM, to actively influence cell behaviour and regulate tissue function [56]. Hydrogels are well-known for their biocompatibility and high water retention capacity. Therefore, hydrogels are commonly used for developing scaffolds with various densities and mechanical crosslinking chemistry [57]. Although hydrogels generally provide extensive cell-binding moieties and a viable microenvironment for improved cell adhesion, the inherently low viscoelasticity and fast degradation rates restrict cell proliferation [58]. Silicate-based minerals can be used to improve hydrogel viscoelastic behaviour and mechanical strength without sacrificing their biocompatibility. In addition, silicate-based nanocomposites can increase the surface area and connection points of the hydrogel, which enhances cell spreading and proliferation [55].

1.2.4.2.1. Bioinks for Extrusion 3D printing

Among various scaffold fabrication techniques, 3D printing has to gain prominence due to its ability to build complicated and functional tissues [56]. 3D printing is commonly used for producing complex biomimetic constructs for tissue engineering applications [59]. Each particular printing technique, which includes extrusion printing, injection printing, stereolithography printing, and laser printing, requires a bioink to have specific chemical and rheological properties. Extrusion-based printing is the most adaptable and versatile of the aforementioned techniques and enables a wide variety of bioinks to be processed for biomedical applications [60]. The optimal formulation of the polymer matrix and filler materials in a bioink should maintain the mechanical integrity of the printed filaments, without compromising the bioinks ease of injection [61-62]. Bioinks actively interact with cells and imitate their extracellular matrix and natural biological microenvironment.

Therefore, optimal hydrogel and nanoparticle concentrations allow for steady extrusion and prevent cellular damage during printing [63]. Silicate-based nanocomposites are notable due to their numerous attachment sites and large surface area stemming from a high aspect ratio. Additionally, silicate-based nanocomposites possess optimal viscosity, shear-thinning capacity, and the ability to form uniform filaments; characteristics, that originate from the non-silicate hydrogel component [64-65]. Accordingly, silicate-based hydrogels are among the most popular nanocomposites that revert to their initial viscosity after extrusion. These unique properties allow for a fast and reproducible fabrication process [60].

1.3.Research Objectives

The research objective of this dissertation is to produce and characterize injectable silicate-based nanocomposite hydrogels for drug delivery and tissue engineering applications. The formulation of each fabricated biomaterial is followed by microstructural and chemical analysis using various experiments, including, zeta potential, X-ray diffraction (XRD), FTIR, and scanning electron microscopy (SEM). Furthermore, mechanical properties and shear-thinning characteristics of these injectable nanocomposite hydrogels are evaluated by several rheological analyses. In addition to this general analysis, more specific experiments are conducted to assess the final application of these biomaterials.

The research objective is broken into three explicit formulations of silicate-based nanocomposite hydrogels for drug delivery and tissue engineering application, as follows: (1) Smart shear-thinning hydrogels as injectable drug delivery systems.

(2) Multifunctional silicate-based electroconductive bioinks for fabricating soft electronics.

(3) Drug-eluting shear-thinning biomaterial for minimally invasive treatment of cancers.

1.4.Structure of Dissertation

This dissertation includes the current introductory chapter which explains the context and the framework of this manuscript and links the following chapters in terms of research motivation and objectives. A summary of key research results is described in Chapter 2. The integration of Laponite nanoparticles as an example of a silicate-based clay mineral with organic and inorganic materials is investigated in Chapters 3 to 5. Each of these chapters presents the formulation and characterization of a silicate-based nanocomposite hydrogel for a specific biomedical application.

In particular, the fabrication and characterization of two stimuli-responsive drug carriers consisting of Laponite/gelatin, and chitosan or poly N-isopropyl acrylamide-co-acrylic acid (PNIPAM) microgels are described in Chapter 3. This chapter presents a published paper [41] and explains the formulation and production of a smart silicate-based nanocomposite hydrogel for on-demand drug delivery applications. Chitosan and PNIPAM microgels are synthesized and utilized as pH-responsive components that release the therapeutic agents upon exposure to various biological environments.

The chemical and rheological properties of these nanocomposite hydrogels, including swelling characteristics, degradability, zeta potential, and release studies are investigated by various experiments. The results of these experiments demonstrate the effective pH responsivity and excellent shear-thinning properties of these hydrogels.

Chapter 4 discusses the development of a silicate-based nanocomposite hydrogel bioink for extrusion-based 3D printing that is composed of alginate, graphene oxide, and Laponite. The shear-thinning properties, viscoelastic behaviour, and electroconductivity of these nanocomposites are investigated by mechanical and chemical analyses, as presented in Chapter 4. The optimum formulation of this bioink is obtained by conducting several rheological analyses and extrusion-based printing techniques. Additionally, Chapter 4 presents a new technology for producing a flexible printed conductor using this viscoelastic bioink and an alginate substrate. This technology preserves the flexibility and stretchability of the nanocomposite hydrogel while maintaining the attachments between the bioink and the alginate substrate.

Chapter 5 reports the generation of another drug carrier for drug deposition applications including gelatin and Laponite. This shear-thinning drug carrier eases the injection process by decreasing the viscosity upon exposure to shear stress. Additionally, the mechanical integrity of this nanocomposite hydrogel after injection stops the drug from being washed away with blood circulation. The Swelling, degradability, chemical properties, and drug uptake capacity of this nanocomposite were evaluated through various experiments. The results from these experiments indicate the substantial effects of chemical compositions of Laponite nanoparticles for improving the drug solubility and providing improved control over release profile. Finally, conclusions from all contributions as well as suggestions for possible future works are presented in Chapter 6.

Chapter 2

2. Summary of Key Results

This chapter presents a summary of key results from three research subjects of this dissertation. Each chapter presents a silicate-based injectable nanocomposite hydrogel for a biomedical application. Specifically, Chapter 3 and Chapter 5 describe the fabrication and characterization of silicate-based drug carriers for on-demand drug delivery applications. Furthermore, Chapter 4 presents the fabrication of an electroconductive silicate-based bioink for extrusion-based 3D printing and tissue engineering applications.

2.1.Smart Shear-thinning Hydrogels as Injectable Drug Delivery Systems

This section describes the fabrication of two injectable pH-sensitive biomaterials which can be utilized for depositing therapeutic agents to the site of interest. The injection process is followed by on-demand drug release upon exposure of these biomaterials to local basic pH in biological environments. Variation in pH is a substantial indicator of disease progression and can be correlated to angiogenesis, protease activity, and bacterial infection [66]. Accordingly, these biomaterials can be utilized for detecting and treatment of various disease progression.

The main objective of this study is (1) to employ pH-sensitive chitosan or PNIPAM microgels to produce a silicate-based, injectable, and stimuli-responsive drug delivery system using gelatin and Laponite materials. Producing multifunctional nanocomposite hydrogels with these properties requires various experiments to optimize the formulation of the final composition. Therefore, the secondary objective of this work is to (2) evaluate the chemical, rheological, and morphological properties of various formulations of nanocomposite hydrogels. For instance, the effect of utilizing various concentrations of

Laponite is studied for viscoelastic behaviour and shear-thinning properties of the nanocomposite hydrogel. Accordingly, the results from these experiments indicate the optimum concentration and total solid weight of Laponite with favourable rheological properties. After the addition of chitosan or PNIPAM microgels to the optimal formulation of Laponite/gelatin, the drug release behaviour of the final compositions is investigated at three different pH values. The results from release-related experiments, including swelling, degradability, and Rhodamine B (Rd) release suggest that the shear-thinning biomaterials exhibit pH-sensitive behaviours.

The key results of this study are as follows: (1) The highest swelling ratio, degradation rate, and Rd release were achieved at pH 9.18, (2) the optimal formulation of these nanocomposite hydrogels consists of 6wt% total solid weight, which is comprised of 2wt% Laponite and 4wt% gelatin. The mixture is produced by combining equal parts of Laponite 9wt% and gelatin 18wt% and diluting the resulting mixture to obtain 6wt% total solid weight. (3) Furthermore, the addition of PNIPAM has a minimal effect on the rheological properties of the Laponite/gelatin compositions, however, the addition of chitosan has a more significant effect. Therefore, the final compositions of Laponite/gelatin with chitosan or PNIPAM microgels are tuned to have shear-thinning properties. Due to the aforementioned properties, these silicate-based injectable nanocomposite hydrogels can be potentially used to develop pH-sensitive drug delivery systems.

This study is published in the Journal of Polymers and is presented in Chapter 3.

2.2. Multifunctional Silicate-based Electroconductive Bioinks for Fabricating Soft Electronics

This study presents the fabrication of a silicate-based nanocomposite hydrogel that combines the shear-thinning properties of alginate/Laponite and the electroconductive properties of graphene oxides. This bioink, which is then printed and embedded in an alginate substrate, introduces a new technology for developing conductors. In fact, this technology allows for producing flexible printed conductors with complex geometries for potential tissue engineering applications.

The overall objective of this study is to produce a highly stretchable, viscoelastic, and durable electroconductive biomaterial. This objective is broken into two categories: (1) the formulation of a silicate-based electroconductive bioink using alginate, Laponite, and graphene oxide for extrusion-based 3D printing, (2) development of a technology for printing and embedding the proposed bioink in alginate sheets in order to form flexible and durable conductors with complex geometries.

The fabrication process of the silicate-based nanocomposite hydrogel is followed by an evaluation of the shear-thinning properties which are essential for developing a bioink for extrusion-based 3D printing. The effect of adding various concentrations of graphene oxide is investigated by multiple rheological, chemical, and morphological analyses. The results of these experiments indicate that the addition of various concentrations of graphene oxide on the shear-thinning properties of the nanocomposite hydrogel is negligible. After extruding and embedding the bioink in an alginate substrate, the reproducibility and durability of the flexible conductor are evaluated by various mechanical analyses. In fact, these experiments were conducted to indicate the exceptional

control over extrusion printing and the substantial stability of the printed conductor after crosslinking with $CaCl_2$.

The key results of this study are as follows: (1) This silicate-based electroconductive bioink has a shear-thinning property that preserves the cylindrical geometry of the stacked layers of filaments upon extrusion. (2) The addition of various concentrations of graphene oxide has negligible effects on the shear-thinning, morphological, and chemical properties of the final composition. (3) The shear-thinning properties of the bioink and extrusion-based 3D printing technique allow for producing flexible conductors with different fibre diameters and complex geometries. Accordingly, the fundamental control over the fabrication process of these conductors illustrates the high reducibility of the proposed technique. (4) The results from various mechanical analyses illustrate the stability of this flexible conductor under stretching and bending without any conductive or mechanical failures. Based on these properties, the silicate-based bioink can be used for extrusion-based 3D printing and the proposed electroconductive bioink can be used for developing flexible conductors with complex geometries which can be potentially utilized for tissue engineering applications, e.g. electrically stimulated nerve and/or muscle tissue.

2.3. Doxorubicin Loaded Shear-thinning Biomaterial for Minimally Invasive Treatment of Brain Tumors

This section describes a shear-thinning biomaterial as a drug vehicle for intra-tumoral drug delivery application over long periods. This biomaterial allows the drug to be deposited in surgically unreachable regions of a brain tumour and provides a sustainable and prolonged release at the site of interest. In addition, the drug injection to a feeding

vessel of a tumour is then followed by clotting the blood and blocking the oxygen and nutrients.

The general objectives of this study are as follows: (1) to produce a silicate-based shear-thinning nanocomposite for intra-tumoral drug delivery applications. Laponite nanoparticles are added to gelatin for enhancing the rheological properties of the nanocomposite hydrogel and controlling the drug release. In fact, the Laponite concentration plays a key role in adjusting the shear-thinning properties, drug loading capacity, and release behaviour of the nanocomposite hydrogel. Accordingly, the first objective of this research is followed by (2) the chemical and rheological characterization of various formulations of this nanocomposite hydrogel for optimization of the total solid weight and Laponite concentration. The optimum formulation of this nanocomposite hydrogel is evaluated by several morphological analysis and release-related experiments, including swelling, degradation, and chemotherapy drug release.

The results from the morphological characterization illustrate the effect of adding various concentrations of Laponite on the microstructure of the nanocomposite hydrogel. In fact, SEM images show greater pore size and non-uniform pore distributions for lower concentrations of Laponite. These differences in porosity might be associated with electrostatic interactions between Laponite and gelatin which are supported by zeta potential and FTIR analysis. These interactions may also affect the drug loading capacity and drug release, which are functions of swelling and degradation rates.

The key results of this study are as follows: (1) The results from the release-related experiments indicate the significant effects of adding various concentrations of Laponite

on swelling and degradation rate, (2) the highest drug loading capacity and the lowest release is achieved with the highest concentration of Laponite.

Therefore, the optimal formulation of these nanocomposite hydrogels depends on the final application and the defined requirements for each specific drug carrier. Due to the favourable shear-thinning properties and substantial control over drug release, the proposed silicate-based nanocomposite hydrogel can be potentially utilized for minimally invasive cancer treatment.

Chapter 3

3. Smart Shear-thinning Hydrogels as Injectable Drug Delivery Systems

Smart Shear-Thinning Hydrogels as Injectable Drug Delivery Systems

Polymers (Basel). 2018, 10, 1317.

Reproduced with permission from MDPI

Preamble

The primary objective of this research is to employ pH-sensitive chitosan or PNIPAM microgels to produce a silicate-based, injectable, and stimuli-responsive drug delivery system using gelatin and Laponite. The proposed nanocomposite hydrogels can be utilized for the deposition of therapeutic agents to the site of interest, which then remains at the same location without being washed away with blood circulation. This multifunctional biomaterial is also capable of releasing the therapeutic agents upon exposure to different pH values. Therefore, chemical, morphological, and rheological characterization is employed to optimize the formulation and evaluate the aforementioned properties of the proposed biomaterial.

The content of this chapter was published in Polymer journal.

Abstract

In this study, we fabricated and characterized a smart shear-thinning hydrogel composed of gelatin and laponite for localized drug delivery. We added chitosan (Chi) and poly N-isopropyl acrylamide-co-Acrylic acid (PNIPAM) particles to the shear-thinning gel to render it pH-responsive. The effects of total solid weight and the percentage of laponite

in a solid mass on the rheological behaviour and mechanical properties were investigated to obtain the optimum formulation. The nanocomposite gel and particles were characterized using Fourier-transform infrared spectroscopy (FTIR), scanning electron microscope (SEM), zeta potential, and dynamic light scattering techniques. Finally, release-related experiments including degradability, swelling and Rhodamine B (Rd) release at various pH were performed. The results suggest that the incorporation of silicate nanoplatelets in the gelatin led to the formation of a tunable porous composite, with a microstructure that was affected by introducing particles. Besides, the optimum formulation possessed shear-thinning properties with modified rheological and mechanical properties which preserved its mechanical properties while incubated in physiological conditions. The release-related experiments showed that the shear-thinning materials offer pH-sensitive behaviour so that the highest swelling ratio, degradation rate, and Rd release were obtained at pH 9.18. Therefore, this nanocomposite gel can be potentially used to develop pH-sensitive systems.

3.1.Introduction

Hydrogels are three-dimensional (3D) networks of hydrophilic polymers that can absorb water up to thousands of times of their dry weight while preserving their structure [5]. They are formed by crosslinking polymer chains, using ionic bonds, covalent bonds, hydrogen bonds, and van der Waals interactions. Hydrogels have been widely used in biomedical researches as cell culture substrates and drug depots for tissue engineering and delivery of therapeutic applications[1,67-68]. In addition, they are potentially able to have environmental stimuli-responsive properties so that they can undergo a volumetric phase transition in response to pH or ion changes in the environment [1]. Recently, injectable

hydrogels have received significant attention because they can be delivered to the site of interest using minimally invasive approaches.

Generally, the initial precursor solution of these hydrogels is injected into the desired area and then crosslinked in situ using ultraviolet (UV) light [69], enzymes [70], ions [71], or temperature [72]. Targeted delivery of therapeutic molecules to the desired area with injectable hydrogels can be carried out by incorporating these agents into the precursor solution. However, it is possible that the bioactive agents incorporated in an injectable hydrogel being damaged by exposing them to toxic agents or inducing non-physiological conditions[73]. For instance, 2-hydroxy-1-[4-(2-hydroxyethyl) phenyl]-2-methyl-1-propanone-1-one (Irgacure 2959), a typical photoinitiator used for UV crosslinking of photocrosslinkable hydrogels, showed high cytotoxicity even at low dosages to human aortic smooth muscle cells [74]. Moreover, in situ crosslinking of the hydrogels can either result in the leakage of initial precursor solution to the adjacent tissue or blood stream, or blockage of the catheters due to premature polymerization [73].

To circumvent the problems inherent in *in-situ* forming hydrogels, shear-thinning gels have been engineered such that their viscosity reduces under higher shear rates. As such, these gels deform easier through needles and catheters and rapidly retain their original form after the removal of the mechanical force. This restoration to solid gel minimizes the limitations associated with typical injectable hydrogels. In addition, bioactive molecules such as drugs and cells can be incorporated into the main preformed hydrogel and delivered to the injection site and remain in the location as the gel recovers [75-77]. Recently, we engineered a shear-thinning biomaterial by blending silicate nanoplatelets and gelatin and used it as an embolic agent for endovascular embolization

procedures[78]. The feasibility of using this material for endovascular embolization was demonstrated with murine and porcine *in-vivo* models.

In this study, we engineer a smart injectable material by incorporating pH-responsive microgels within our previously developed shear-thinning gel. The proposed gel can be deployed to the site of interest using a needle and can deliver therapeutic agents in response to local pH variations. We chose pH as an external stimulus as it is an important indicator of disease progression and can be correlated to angiogenesis, protease activity, and bacterial infection [66]. We develop a nanocomposite of gelatin and Laponite loaded with Poly(N-isopropyl acrylamide)-co-Acrylic acid (PNIPAM-co-AA) or Chi that are known as pH-sensitive drug carriers. Laponite is a charged synthetic silicate nanoplatelet (20-30 nm in diameter and 1 nm in thickness) in which the charges are distributed anisotropically so that the top and bottom surfaces possess negative charges while the positive charges are distributed along the edges [35]. On the other hand, the polymeric chain of gelatin has negatively and positively charged regions which enable intense interaction between these regions and sites of Laponite with opposite charges [79]. These interactions lead to the fabrication of gelatin/Laponite nanocomposite. We investigated the shear-thinning behaviour of different ratios of gelatin and Laponite by performing rheological and mechanical tests to optimize the formulation of the fabricated nanocomposite. Then, positively charged Chi particles or negatively charged PNIPAM-co-AA particles were incorporated into the composite to study the drug release behaviour of the gel at three different pH.

3.2.Materials and Methods

3.2.1. Materials

Gelatin type A obtained from porcine skin, chitosan (448877-medium molecular weight (190,000-310,000 Da) and deacetylation degree of 75-85%), N-isopropyl acrylamide monomers (NIPAM), acrylic acid (AA), N, N'-methylene bisacrylamide (BIS), ammonium persulfate (APS), sodium dodecyl sulphate (SDS), Span 80, glutaraldehyde, Rhodamine B (Rd) and PBS tablets were purchased from Sigma-Aldrich (St. Louis, MI). Synthetic silicate nanoplatelets (Laponite XLG) were obtained from Southern Clay Products, Inc. (Louisville, KY). The rest of the materials were provided by the following companies: sodium acetate (Bio Basic, Canada), Heavy mineral oil and n-hexane (Fisher Scientific, USA), ethanol (Commercial Alcohols, Canada), acetic acid and toluene (vwr, USA), and dialysis bags (Spectrum Lab, USA).

3.2.2. Shear-thinning Gel Fabrication

A stock solution of 18% (w/w) gelatin was prepared by dissolving gelatin in Milli-Q water and heating to 40˚C to ensure that the gelatin was completely dissolved. A 9% (w/w) Laponite stock solution was made in 4˚C water to prevent the gelation of Laponite nanoplatelets and ensure complete dissolution of the nanoclay particles. Preparation of different formulations of shear-thinning gel, as listed in Table 3.1, was carried out by vortexing predefined amounts of gelatin and Laponite stock solutions with Milli-Q water at 3000 rpm for 5 minutes to obtain the desired total solid concentrations and Laponite loading. This was followed by reheating the obtained gel and vortexing for better dispersion of nanoplatelets. The shear-thinning gels were then stored at 4˚C. In order to prepare shear-thinning gel loaded with pH-sensitive particles, particles in the amount of 1

wt% of gel were suspended in Milli-Q water. Then, the suspension was mixed with gelatin and Laponite solutions through vortexing as explained before. The rest of the procedure was similar to the preparation of gelatin/Laponite nanocomposite.

Table 3.1. Composition of nanocomposites.

Nanocomposite	Gelatin (g/ml)	Laponite (g/ml)	Chi (g/g)	PNIPAM (g/g)
3NC50	0.015	0.015	0.000	0.000
6NC0	0.060	0.000	0.000	0.000
6NC25	0.045	0.015	0.000	0.000
6NC50	0.030	0.030	0.000	0.000
6NC75	0.015	0.045	0.000	0.000
6NC100	0.000	0.060	0.000	0.000
9NC50	0.045	0.045	0.000	0.000
6NC50-Chi	0.030	0.030	0.010	0.000
6NC50-PNIPAM	0.030	0.030	0.000	0.010

Nomenclature will be described in section 3.3.1

3.2.3. PNIPAM-co-AA Synthetization

A 97 ml aqueous solution containing 10 mmol of NIPAM, 0.20 mmol of BIS, 0.1 mmol of AA and 0.12 mmol of SDS was prepared and transferred to a 3-necked, round-bottom flask. The solution was continuously purged with nitrogen during heating to polymerization temperature (70˚C). Polymerization was initiated as 3.0 ml of an aqueous solution containing 0.10 mmol of APS was injected into the continuously stirring solution and allowed to react for 5 hours. Purification of PNIPAM-co-AA was carried out by dialyzing against deionized water for 1 week with a daily water change and lyophilizing the solution using Freezemobile Virtis lyophilizer.

3.2.4. Chitosan Fabrication

An aqueous solution of Chi as the water phase was prepared through dissolving 1.5 wt% of Chi and 0.9 wt% of NaCl in acetic acid 1 (v/v)%. Then, it was emulsified by dripping the mixture into a continuous phase (oil phase) composed of mineral oil and 5% (v/v) span 80 and homogenizing at 1000 rpm for 30 minutes. In order to crosslink Chi, a chemical crosslinking agent (Glutaraldehyde Saturated Toluene) was added dropwise into the Water/Oil mixture while agitating at 300 rpm. After one hour, the mixture was centrifuged at 2000 g for 5 minutes to separate particles from the oil. The particles were further washed with hexane, ethanol 50% containing 1% Tween 20, and distilled water (5 times). Finally, the particles were lyophilized.

3.2.5. Rheological and Mechanical Analysis

Rheology and stress recovery tests were carried out based on a previously published protocol [79]. Variations of shear stress were recorded over the shear rate sweeps from 0.001 to 10 s^{-1} at room temperature for samples with different total solid weights (3, 6, and 9 %). Similar rheology tests along with nondestructive mechanical analysis were performed to optimize the content of Laponite in the gel. The mechanical test was conducted using ElastoSensTM Bio2 (Rheolution Instruments) to obtain the storage modulus (G') and loss modulus (G") at 37 ˚C. Injectability was further performed on the optimized content of gelatin and Laponite as well as microgel loaded nanocomposite by employing a recovery analysis in which the nanocomposite was subjected to a high strain rate (100%) followed by a low (1%) strain rate at 1 Hz for 5 minutes.

3.2.6. Zeta Potential and Particle Size

Chi and PNIPAM particles, with a mixture of gelatin and Laponite, were suspended in acidic, neutral, and basic media to obtain the zeta potential and the hydrodynamic dimension of particles. Each sample was diluted to 0.2 wt % and vortexed for 5 minutes before conducting the experiments to decrease the viscosity and facilitate charge measurements. A Brookhaven BI-ZR3 Zeta Potential Analyzer with a 660 nm wavelength laser was used to determine the zeta potential and hydro dynamic dimensions of the samples at room temperature.

3.2.7. Scanning Electron Microscopy

SEM images were taken to study the microstructure of the shear-thinning gel and determine the effects of the introduction of particles on the microstructure of nanocomposite. Samples were freeze-dried at -80˚C and then coated with gold prior to imaging on a Hitachi S-4800 FESEM microscope at an accelerating voltage of 1 kV.

3.2.8. Fourier-transform Infrared Spectroscopy

A PerkinElmer Spectrum Two Fourier transform infrared spectrometer (USA) was used to obtain FTIR spectra by Potassium Bromide (KBr) technique. Freeze-dried samples were grounded and mixed with KBr powder to investigate the formation of nanocomposites and determine the interaction between the components. The spectra were collected within the range of 400−4000 cm^{-1}.

3.2.9. Degradation and Swelling Studies

The degradation rate of the shear-thinning gel was carried out by placing an accurately weighted amount of gel in an Eppendorf tube and soaking it in buffer solutions

with pH 5, 7.4, and 9.18 at 37˚C. At predetermined time intervals, the gels were centrifuged to remove the supernatant and reweigh the gel. The degradation rate was measured based on the following equation:

$$\text{Remaining Weight \%} = \frac{Wt}{Wi} \times 100 \qquad (1)$$

where Wt is the instant weight of the sample and Wi is the initial weight.

The swelling experiment was performed by immersing accurately weighted freeze-dried shear-thinning gel in a buffer solution with different pH values. At a certain time point, the samples were removed from the media and weighted. The swelling rate was calculated as:

$$\text{The degree of swelling \%} = \frac{Ws-Wd}{Wd} \times 100 \qquad (2)$$

Where Ws is the weight of swollen gel and Wd is the weight of dry gel.

3.2.10. Loading Rd

30 mg of lyophilized PNIPAM-co-AA was immersed in a 0.1 mg/ml solution of Rd and stored in a fridge for 24 hours to uptake Rd. After that, the mixture was centrifuged and washed three times with distilled water. Rd entrapment efficiency was calculated according to the following equation:

$$\text{EE \%} = \frac{Ci-Cw}{Ci} \times 100 \qquad (3)$$

where Ci is the initial concentration of Rd and Cw is the concentration of Rd in the washing supernatants. The concentration of Rd was calculated by measuring the

fluorescence intensity of the solution using a plate reader. A calibration curve was developed to determine the concentration of Rd based on the associated fluorescence intensity of the solution. This experiment carried out by measuring the fluorescent intensity of 15 Rd concentrations between 0 to 50 μg/ml. the solutions with various concentrations of Rd were prepared through serial dilution of 50 μg/ml sample. Each sample had three replicate to insure the accuracy of measurement. This measurement was employed to analyse the Rd concentration of samples from the release study.

Loading Rd on Chi particles was carried out by incorporating Rd in the initial Chi solution so that the weight ratio of Rd to Chi was 0.01. The rest of the steps was as of Chi particle preparation. The entrapment efficiency was determined by immersing and shaking the predefined weight of Chi particles in acetic acid 3% (v/v). After 24 hours, the suspension was sonicated for 30 minutes and centrifuged. Rd entrapment efficiency was obtained using the following equation:

$$\text{EE \%} = \frac{Ca}{Ct} \times 100 \qquad (4)$$

where Ca is the concentration of Rd in the aliquots and Ct is the theoretical concentration of Rd.

3.2.11. Drug Release

0.1g of different loaded gel formulations were incubated in 1 ml of pH 5, 7.4, and 9.18 buffer solutions to investigate the pH sensitivity of fabricated shear-thinning gels. At predetermined time intervals, samples were centrifuged, and the release media was replaced by 1 ml of buffer with the same pH to maintain a constant volume of release medium. The fluorescent intensity of the withdrawn media at each time point was measured

with a Tecan infinite 200 pro plate reader (λ ex 543 nm and λ em 580 nm). The obtained fluorescence intensity was converted to concentration (μg/ml) using a calibration curve. The release experiment was done in triplicate.

3.2.12. Statistical Analysis

The data were presented as mean ± standard deviation. In addition, statistical analysis was carried out using One-way ANOVA with Turkey's Honest Significant Difference (Turkey HSD) post hoc test by SPSS statistics 23 software. $P < 0.05$ was reported as significant for all statistical tests (*$p < 0.05$, **$p < 0.01$, ***$p < 0.001$).

3.3.Results and Discussion

3.3.1. Fabrication and Particle Characterization

Figure 3.1 A illustrates the schematic of the method employed to fabricate pH-responsive shear-thinning gel. The gelation process was carried out by the physical mixing of synthetic silicate nanoplatelets with porcine gelatin (Type A). Briefly, Laponite was suspended in ultrapure water (Mili-Q) using a shaker which caused an enhancement in nanoparticles surface area and subsequently better interaction with gelatin. Then, gelatin stock solution was added to the prepared silicate suspension under vigorous agitation to prevent agglomeration of Laponite nanoplatelets. The solution became a turbid, gel-like mixture within a few minutes due to physical crosslinking of the shear-thinning particles through an intensive electrostatic interaction between gelatin and Laponite. This can be attributed to the interaction between the negatively charged sides of silicate nanoplatelets and the positive sides of the gelatin chain. Different compositions of shear-thinning hydrogel composites are labelled as xNCy (Table. 3. 1) where x is the total solid weight percent% (w/v) and y represents the percentage of Laponite in solid mass % (w/w).

Since gelatin is a polyampholyte composed of carboxyl and amino groups, its electrical charge is highly influenced by variations in pH. It has been reported that gelatin's zeta potential constantly decreases from positive to negative values in response to a pH increase from 2-10, and reached its isoelectric point at pH=8.3 [80]. On the other hand, Laponite‘s zeta potential is always negative in this pH range and decreases with an increase in the pH [81]. Therefore, there is an electrostatic attraction between gelatin and the silicate nanoplatelets within the range of 2-8.3 and repulsion above this range. These electrostatic interactions will enable the shear-thinning gel to act as a pH-responsive carrier for the release of therapeutic agents.

These therapeutic agents can be directly incorporated into the initial silicate suspension/gelatin solution or they can be entrapped into different carriers and incorporated into each of the primary components. In this work, we load Rd as a drug model on PNIPAM-co-Acrylic acid and Chi, both of which have been extensively studied as pH-sensitive drug carriers [82-85]. The loaded particles were suspended in Milli-Q water and dispersed in the shear-thinning gel by adding the suspension to the gelatin/Laponite mixture followed by vigorous agitation.

The size and zeta potential variations of Chi and PNIPAM-co-AA particles in response to pH variations are shown in Figure 3.1 B-F. It has been reported that the zeta potential of Chi particles is influenced by a molecular weight of Chi, the ratio between Chi and the crosslinking agent, the concentration of Chi, pH, and measurement medium [86]. In this study, we investigated size and zeta potential changes as a function of pH in residing aqueous environments. The hydrodynamic size and zeta potential of Chi particles followed a descending trend as the pH increased. In acidic pH, the amine group in the back bone of

Chi became protonated (NH_3) and caused zeta potential to become positive. In addition, the increased hydrodynamic particle size can be attributed to the repulsion between NH_3 which facilitated transportation of water from surrounding media inside the particles. As the pH increased from the pKa of Chi (≈ 6.5), this polymer was deprotonated and its zeta potential showed nearly neutral value, at pH 7.4 [87-88]. A subsequent decrease in particle size and zeta potential to 328.2 nm and -20 mV was observed when the pH value of the solution increased to 9.18 (Figure 3.1 B and F). It has been shown that Chi particles reached the isoelectric point within the range of 7-7.4 [89]. In addition, Shu et al [90] showed that ionization of the amine group of Chi was highly influenced by pH so that a sharp decrease in the degree of ionization was observed as the pH value of solution increased above 6. The zeta potential trend in this study is consistent with previously published works in which the zeta potential of Chi particles continuously decreased with pH increase and reached negative values in alkaline pH [86,89].

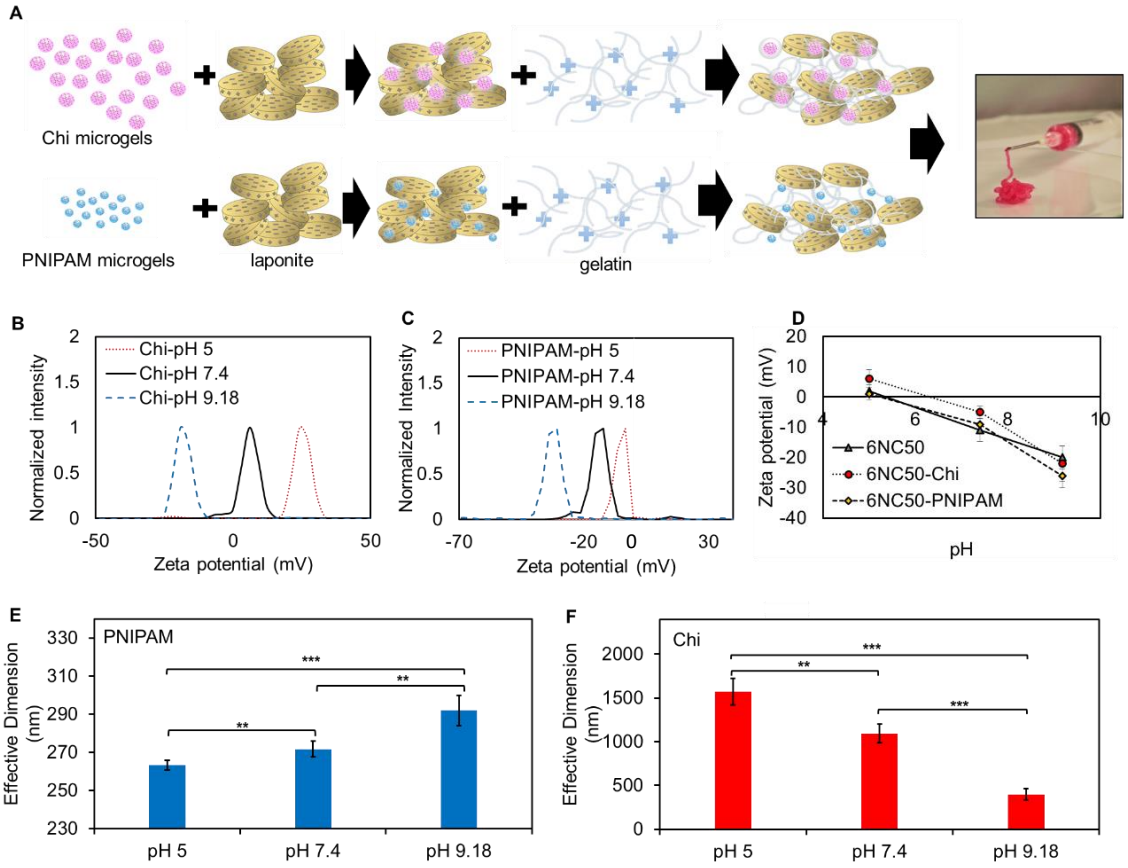

Figure 3.1. Fabrication and particle characterization. Electrostatic interactions between gelatin and Laponite resulted in the formation of the pH-responsive nanocomposite. A) schematic of fabrication of shear-thinning gel containing pH-responsive microgels B) zeta potential of Chi particles at different pH; C) zeta potential of PNIPAM particles at different pH; D) zeta potential of 6NC50 and 6NC50 loaded with Chi and PNIPAM particles at different pH; E) effective diameter of PNIPAM particles at different pH; F) effective hydrodynamic dimension of Chi particles at different pH.

On the other hand, PNIPAM is the most frequently used thermosensitive polymer with a lower critical solution temperature (LCST) around 32 ˚C. It has been reported that pure NIPAM has a low density of ionizable functional groups, which are essential in pH-responsive materials. Copolymerizing PNIPAM with acrylic acid not only increases the LCST to higher temperatures but also induces pH-responsive behaviour to PNIPAM owing to its carboxylic acid group [89]. In order to simplify the text, PNIPAM-co-AA is hereafter replaced as PNIPAM in the labelling of samples. At pH values above the pKa of acrylic

acid (≈4.2), COOH deprotonates and becomes COO^- which induces a negative charge to the polymeric network. The obtained result of zeta potential was consistent with this phenomena so that it decreased from -0.23 to -12.3 and -30.9 mV as the pH increased from 5 to 7.4 and 9.18, respectively. In addition, this transportation creates an electrostatic repulsion between the adjacent carboxylate ions within the polymeric chain and subsequently increases the hydrophilicity of the particles [91]. Therefore, the enhancement observed in the hydrodynamic diameter of PNIPAM when pH increased is in keeping with the theory (Figure 3.1 E).

Zeta potential of the shear-thinning gel at different pH after incorporation particles is illustrated in Figure 3.1 D. Zeta potentials in all formulations of the gel had descending trends owing to the decrease in the zeta potential of each component. Additionally, the zeta potential of gelatin and Laponite played a major role in the complex material since the difference between the curves was negligible.

3.3.2. Chemical and Morphological Characterization

The FTIR spectra of PNIPAM, gelatin-Laponite, and gelatin-Laponite-PNIPAM composites were plotted in Figures 3.2 A and B shows the FTIR spectra of Chi, gelatin-Laponite, gelatin-Laponite-Chi. Since a small amount of Chi and PNIPAM (1 wt% of gel) was incorporated in the shear-thinning composite, the majority of the peaks were overlapped, with intense peaks for gelatin and Laponite. So, subtracted spectra of [6NC50-NIPAM-6NC50] and [6NC50-Chi-6NC50] were plotted in Figure 3.2 A and B, respectively, to compare with the original spectra of PNIPAM and Chi for detecting their functional groups in the composite sample. As we can see, 6NC50 and 6NC50-PNIPAM show typical bands of the main component. The stretching bands observed at 2931 and

1663 cm^{-1} correspond to C-H and C=O of carboxamide [92]. The characteristic peak related to Si-O stretching of the Laponite component was detected at 1003 cm^{-1}. In addition, the peak appearing in the high-frequency region at 3439 cm^{-1} originated from stretching of NH and O-H in the amide group and nanoclay [92-93]. The weak bands observed in subtracted spectra in 1650-1750 cm^{-1} arose from the carboxyl of NIPAM and acrylic acid. Moreover, the bands corresponding to -CH_3 symmetric stretching, asymmetric CH_2 stretching, and CH_3 asymmetric stretching was detected within 2850-2975 cm^{-1} [94]. Negligible changes in the peak position along with similarity in FTIR pattern suggest that adding NIPAM to the shear-thinning gel did not remarkably affect its chemical structure. The characteristic bands of the shear-thinning gel appeared in the spectra of gelatin-Laponite-Chi, as well. Besides, the similarity between the spectra of subtracted [6NC50-Chi-6NC50] and Chi confirmed proper incorporation of Chi in the gel. As shown in the subtracted spectra, the bands related to combined peaks of the OH and NH_2 group appeared at 3416 cm^{-1}. Also, the bands at 1390 and 1630 cm^{-1}correspond to the –C–O stretching of the primary alcoholic group in Chi and N-H bending, respectively [95][96]. Interestingly, the sharp band corresponding to the stretching of C-H slightly shifted to lower wavenumber, indicating some specific interaction between Chi and the gel which caused a slight decrease in the strength of the C-H bond.

Figure 3.2 C displays an SEM micrograph of fabricated gel. The gel was lyophilized before taking the image to preserve the structure and volume after water content removal. The shear-thinning gel has a porous structure with an average pore size of 74 ± 23 µm after the removal of water content. Li et al [92] stated that obtaining pore size can be tuned by introducing different ratios of gelatin to Laponite. The pore size increases parallel with the

increase in the gelatin component owing to the fact that gelatin has a hydrophilic functional group such as COO^- and NH_2, which facilitates network expansion and increases the water content, therefore causing larger pore sizes. On the other hand, a more significant increase in pore size can be obtained as the concentration of Laponite decreases, because it is a multifunctional crosslinker.

Figure 3.2 D and E show SEM micrographs of the shear-thinning gel after incorporation of PNIPAM and Chi particles. Incorporating PNIPAM with negatively charged COO^- in shear-thinning gel facilitates crosslinking, so that the average pore size slightly decreased (62 ± 16 μm). Conversely, positively charged Chi adsorbs on the top and bottom of silicate nanoplatelet and acts as a barrier in gel crosslinking. The presence of very large pores in the micrograph of the 6NC50-Chi gel is evidence for this phenomenon.

3.3.3. Rheological and Mechanical Characterization

The rheological test was performed on a gelatin-Laponite gel to study the shear-thinning behaviour of fabricated hydrogel. The effects of total solid weight (xNC50) and also the ratio of gelatin: Laponite (6NCy) on the variation of shear stress (Pa) as a function of shear rate (1/S) were investigated. Figure 3.3 A and B demonstrate that all the gel formulations showed shear-thinning properties.

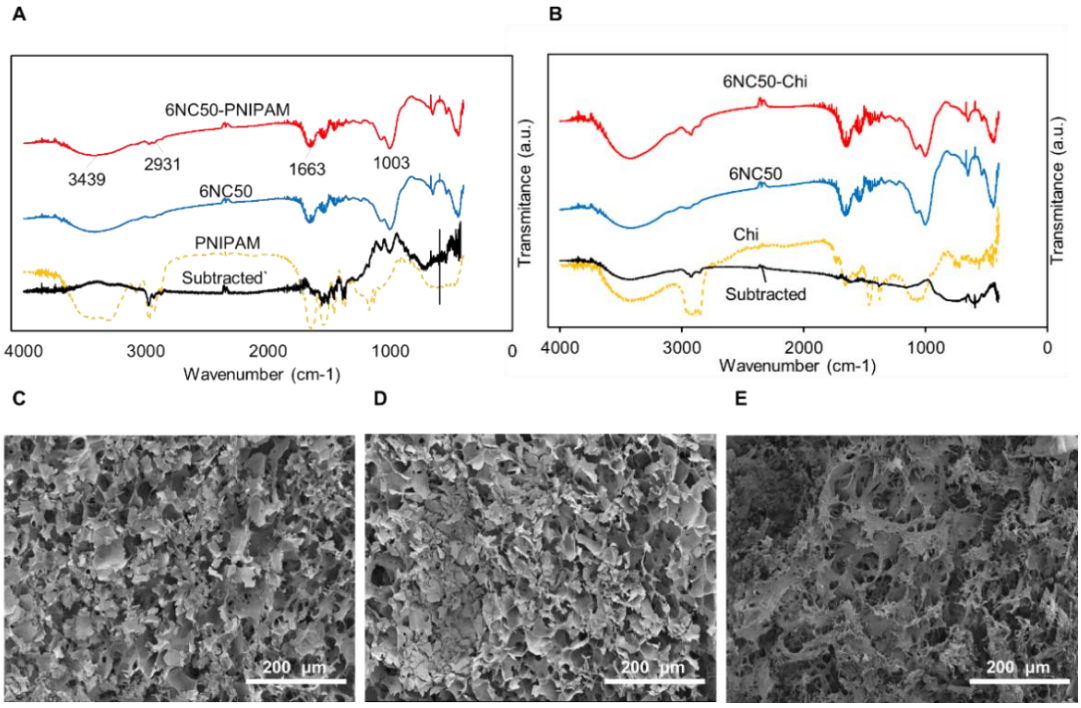

Figure 3.2. Chemical and morphological characterization. A) FTIR spectra of 6NC50 shear-thinning gel loaded with PNIPAM particles; B) FTIR spectra of 6NC50 shear-thinning gel loaded with Chi particles. SEM images illustrate the effect of adding PNIPAM and Chi particles on the microstructure of shear-thinning gel C) 6NC50; D) 6NC50-PNIPAM; E) 6NC50-Chi.

At a low shear rate (10^{-3} S^{-1}), a significant increase in shear stress was observable by increasing the total solid weight from 3 to 9 so that the shear stress enhanced from 2.4 Pa in 3NC50 to 147 and 551 Pa in 6NC50 and 9NC50, respectively. It is noteworthy that a sharp increase in the shear stress to a stable level followed by a negligible decrease at a high shear rate in 6NC50 suggests a controllable injection of this sample with respect to the other samples. Therefore, 6NCy was chosen as the optimum condition for further rheological and mechanical analysis. Incorporation of nanoclay platelets with gelatin enhanced shear stress which was due to the electrostatic interaction between negatively charged Laponite and positively charged gelatin chain [80]. However, the increase in the content of Laponite did not significantly affect rheological properties as the shear stress

versus shear rate curve of 6NC25, 6NC50, and 6NC75 presented similar patterns. These results were consistent with previously published work [78].

The storage (G') and loss (G") moduli were determined at 37°C using an ElastoSensTM Bio2 which is a non-destructive method of monitoring mechanical properties of viscoelastic materials.

The dynamic complex modulus can be obtained as shown below:

$$G = G' + iG'' \quad (5)$$

$$G' = G \cos \delta \quad (6)$$

$$G'' = G \sin \delta \quad (7)$$

G' represents the amount of energy stored during the loading cycle which is the indication of the elastic part of the material. On the other hand, the viscous part is presented by G" which is the amount of dissipated energy during the loading cycle. In viscoelastic materials, the ratio between loss modulus and elastic modulus, called loss factor, refers to mechanical damping:

$$Q\text{-}1 = \frac{G''}{G} = \frac{G \sin \delta}{G \cos \delta} = \tan \delta \quad (8)$$

where Q-1 is the loss factor and δ represents the phase difference between dynamic stress and dynamic strain. The loss factor is being used to determine the behaviour of material so that the material has solid-like behaviour as Q-1<1 and liquid-like behaviour when Q-1>1 [97].

According to Figure 3.3 C, G' is bigger than G" for all samples, which indicates that all the 6NCy samples have solid-like behaviour. The storage modulus gradually

increased from 492 Pa in 6NC0 to 731 Pa in 6NC50 followed by a sharp enhancement to 2246 Pa and 2994 Pa in 6NC75 and 6NC100 respectively. As shown by Figure 3.3 C, the loss factor remarkably decreases as the content of Laponite exceeds 50%, which may cause increasing the solid-like behaviour and losing control of continuous injection of the shear-thinning gel. Also, the shear stress of the 6NC25 sample experienced a sharp decrease when it reached its peak which may induce the same error during injecting the materials (Figure 3.3 B). Therefore, 6NC50 was chosen to conduct further experiments.

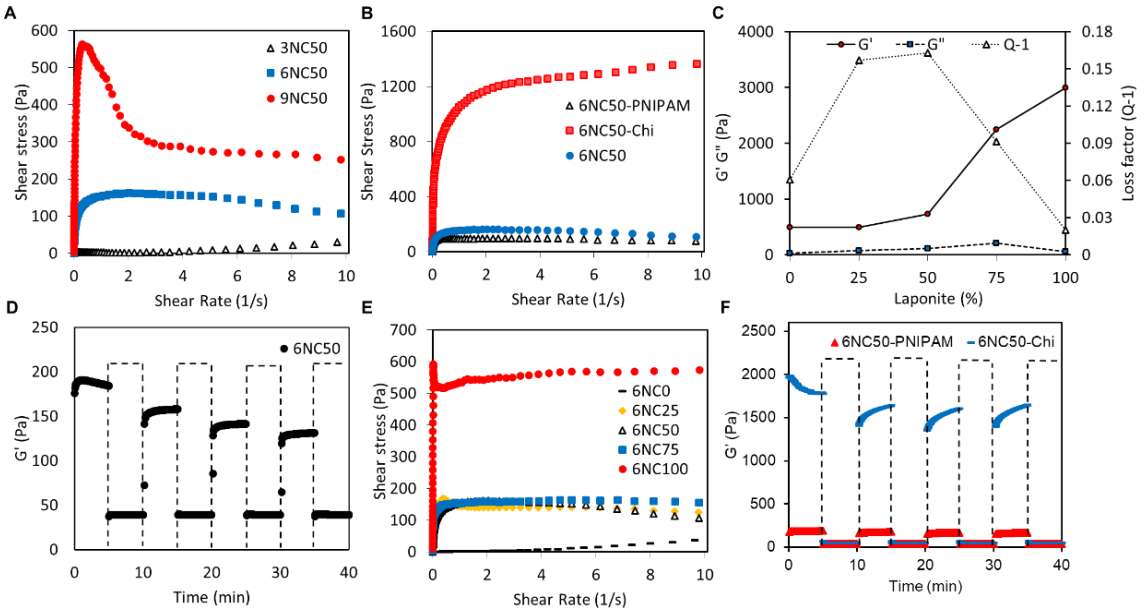

Figure 3.3. Rheological and mechanical characterization. A plot of shear stress versus shear rate as a function of A) total solid weight (3NC50,6NC50 and 9NC50) and B) a percentage of Laponite in solid mass (0,25,50,75, and 100); C) storage modulus (G'), loss modulus (G"), and loss factor of 6NCy as a function of Laponite concentration; D) G' of 6NC50 after repeated application of high strain (100% strain) and low strain (1% strain) over time (high strain condition is the regions in box); E) plot of shear stress as a function of shear rate for 6NC containing pH-sensitive particles; F) G' recovery of 6NC-PNIPAM and 6NC50-Chi after subjecting the gels to alternating high strain and low strain condition.

Figure 3.3 D demonstrates the 6NC50 stress recovery curve after repeated application of high strain shear rate (100%) and low shear strain rate (1%) over the span of 40 minutes. As we can see, the storage modulus remarkably decreased when a high-strain

shear rate was applied to the gel and it presented a liquid-like behaviour at this strain rate. While a significant increase in the storage modulus was observed at low strain rates in which gel had solid-like behaviour, the results indicated that the gel successfully recovered to solid-like behaviour after application of a high strain shear rate. In addition, rheological tests along with stress-recovery analysis were carried out to examine shear-thinning properties of the gel after introducing microgels. In Figure 3.3 E the variations of shear stress versus shear rate in 6NC50-PNIPAM were similar to that of 6NC50, indicating that shear-thinning properties were not influenced by introducing PNIPAM. In contrast, adding Chi to the gel led to a significant shift to higher shear stress. This increase can be attributed to the adsorption of Chi on the surface of Laponite disks, which limits the slipping of Laponite nanoplatelets. Moreover, the recovery of 6NC50-PNIPAM and 6NC50-Chi after repeated application of high strain and low strain are presented in Figure 3.3 F. The results indicate that 6NC50-PNIPAM and 6NC50-Chi recovered very fast, which is essential for avoiding the unwanted flow of materials as they are injected. After three cycles of high and low strain conditions, the resulting modulus at high, 100% strain for both formulations was below 50 Pa by the end of 10 minutes of high strain condition, indicating rapid network disruption. After three strain cycles, a 13.5 % and 17.5 % decreased in storage modulus was observed in 6NC50-PNIPAM and 6NC50-Chi, respectively.

3.3.4. Release Characterization

3.3.4.1. Degradation and Swelling

Fig. 4 A and B demonstrate the degradation rate of 6NC50-PNIPAM and 6NC50-Chi in three different pH values at 37˚C within 24 hours. The results showed that the main weight loss at each formulation occurred in the first 2 hours. Also, both gel formulations

had a lower degradation rate at neutral pH so that more than 70% of gels were preserved during the experiment. In addition, both formulations degrade faster in pH 9.18, and weight loss was significantly higher (***P<0.001 and **P<0.01 6NC50-Chi and 6NC50-PNIPAM, respectively) than another pH due to repulsion between the main components.

Degradation and swelling rates and their kinetics are important parameters of a drug carrier owing to their significant effects on release rate. Swelling kinetics and the ratio of 6NC50-PNIPAM and 6NC50-Chi in different pH (5, 7.4, and 9.18) are shown in Fig. 4 (C) and (D). The swelling ratio was increased in both formulations by increasing the pH of surrounding media so that the lowest and highest swelling ratios were observed in pH 5 and 9.18, respectively. A continuous weight gain through the first 2 hours of swelling time was observed in all samples, a result of the penetration of water from surrounding media, driven by osmotic pressure [98], to the porous structure of the shear-thinning gel. This was followed by a slight weight decrease for the rest of the swelling time in samples immersed in pH 5 and pH 7.4 buffers in which there was an electrostatic attraction between gelatin and Laponite. In contrast, the highest swelling ratio of both formulations was obtained in pH 9.18 when the electrostatic repulsion between main components increased the distance between polymer chains to facilitate water penetration. In addition, shear-thinning gel exposed to pH 9.18 followed a degrading pattern after reaching the maximum swelling ratio which can be attributed to partial dissolution of the gel in surrounding media. The difference between maximum swelling ratios of gel in pH 9.18 buffer and other buffers were statically significant for both 6NC50-PNIPAM and 6NC50-Chi (**P<0.01 and ***P<0.001 6NC50-Chi and 6NC50-PNIPAM, respectively). Also, there was a significant difference (**P<0.01) between the maximum swelling ratio of 6NC50-PNIPAM in pH 5

and 7.4 while, this difference was insignificant for 6NC50-Chi. Shear-thinning gels containing PNIPAM had a higher maximum swelling ratio at every experimental condition which can be attributed to the low capability of Chi particles to uptake water in pH 7.4 and 9.18.

3.3.4.2. Cumulative Release

Release experiments were carried out at three different pH over the course of 22 days by loading Rd with a molecular weight of 479.01 g/mol on 6NC50-PNIPAM and 6NC50-Chi. Rd is an extensively used drug model with a molecular weight similar to that of most commercial antibiotics [99]. The encapsulation efficiency (EE) of drugs on carriers can be affected by various parameters such as drug loading method, type of drug, intrinsic behaviour of carrier, particle size, and etc [100]. Here, the drug was loaded on Chi particles through the preparation of Chi particles which resulted in very low entrapment efficiency. This low entrapment efficiency can be attributed to electrostatic repulsion between a positively charged functional group of Chi and Rd. On the other hand, a 17.9% EE was obtained as PNIPAM was immersed in Rd solution and kept at 4˚C where the particles swelling ratio was the highest, allowing Rd molecules to penetrate inside the particles. This EE is reported elsewhere [90].

Figure 3.4 E and F show the cumulative release profile from 6NC50-PNIPAM and 6NC50-Chi, respectively. The results indicated that both shear-thinning gels had a pH-responsive release profile so that they were in off-state of release at pH 5 and 7.4 and went to on-state of release at pH 9.18. As we can see, the release rate was negligible at pH 5 and 7.4 while at pH 9.18 it was significantly higher (***$p < 0.001$) than the other two pH. These results along with degradation results are suggesting that degradation of the shear-

thinning gel was the main mechanism for the higher level of drug release at pH 9.18. As discussed before, the considerable degradation of nanocomposite gel in this condition is being attributed to the repulsion between gelatin and Laponite, since both of them are negatively charged at this pH [80-81].

As to be shown in Figure 3.4 E, the release of Rd from PNIPAM particle seemed to be diffusive, since no burst release was observed at any release conditions. At pH 9.18, the release rate gradually increased to more than 3.7 (μg/ml) after 384 hours followed by a slight increase for the rest of the release experiment. The major portion of entrapped Rd on the PNIPAM was released over the 22 days of an experiment, which was caused by the swelling of PNIPAM particles in pH 9.18 as evidenced by hydrodynamic size variations (Figure 3.1 E). In contrast, 6NC50-Chi showed a significantly lower release rate compared to 6NC50-PNIPAM in pH 9.18, where the highest degradation rate was obtained for both gels. Although the gel was destroyed at pH 9.18, the Chi particles shrank and the detected 7.3 (ng/ml) Rd in media after 22 days was due to the diffusion of physically entrapped Rd. Also, low EE is another noticeable factor for the low rate of release from 6NC50-Chi.

The obtained release profiles suggest that 6NC50-PNIPAM and 6NC50-Chi show pH-responsive behaviour. In addition, the shear-thinning behaviour of nanocomposite gel loaded with PNIPAM and Chi enable minimal invasive injection of the gel to the desired area for local delivery of drugs or other therapeutic agents. This is particularly useful in the treatment of wounds in which the infections are multi-strain and the pH changes significantly depending on the type of bacterial infections. This is also pertinent in the treatment of bacterial infections caused by Pseudomonas and Escherichia coli where the pH of the wound area shifts to alkaline conditions [101].

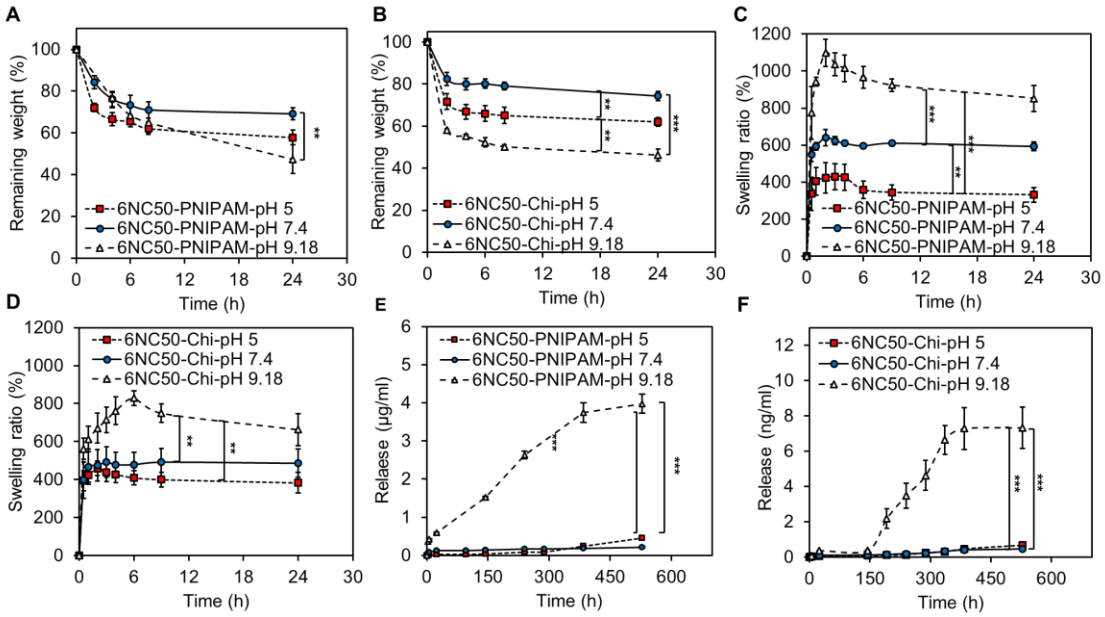

Figure 3.4. Release characterization. Degradation, swelling, and release of Rd increase by increasing pH from 5 to 9. Degradation of A) 6NC50-PNIPAM and B) 6NC50-Chi at different pH; Swelling kinetics of C) 6NC50-PNIPAM and D) 6NC50-Chi at different pH. The highest swelling degree for both types of gel was observed in pH 9.18; cumulative Rd release from E) 6NC50-PNIPAM and F) 6NC50-Chi over the span of 22 days in different pH. The release was significantly higher (***P<0.001) in pH 9.18 with respect to another pH.

3.4.Conclusions

This study presents a smart, injectable drug delivery system, engineered by introducing Chi and PNIPAM pH-responsive particles to a gelatin-Laponite shear-thinning gel. The addition of PNIPAM to the nanocomposite resulted in a decrease in the pore size of the gel, while notably large pores were formed as Chi was incorporated within the shear-thinning gel. In addition, the injectability of the gel decreased as Chi particles were introduced to the shear-thinning nanocomposite, while PNIPAM had a negligible effect on injectability. In addition, gelatin-Laponite composite loaded with microgels presented desirable stress-recovery behaviour so that the gel recovered very fast after shear stress removal. Furthermore, the shear-thinning gel offered the possibility of pH-responsive behaviour, since degradation and swelling rates of the gel were highly influenced by the

pH of surrounding media. The degradation and swelling ratios of gel in pH 9.18 buffer were significantly higher than other buffers owing to electrostatic repulsion between the main components. Besides, the pH sensitivity of the shear-thinning gel was further verified by the release experiment as the release profile for both incorporated drug carriers show negligible release at acidic and neutral conditions, while the release rate notably increased in basic pH. Notably, the shear-thinning gel that contained PNIPAM particles presented better pH responsivity than the Chi one. In summary, the prepared shear-thinning nanocomposite loaded with pH-responsive PNIPAM microgels presented a high potential for site delivery of therapeutic agents in which the delivery is activated in response to local basic pH.

Chapter 4

4. Multifunctional Silicate-based Electroconductive Bioinks for Fabricating Soft Electronics

Preamble

The first objective of this research is to fabricate silicate-based electroconductive hydrogel bioinks using Laponite, alginate, and graphene oxide for the 3D printing of soft electronics. The second objective is to introduce new technology for printing flexible and durable conductors on alginate sheets, for potential tissue engineering applications. The high reducibility of this technique is achieved from high control over the fabrication process. The shear-thinning properties of this bioink maintain the cylindrical shape of the stacked layers of filaments and enable the fabrication of filaments with different diameters. The fabrication process is then followed by various mechanical analyses to evaluate the flexibility and durability of the printed conductors. In addition, the viscoelasticity and electroconductivity of the bioink can be adjusted through the addition of various concentrations of Laponite and graphene oxide.

Abstract

Hydrogel-based bio-inks have been extensively used for developing three-dimensional (3D) biomaterials for biomedical applications. However, the poor mechanical performance and inability to conduct electricity limit their application and wearable sensors. In this work, we developed a novel electro-conductive bio-ink made of silicate nanosheets and graphene oxide to alginate to generate a stretchable, soft, but durable electro-conductive material. This material is suitable for utilization as a novel electro-conductive bio-ink for extrusion printing of flexible electronics. A series of tensile tests

were performed on the material, indicating excellent stability under significant stretching and bending without any conductive or mechanical failures. Rheological characterization revealed that the addition of Laponite enhanced the hydrogel's mechanical properties including stiffness, shear-thinning, and stretchability. We also illustrate the reproducibility and generalizability of our fabrication process by extrusion bioprinting various patterns with different fibre diameters. Developing an electro-conductive bio-ink with favourable mechanical and electrical properties offers a new platform for advanced tissue engineering.

4.1.Introduction

Engineered materials that can imitate native tissue properties are promising tools for treating a wide variety of clinical problems in patients and for use in research labs. In particular, conductive engineered material can be used to produce flexible biocompatible sensors for the in-vivo recording of bio-signals and biomolecules or in tissue engineering applications [102]. However, designing systems capable of generating the desired three-dimensional (3D) structures with the necessary physical properties, biocompatibility and scalability are not trivial. 3D printing is a technology that is ideal for the intensive manufacturing of these structures and sensors for both in-vivo applications [103-104]. 3D printing provides high reproducibility and precise control in an automated manner and has the potential for mass production [105]. A limiting factor preventing the widespread adoption of bio-printing for this purpose is the paucity of bio-inks that are both printable and possess the necessary physical properties after being printed.

Engineering electro-responsive sensors and soft electronics using 3D printing require a bio-ink that has similar physical characteristics to the underlying tissue while being electro-conductive [106-107]. Conductive hydrogels enable to provide uniform

electrical paths to living cells to improve electrical signal propagation, cell adhesion, and differentiation within the desired 3D scaffold for tissue engineering applications [108]. Additionally, flexible conductors have gained significant attention for producing epidermal sensors, artificial skin, and implantable medical devices. In the meanwhile, bioprinting is a developing fabrication method for the rapid assembly of soft electronics [109]. Therefore, generating an electro-conductive bio-ink enables the production of soft electronics with a wide range of biomedical applications.

These hydrogel-based bio-inks should also be flexible, physically robust and capable of withstanding the host tissue's physical activity and movement. Additionally, the bio-ink must have suitable electro-conductive properties for conducting currents generated by in-vivo sensors or by the living tissue itself (e.g., cardiac or neural action potential). Hydrogels with shear-thinning properties are good candidates for use as inks for application in 3D printing of tissue and soft electronics [110]. This is due to their non-Newtonian [111] viscoelastic behaviour under shear stress, which makes them extrudable through existing printheads, but fairly robust in the relaxed state upon extrusion. Furthermore, hydrogels can be used to print a variety of complex patterns and are generally biocompatible and well-tolerated, making them ideal candidates for tissue engineering applications [112]. Some of the most common polymers used for printing soft structures include hyaluronic acid (HA), [113] agarose, [114] alginate, [115] gelatin methacrylate (GelMA), [116] silk proteins, [117] elastin, [118] and poly (ethylene oxide/glycol) [119]. The property that enables the use of all of these aforementioned polymers for printing applications is their non-Newtonian behaviour under shear stress. However, low viscosity and slow cross-linking process eliminate maintaining a high shape fidelity after printing

[108]. Alginate is the most used hydrogel for bioprinting due to its excellent biocompatibility, availability, and mild ionic gelation process [120]. Due to these properties, alginate was chosen to form the basis of this bio-ink. However, it lacks biologically active moieties, alginate has minimal cellular adhesion properties and does not promote cell proliferation and differentiation [121]. Moreover, it should be noted that alginate-based hydrogel bio-inks are oftentimes constrained by their mechanical weakness and limited shape fidelity after printing [122].

To alleviate the physical strength limitations of alginate hydrogels, silicate nanoclays have been added to alginate hydrogels [123]. Synthetic silicates are charged disks with high aspect ratios, approximately 20–30 nm in diameter and 1 nm in thickness [124]. Laponite is an example of a silicate nanoclay and is a synthetic, lithium–magnesium–sodium silicate of the smectite group. Laponite has been added to alginate-based hydrogel to simultaneously improve the physical properties of the hydrogels and to provide a base for cellular attachment [20]. This improvement is hypothesized to be a result of hydrostatic interactions between the anionic polymer (alginate) and the positive charge on Laponite's surface that help in stabilizing the hydrogel [61,125]. An example of an alginate Laponite hydrogels for bio-printing is provided by Ahfeld et al [126]. They blended alginate and methylcellulose with Laponite, to fabricate a bio-ink and produce scaffolds utilizing the extrusion-based method 3D plotting [126]. Similarly, Ahasan Habib et al. developed a bio-ink composed of alginate, carboxymethyl cellulose and montmorillonite clay instead of Laponite that had suitable physical properties for bioprinting [127]. While silicates enhanced alginate hydrogel bio-inks have been

extensively studied for their physical properties, their electro-conductive properties and the possibility of modification with electro-conductive material remain unexamined [128].

Some electro-conductive materials that have been used for engineering bio-inks include metals such as gold, [129] copper, [129] and silver, [130] and organic materials such as carbon nano-tubes(CNT) [109], and graphene. [131-132] For example, Zhu et al. developed a gold nanorod (GNR) incorporated gelatin methacryloyl (GelMA) based bio-ink for printing 3D functional cardiac tissue constructs [59]. In another study, He et al. fabricated ultrathin and electrically parallel arrays of reduced graphene oxide (rGO) films on various substrates including the flexible polyethylene terephthalate (PET) films They used these nanocomposite films as a chemical and biological sensor to detect the cellular secretion of biomolecules [63]. Graphene and graphene oxide is of particular interest due to their electro-conductive properties. This is due to their sp^2 hybridized orbital structure and free electrons, which gives them outstanding thermal and electrical conductive properties [133]. Graphene oxide is an oxidized form of graphene with carboxylic acid and hydroxyl functional groups in the plane [134].

Printable highly elastic bio-inks with low electrical resistance and high flexibility have gained increasing attention in biomedical applications such as flexible displays, [135] smart sutures, [136] epidermal sensors, [137] elastomeric circuits, [138] implantable devices, smart wound dressings, [109,139] and soft contact lenses. [140] However, the interface between the bio-ink and the surface of the tissue is also an area that needs further attention. This is a particularly acute problem as in most applications, the bio-ink cannot be directly printed onto the patient's tissue or body, so that the bio-ink must be printed on another substrate and then applied to the body. It needs to be printed on a substrate that is

flexible, durable, and is not cytotoxic among other conditions. However, providing stretchable, durable, and cost-effective fabrication methods remains a constant challenge. [102] Various substrates have been introduced to provide a flexible and biodegradable layer for organic conductor patterns. Based on the literature silk, poly(lactic-co-glycolic) acid PLGA, poly(imide), poly(4-vinyl pyridine), and poly(styrene-block-butadiene-block styrene) have been regularly utilized to provide a flexible substrate. [141] Tunnel injection and metallic microstrips have been employed to form conformal contacts and sufficient attachment to curved surfaces. However, maintaining the attachment without affecting the physical properties remains challenging. A variety of techniques, such as inkjet printing, screen printing, and contact printing, [109] have been employed for printing cost-effective conductors on paper. However, paper-based conductors are not stretchable and soften in aqueous environments. Poly (dimethylsiloxane) and electrospinning techniques have been widely used to produce an elastic and cost-effective substrate for fabricating flexible conductors. [142-143]. Although PDMS is a cost-effective material and provides a decent amount of flexibility, the hydrophobic nature of this polymer prevents biodegradability and permeability, which are necessary traits for drug delivery and biomedical applications. Despite, electrospinning allowing the fabrication of nanoscale fibres from a wide variety of polymer solutions, a complex fabrication process and a lack of generating consistent samples remain as challenges in electrospinning.

In the present work, we report a novel silicate-based conductive bio-ink composed of alginate, Laponite, and graphene oxide. This material composition provides a printable, low electrical resistant and flexible hydrogel structure which is then embedded in a multilayered hydrogel bed using a multi-step process. The properties of the novel bio-ink

including its structural morphology, rheological characteristics, and conductivity under different physical conditions were analyzed. Furthermore, we stretched and sutured the printed bio-ink-system to show their potential function in the simulated clinical applications in stretchable electronics and in tissue engineering. To the best of our knowledge, we were able for the first time to produce a material composition that combines the printable rheological properties of alginate-silicate hydrogels and the electro-conductive properties of graphene oxides. The printed conductive bioink on a multilayered hydrogel bed generated a flexible electric conductor with the potential functions in in-vivo clinical applications.

4.2.Materials and Methods

4.2.1. Materials

Alginic acid sodium salt (alginate), graphene oxide, gelatin from porcine skin (type A, 300 bloom gel strength), agarose, and calcium chloride were all obtained from Sigma Aldrich, St. Louis, Missouri. Laponite XLG, a synthetic nanosilicate, was acquired from BYK additives, Germany.

4.2.2. Preparation of Bio-inks

0.5% (w/v) alginate, 6% (w/v) Laponite, and 5mg/ml graphene oxide were prepared by, first, dispersing the graphene oxide in deionized water. The suspension was then sonicated for 5 minutes alginate was dissolved in the graphene oxide suspension and the solution was cooled to 5℃. Laponite was added to the solution and immediately vortexed for 5 minutes to ensure the homogenous distribution of Laponite nanoplatelet in solution. In order to prepare different formulations of the bio-ink, different concentrations of the

graphene oxide and Laponite were added to the solution and the rest of the procedure was followed as explained above. A list of different formulations of the bio-ink is given in table 4. 1.

Table 4.1. A list of different formulations of the bio-ink.

Sample code	Laponite (wt)%	Graphene oxide (wt)%
S1	3	0
S2	3	3
S3	3	5
S4	6	0
S5	6	3
S6	6	5
S7	9	0
S8	9	3
S9	9	5

All the formulations have 0.5 wt% Alginate

4.2.3. Zeta Potential

Zeta potential tests were conducted using Brookjaven BI-ZR3 Zeta Potential Analyzer with a 600 nm wavelength laser at room temperature. Samples with 0.5% (w/v) alginate, 6% (w/v) Laponite, and 0, 3, 6% (w/v) graphene oxide were diluted to 0.2% (w/v) and sonicated for 5 minutes to ensure a uniform distribution of graphene oxide and Laponite. This test was conducted to study the effect of the introduction of different concentrations of graphene oxide on the zeta potential of the bio-ink.

4.2.4. Fourier-Transform Infrared Spectroscopy (FTIR)

The chemical structure of Laponite/alginate with various concentrations of graphene oxide was analyzed by a PerkinElmer Spectrum Two Fourier transform infrared spectrometer (USA) to obtain FTIR spectra by potassium bromide (KBr) technique. Samples were firstly freeze-dried and then ground into powder and mixed with KBr to collect the spectra and determine the interactions between the components within the range of 400-4000 cm^{-1}.

4.2.5. X-Ray Diffraction (XRD)

Firstly, samples were freeze-dried and grounded into a powder. The crystal structure of the bio-ink with different concentrations of graphene oxide was analyzed using a PANalytical Empyrean X-Ray Diffractometer at room temperature with a current of 40 mA and a voltage of 45 kV over the diffraction angle range of 10°-90° (2θ).

4.2.6. Scanning Electron Microscopy (SEM):

SEM images were acquired using Hitachi S-4800 FESEM microscope at an accelerating voltage of 1kV. Samples were freeze-dried by storing them in a -80°C freezer for 24hr, lyophilized for 2 days, tapped to the SEM stubs and then coated with gold-palladium. SEM images were employed to investigate the microstructural differences between bio-ink formulations with various concentrations of graphene oxide (0, 3, and 5 mg/ml), with 0.5% (w/v) alginate and 6% (w/v) Laponite.

4.2.7. Rheometer and Mechanical Analysis

The Young's modulus, storage modulus, shear stress, and viscosity of the bulk bio-inks with different concentrations of the graphene oxide (0, 3, 5 mg/ml) were measured using an Anton Paar MCR 502 rheometer (Graz, Austria) over shear rate sweeps of 0.001 to 10 Hz at room temperature. Viscosity was measured under a constant shear rate over

300 seconds and stress recovery measurements were conducted at 1 Hz by alternating the application of 100% strain and 1% strain for 5-minute intervals on the bulk bio-inks.

4.2.8. 3D Bioprinting Process

All 3D-bioprinting experiments for the present work were conducted employing a Cellink Inkredible+ (Cellink, Sweden) microextrusion 3D-bioprinter with pneumatic pressure for extruding materials. Repetier and Slic3r software were used to manually generate codes for the 3D bioprinting of rectangular patterns. In order to print serpentine and spiral patterns, AutoCAD was employed to develop the drawings and Cura was used to developing the final codes for bioprinting. Different formulations were used to study the printability of the bio-inks Figure. 4.3 B. In order to provide the requisite control over the diameter of printed fibres, print-head nozzle moving speed was optimized with different printing air pressures for feeding pressure Figure. 4.3 C. The nozzle moving speed and the printing feeding pressure were determined for the bio-ink with 6% (w/v) Laponite, 5 mg/ml graphene oxide, and 0.5% (w/v) alginate. The electro-conductive bio-ink with alginate 0.5% (w/v), Laponite 6% (w/v), graphene oxide 5 mg/ml, and 2% (w/v) $CaCl_2$ were used to print the patterns for this study. Three different feeding pressures: 150, 180, 210 (kPa) and nozzle moving speeds: 150, 350, 550 (mm/s) were employed to optimize the printing process. After optimizing the printing process, Repetier software was used to customize the codes and the patterns were printed with three different spacing between printed fibres including 1, 3, and 5 mm (see Figure 4.4 G). Besides, three different needle gauges of 18, 22, and 25 with an inner diameter of 0.84, 0.41, and 0.26 mm respectively, were used to produce fibre sizes of 0.5, 1, and 2 mm for rectangular patterns. All the patterns were allowed to crosslink with 2% $CaCl_2$ for 30 minutes at room temperature. The

electrical conductivity of the rectangular pattern was measured using a multimeter at room temperature.

4.2.9. 3D Bioprinting on Alginate Substrate

4% (w/v) alginate was chosen to develop a flexible substrate for printing an electrically conductive pattern. The first step to develop a flexible printed pattern was spreading 4% (w/v) alginate solution in a 100 mm Petri-dish and crosslink it with 4% (w/v) $CaCl_2$. New technology was developed in order to provide sufficient attachment between the electrically conductive printed pattern and the alginate sheet. The following method was employed to fabricate the flexible substrate. 1.5% (w/v) agarose solution was prepared by suspending 1.5 g agarose powder in 100 ml deionized water and dissolving at 70°c to form a clear solution. 4% (w/v) $CaCl_2$ the solution was then added to the clear agarose solution and 15 ml of the final solution was spread in a 100 mm Petri-dish and cooled down to room temperature to form a flat sheet of agarose containing $CaCl_2$. 15 ml of 4% (w/v) alginate was then spread to the same Petri-dish at the top of the agarose sheet. The agarose sheet containing 4% (w/v) $CaCl_2$ was employed to provide more control over the crosslinking process of the alginate sheet by eliminating the non-uniform topography of the alginate sheets as a result of direct contact with $CaCl_2$ solution and adjusting the crosslinking time by changing the concentration of the $CaCl_2$ solution.

After preparing the alginate sheet, developing printing codes, and choosing an optimum formulation of the bio-ink, different patterns were printed on the substrate. The most significant challenge in this process was trapping the printed pattern inside a half-crosslinked alginate sheet to provide a strong attachment between the printed patterns to the alginate sheet. Therefore, the prolonged crosslinking method played a significant role

in providing control over the crosslinking procedure. The various volume of alginate solution was prepared and crosslinked with 1.5% (w/v) agarose sheet containing 4% (w/v) $CaCl_2$ the solution to monitor the crosslinking velocity (mm/min). After exposing the 4% (w/v) alginate solution to the agarose sheet for 20 minutes, 2 mm of the alginate solution was crosslinked to provide sufficient support and to maintain the printed pattern on the alginate sheet. Partially crosslinking the alginate solution is necessary for forming layers of alginate sheets from the bottom to the top of the solution. The layers of alginate sheets tolerate the weight of the bio-ink and prevent any deformations of the bio-ink after printing on alginate and eliminate sinking the pattern to unwanted levels of alginate substrate. After printing the pattern, the sample was crosslinked for 20 more minutes to be fully crosslinked. During the next 20 minutes, printed patterns and the alginate sheet were crosslinked in parallel.

4.2.10. Electrical Conductivity Measurement

The electrical conductivity of the rectangular patterns was measured using four conductive copper rods with a 1 mm diameter. The distance between every two sets of rods plays an important role in keeping the consistency of the measurement. AutoCAD was used to develop a drawing and the sample was later laser cute to form the mould.

Besides, a spiral pattern was chosen to monitor the variations of electrical resistance of different fibre diameters, lengths, and printing patterns on alginate sheets. In addition, electrically conductive bio-ink was printed in three different patterns on alginate sheets to study the effect of printing patterns on the electrical resistance of the samples.

4.2.11. Tensile Test

Mechanical properties of the serpentine pattern on alginate sheets were measured using MTI Electromechanical Universal Testing Machine Systems, with a 1kN load cell. In order to secure the alginate sheet inside the grips, samples were cut into rectangular shapes (10×5 cm) and glued to sandpapers from two ends and then sandpapers were fixed inside two grips. This method successfully prevents any undesired ruptures in prepared samples as a result of direct contact of the alginate sheets and grips during the measurement. For the cyclic tensile test, the samples were stretched with a linear velocity of 1mm/min and the test was repeated for 7 cycles with a maximum strain of 10%. The electrical conductivity of the printed pattern on the alginate sheets was measured after each cycle and during the first cycle using a multimeter.

4.3.Results and Discussion

4.3.1. Hydrogel Preparation

Partially exfoliated graphite crystals were used in this research. The exfoliation process involves expanding the graphite platelets up to hundreds of times in order to eliminate aggregation and improve the lubricity and flexibility of this material [108]. Partially exfoliated graphite crystals are not stable in aqueous solutions. This is due to the low energy barrier of the van der Waals forces in the graphite crystals, which translates to the sedimentation and aggregation of graphene in water [144]. In order to prevent sedimentation and produce sufficiently large energy barriers between the graphene layers, covalent or noncovalent bonds between the layers are necessary [145]. Surface modification of graphene is the most popular approach for adding the aforementioned bonds and exfoliating graphene in water [146]. Chemical oxidation is commonly used to form the necessary covalent bonds to produce graphene oxide, which is readily dispersible

in water in strongly alkaline conditions [147-148]. However, the carboxylic groups of the graphene oxide produce an acidic pH, which results in restacking and the precipitation of the graphene interlayers. In order to overcome the van der Waals forces of graphene oxide, electrostatic repulsion or steric hindrance is necessary. The addition of Laponite to graphene oxide results in electrostatic repulsion, which translates to stable aqueous graphene oxide [149]. Laponite is a platelet that is 25 nm in diameter and 1 nm in height and has positive charges on its edges and negative charges on its surface [150]. The negative charge density of the surface is due to the isomorphic substitution of Mg^{2+} by Li^{+} in the crystal lattice and imparts charge repulsion. Accordingly, Laponite shows a remarkable swelling ratio in water [151-152]. This unique replacement reaction and the charge distribution give Laponite the ability to interact electrostatically with both anionic and cationic polymers and to modify their rheological properties. Laponite adopts a stable colloid form in water and provides an alkaline pH which improves the stable dispersion of graphene oxide [153].

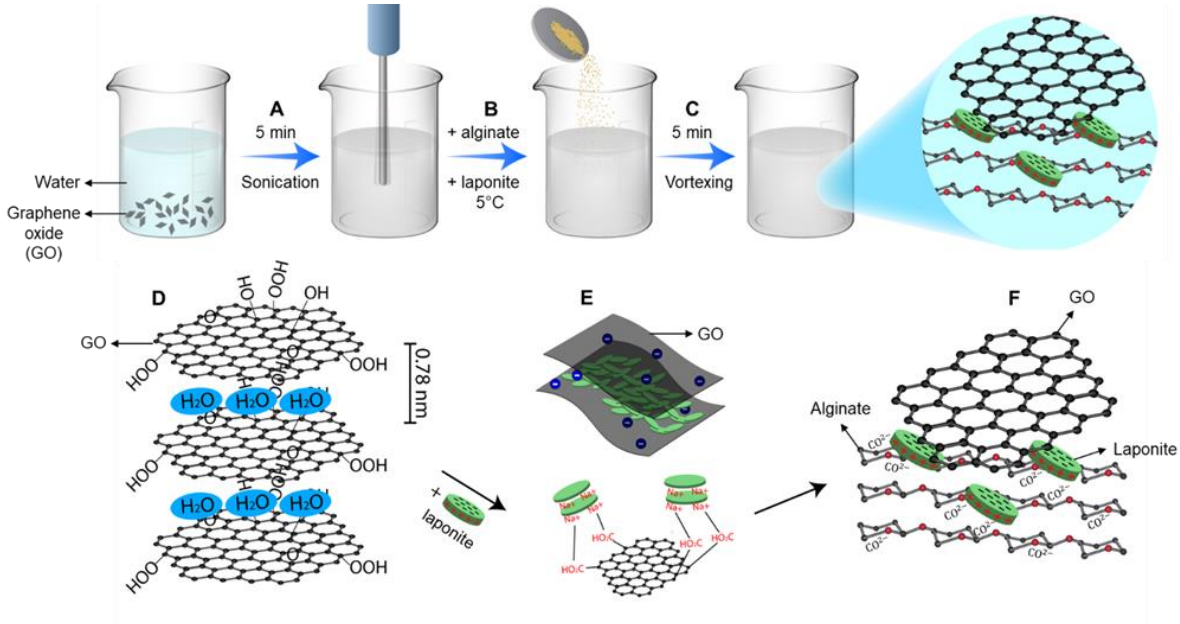

Figure 4.1. Schematic of the fabrication process. A) preparation of a uniform colloid from 3 and 5 mg/ml graphene oxide in deionized water. B) Addition of alginate at room temperature and Laponite at 4°C. C) Formation of a viscose nanocomposite hydrogel by vortexing. D) Macromolecular structure of graphene oxide dispersions in water, E) Electrostatic interactions of graphene oxide and Laponite, F) Molecular interactions of and alginate/Laponite/graphene oxide.

In this study, the aqueous suspension of graphene oxide was prepared by, first, dispersing 5 and 3 mg/ml graphene oxide in deionized water and then sonicating the dispersion for 5 minutes to form a uniform colloid, as shown in Figure 4.1 A. The individual concentration for each material was chosen based on desired mechanical properties to achieve a high shape fidelity of the printed pattern, desired cell adhesion, electrical conductivity, and flexibility based on literature [154-157]. Additionally, final concentrations were chosen based on desired chemical, rheological, and physical properties of the hydrogel for developing shear-thinning electro-conductive soft electronics. As observed in the schematic of the sample preparation, Figure 4.1 B after the very gradual addition of 0.5% (w/v) alginate and vortexing the solution to dissolve all of the particles, 6% (w/v) Laponite was added to the 4°C solutions of alginate/graphene oxide and vortexed vigorously for 5 minutes to form a final gel, as shown in Figure 4.1 C. The molecular interactions of graphene oxide in deionized water are also shown in Figure 4.1 D. The addition of Laponite prevents the aggregation of graphene oxide in water and improves the stability of the colloid. Due to the charge repulsion between Laponite platelets, the laponite particles on the graphene plates prevent the platelets from aggregating as shown in Figure 4.1 E. Additionally, the electrostatic interactions between the negatively charged alginate and the positive charges on the Laponite nanoplatelets result in the crosslinking of the hydrogel nanocomposite and improve the mechanical properties of the hydrogel bio-ink.

4.4. Chemical and physical characterization

4.4.1. Zeta potential

Zeta potential analysis of the prepared hydrogels provides insight in discussing the electrostatic interactions of the nanocomposite hydrogels. According to the literature, the zeta potential of the Laponite is consistently negative in both acidic and basic pH range [81]. The zeta potential of the Laponite which was reported to be around -40 mV, decreases to around -50 mV in the presence of the carboxylate groups of the alginate [61]. Furthermore, adding 3 mg/ml of graphene oxide made the zeta potential even more negative, as illustrated in Figure 4.2 A. In addition, by increasing the concentration of the graphene oxide from 3 to 5 mg/ml, the zeta potential of the nanocomposite hydrogel slightly decreased to the value of -70 mV. This non-significant change might be attributed to the existence of negatively charged functional groups, such as carboxyl and hydroxyl anions, in the structure of graphene oxide. The negatively charged functional groups of the graphene oxide have repulsive interactions with the carboxylate groups of the alginate and negative charges of the Laponite nanoplatelets is shifted the zeta potential to a more negative value [158].

4.4.2. Fourier-Transform Infrared Spectroscopy

Figure 4.2 B depicts the FTIR spectra of the alginate/Laponite and the nanocomposite hydrogel network with 3 and 5 mg/ml graphene oxide. The incorporation of graphene oxide into Laponite/alginate structure added specific characteristic peaks to the FTIR spectra of Laponite/alginate at 1040 cm^{-1}, which can be attributed to the stretching vibration of the C–O (alkoxy) group in graphene oxide spectra [159]. As shown in Figure 4.2 B, 1040 cm^{-1} peak became sharper in the hydrogel with a graphene oxide

concentration of 5 mg/ml. Similar to observations in the literature, characteristic peaks for graphene oxide representing the stretching vibration of O – H and C = O in COOH appear at 2349 and 1734 cm^{-1}respectively [160]. Additionally, the characteristic peak of the carboxyl group's C − O stretching vibration is shifted to the upper wavelengths, so that just one peak is observed at 1468cm^{-1}. This shift may be attributed to the interaction of Laponite and graphene oxide and has a low intensity in the spectra of Laponite/alginate hydrogel nanocomposites. Moreover, a band at 1414 cm^{-1}correspond to asymmetric COO^{-} stretching vibrations of the carboxylate group of structure and is observed in all three spectra [161]. Furthermore, asymmetric stretching vibration of the C − O bond of carboxylate groups in the structure of the pure alginate shows itself as a small peak at 1405 cm^{-1}, [162] while C − O stretching mode of the alginate/Laponite hydrogel backbone is observed as two peaks at 1298 and 951 cm^{-1} [163]. Since alginate (0.5 (w/v)% of gel) is a minor component of the current nanocomposite hydrogel, some of the alginate's characteristic peaks overlap with the intense peaks of the Laponite. The characteristic peak of the Laponite is observed at 1005 cm^{-1}, which is related to the Si − O stretching of its structure [164]. Moreover, the peak at observed at 648 cm^{-1} correspond to the vibration of the Mg − O bond of Laponite [165]. Similar to alginate, this peak is also not clear due to structural electrostatic interaction between Laponite and graphene oxide. As observed in Figure 4.2 B, all of the samples had peaked at 1625 cm^{-1} . This peak is due to the bending of the O – H bond found in Laponite's, alginate's, and graphene oxide's. In addition, there is another characteristic peak for Laponite which appears between 3700 and 3000 cm^{-1} which is due to the overlap of stretching hydroxyl groups in Si – OH and Mg

– OH bands [166]. This peak, which basically appears at 3600 and 3200 cm^{-1}, overlaps with the structural O – H bonds of alginate.

4.4.3. 2.2.3. X-Ray Diffraction

The XRD analysis was carried out to prove the presence of graphene oxide. Nanosheets in the structure of the dried Laponite/alginate hydrogel. As depicted in Figure 4.2 C Laponite shows a major peak at 2θ ~20.1°, which corresponds to (100) crystallographic plane with crystal plan spacing of around 14Å. Laponite also exhibits some other peaks at 2θ ~,27.4° and 35.1° relating to the (005) and (110) crystallographic planes, respectively [167]. Moreover, the XRD pattern of Laponite/alginate hydrogels irrespective of graphene oxide incorporation, shows a weak and broad diffraction peak at around 17.32°, indicating a rather amorphous structure for alginate [168]. Graphene oxide with a layered nanostructure also shows the characteristic small peak at 2θ ~12° relating to the diffraction of the (001) plane and spacing obtained from Bragg equations as 10.06 Å. The weak intensity of the diffraction peak of (001) for graphene oxide showed the exfoliation of graphene layers in the structure of the nanocomposite hydrogel, [169] so that at a lower concentration of 3 mg/ml there is no peak for (001) plane of the graphene oxide.

4.4.4. Scanning Electron Microscopy

Figure 4.2 D-F demonstrates an SEM image of the fabricated Laponite/alginate bio-ink hydrogel with different concentrations of graphene oxide (0, 3, 5 mg/ml). The pore size of the fabricated hydrogels was analyzed using Image J software. All of the hydrogel-based bio-inks had porous structures and the porosity of the structures increased from 7.5 ± 2.74 μm to 57.62 ± 12.76 μm with an increase in graphene oxide from 0 to 5 mg/ml. The intrinsic porosity of the Laponite/alginate structure is due to the Laponite, which has a large surface

area, forms a dense house-of-cards structure. Additionally, the alginate gives the hydrogel the ability to absorb water, which leads to additional porosities after freeze-drying. Moreover, it is clear that all hydrogel samples exhibit a layered microstructure which indicates the presence of the Laponite as a major phase of the hydrogel. However, as the concentration of the incorporated graphene oxide increases, so does the pore size. This phenomenon may be attributed to the self-organization and electrostatic interaction between positive charge Laponite and negative surface charged graphene oxide layers [148].

4.4.5. Mechanical properties of the bio-ink

Unique isomorphic substitution of Laponite can enhance the shear-thinning properties, plastic behaviours, and high elastic response of hydrogel composites [170]. Specifically, Laponite was shown to significantly improve the shear-thinning properties of alginate and to form a stable colloid with graphene oxide in water [148,61]. This study presents the rheological optimization of Laponite/alginate/Graphene oxide bio-inks for 3D extrusion-based bioprinting. The mechanical properties of an alginate/Laponite bio-ink with different concentrations of graphene oxide were studied.

The electrostatic interactions between Laponite and graphene oxide lead to a stable colloid [43]. Laponite forms an alkaline environment after dissolving in water, and electrostatic repulsion keeps the Laponite platelets dispersed [153]. Graphene oxide, however, has an acidic pH in water, which could decompose the Laponite hydrogel [81]. The viscosity of Laponite decreases under shear stress and recovers after removing the force as shown in Figure 4.2 I. The rheological measurement aims to optimize the graphene oxide concentrations to form a mechanically robust yet extrudable bio-ink. Accordingly,

Young's modulus of bio-inks with different concentrations of graphene oxide, 0, 3, and 5 (mg/ml), were measured to study the effects of graphene oxide on mechanical stiffness. The compressive modulus of bio-inks in the present study was found to be similar to those reported in the literature for alginate/Laponite and graphene oxide/GelMA. For instance, Avery et.al. reported that the addition of Laponite to alginate significantly amplified Young's modulus from 2 to 15 kPa [150]. Based on the literature, Young's modulus increased from 2 to 7 kPa when reduced graphene oxide was added to GelMA and this trend continued until adding 3 mg/ml of alginate's reduced graphene oxide produced a young's modulus of 22 kPa. Interestingly, as reported in the literature, increasing the concentration of the reduced graphene oxide leads to improvement in the mechanical properties of the GelMA hydrogel from a reduction in crosslinking density [171].

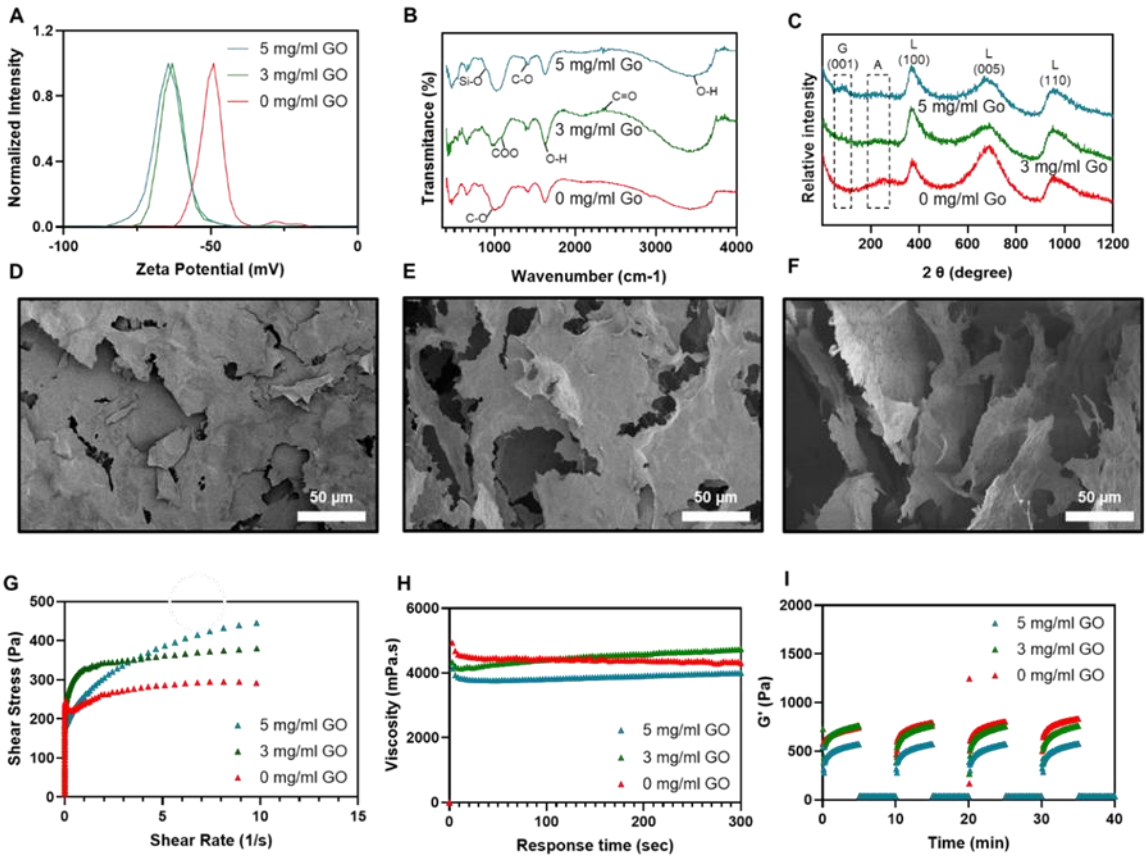

Figure 4.2. Chemical, structural, and rheological characterization. A) Zeta potential of

alginate/Laponite with various concentrations of graphene oxide (Go) : 0, 3, and 5 mg/ml; the inset plot depicts the zeta potential of alginate/Laponite as a function of the graphene oxide concentrations. B) FTIR spectra of alginate/Laponite hydrogels with various concentrations of graphene oxide. C) XRD spectrum of alginate/Laponite with different concentrations of graphene oxide. D-F) SEM images of alginate/Laponite bio-ink with various concentrations of graphene oxide: 0, 3, and 5 mg/ml, respectively. The overall porosity of the gel increased with increasing the concentration of graphene oxide. G) Shear stress as a function of shear rate was plotted to indicate a negligible effect of adding 3 and 5 mg/ml graphene oxide. H) Plot of the viscosity versus response time under constant shear rate was shown a minor decrease by cooperating 5 mg/ml graphene oxide. I) Elastic recovery of the bio-inks was observed by imposing alginate/Laponite with 3 and 5 mg/ml graphene oxide to 100% and 1% oscillatory strain during four cycles over 40 minutes while monitoring storage modulus, results indicate a complete elastic recovery and insignificant effect of graphene oxide on alginate/Laponite bio-ink.

In addition, the results from these experiments show a 9 kPa increase after adding 5 mg/ml graphene oxide to the alginate/Laponite hydrogel. Laponite has been reported to improve the shear-thinning properties of alginate [125]. In order to study the shear-thinning properties of the electro-conductive bio-inks, a rheological analysis was performed under various shear stress (Pa) as a function of shear rate (1/s). Shear-thinning is a well-known property of Laponite dispersions. This shear thinning is mainly due to the electrostatic repulsion of Laponite's charged groups forcing the nanoplatelets to form an extended configuration. Simultaneously, the shielding effect of the electrostatic interactions allows the nanoplatelets to fold up, assuming a more compact conformation [172].

As observed in Figure 4.2 G, all of the bio-inks formulations show shear-thinning properties and provide a suitable amount of control over the extrusion process. This study did not show a significant difference between the formulation with 3 or 5 mg/ml of graphene oxide. All compositions of the bio-ink showed a sharp increase in shear stress at low shear rates before reaching a plateau at a high shear rate. This trend suggests that manufactured bio-inks inherit the yield-stress behaviour and rheological properties of

Laponite. According to the literature, adding alginate, PEGDA, gelatin, PNiPAM, chitosan, and polyacrylamide does not have a substantial effect on the mechanical properties of the Laponite [150,169,41,173].

The shear-thinning properties of different formulations of the bio-ink can be also determined by measuring viscosity under constant shear. The viscosity increased with the addition of 3 mg/ml graphene oxide to the alginate/Laponite bio-inks. This increased viscosity was attributed to the electrostatic interactions between negatively charged graphene oxide and positively charged Laponite as previously mentioned. Adding 3 mg/ml of graphene oxide to alginate/Laponite bio-inks improved the mechanical stiffness and young's modulus of the bio-inks. However, the addition of a higher concentration of graphene oxide did not follow a similar trend. Higher concentrations of graphene oxide led to a decrease in the viscosity of the bio-inks under constant shear rate. As reported in the literature, this trend may be due to the effect of lower pH on the viscosity of the Laponite [174].

In order to characterize the mechanical integrity of the bio-ink upon printing, recovery of the nanocomposite hydrogel was measured from high (100% oscillatory strain) to low strain (1% oscillatory strain) conditions. Previously, Laponite and gelatin showed a rapid elastic recovery in less than 10 seconds [79]. As illustrated in Figure 4.2 I, the storage modulus of the bio-ink decreased at 100% strain and illustrated liquid-like behaviour but recovered immediately after removal of the strain and resumed its solid-like integrity. This rheological test was carried out to compare the effect of in addition to various concertation of graphene oxide on the elastic recovery of the bio-inks. Results indicated that the storage modulus was not influenced by increasing the concentration of graphene oxide. Such rapid

elastic recovery prevents bio-ink flow after printing and maintains the cylindrical shape of the fibres. These results illustrate the fast elastic recovery of the bio-ink at high and low oscillatory strain after four cycles over 40 minutes.

4.4.6. Printing and electrical conductivity measurements of the bio-ink

As previously mentioned, bioprinting is gaining popularity for fabricating biomimetic scaffold for tissue engineering and drug screening; however, developing a biocompatible bio-ink remains a challenge [59]. Particular bio-ink requirements vary depending on the final application and various printing methods such as extrusion, injection, stereolithography, and laser. The polymer networks of a bio-ink must maintain their mechanical integrity, which is essential for supporting the stability of printed patterns, without compromising their cellular compatibility. Additionally, the viscosity and shear thinning properties of a bio-ink play a crucial role in determining and optimizing the extrusion technique [64-65]. For instance, the viscosity of a shear-thinning bio-ink decreases under shear stress and allows fluent extrusion and prevents cellular damage during printing [63]. Due to their high swelling ratio, hydrogels demonstrate a very low young's modulus and mechanical stiffness. Therefore, nanoparticles are incorporated into hydrogels to improve their mechanical properties for producing multifunctional nanocomposite hydrogels [175-176]. Additionally, some tissues such as cardiomyocytes and neurons are electrically conductive, making the addition of electrically conductive material to the bio-ink is beneficial [171].

Only a few existing bio-inks are electro-conductive, and even those are slightly electro-conductive [140]. Metallic and ceramic nanoparticle such as gold, silver, and graphene oxide has been added to biocompatible hydrogels to develop electro conductive

bio-inks [59]. Among these nanoparticles, silver and gold have remarkable electro-conductivity. However, they are very expensive and tend to agglomerate and form clusters. Thus, finding cost-effective alternatives with more stable suspension characteristics has gained attention. In this study, we incorporated graphene oxide mixture to enhance the electrical conductivity of the bio-ink, [177] and Laponite was added to the alginate/graphene oxide to maintain the stability of the graphene oxide colloid in water and to improve the mechanical properties of the nanocomposite hydrogel [146].

Figure 4.3 C shows a schematic of the extrusion and fibre formation of different formulations of the alginate/Laponite bio-ink with various concentrations of graphene oxide. Figure 4.3 C (ii-iv) shows the formed filaments of the bio-inks with 0.5% (w/v), 3% (w/v) Laponite, and 0, 3, and 5 mg/ml of graphene oxide, respectively. These bio-inks were unsuitable for extrusion printing due to the low mechanical integrity of the stacked layer, or their inability to form consistent and cylindrical filaments following extrusion.

In figure 4.3 A the bio-ink with 6% (w/v) Laponite generated cylindrical filaments upon extrusion and provided the desired mechanical integrity for the stacked layer, which hinders the deformation of the pattern. Figure 4.3 A shows the printability chart of the different formulations of the bio-ink. The high viscosity of the alginate/Laponite/graphene oxide bio-inks with 9% (w/v) Laponite disrupted extrusion while employing 3% (w/v) Laponite resulted in droplet formation and deformation of the stacked-layer after printing.

Thus, the nanocomposite hydrogels with 0.5% (w/v) alginate, 6% (w/v) Laponite, and 0, 3, and 5 mg/ml graphene oxide were chosen as the optimum formulations of the electro-conductive bio-ink. Feeding pressure and moving nozzle speed are determinative

parameters for controlling the printability, filament formation consistency, and fibre diameter.

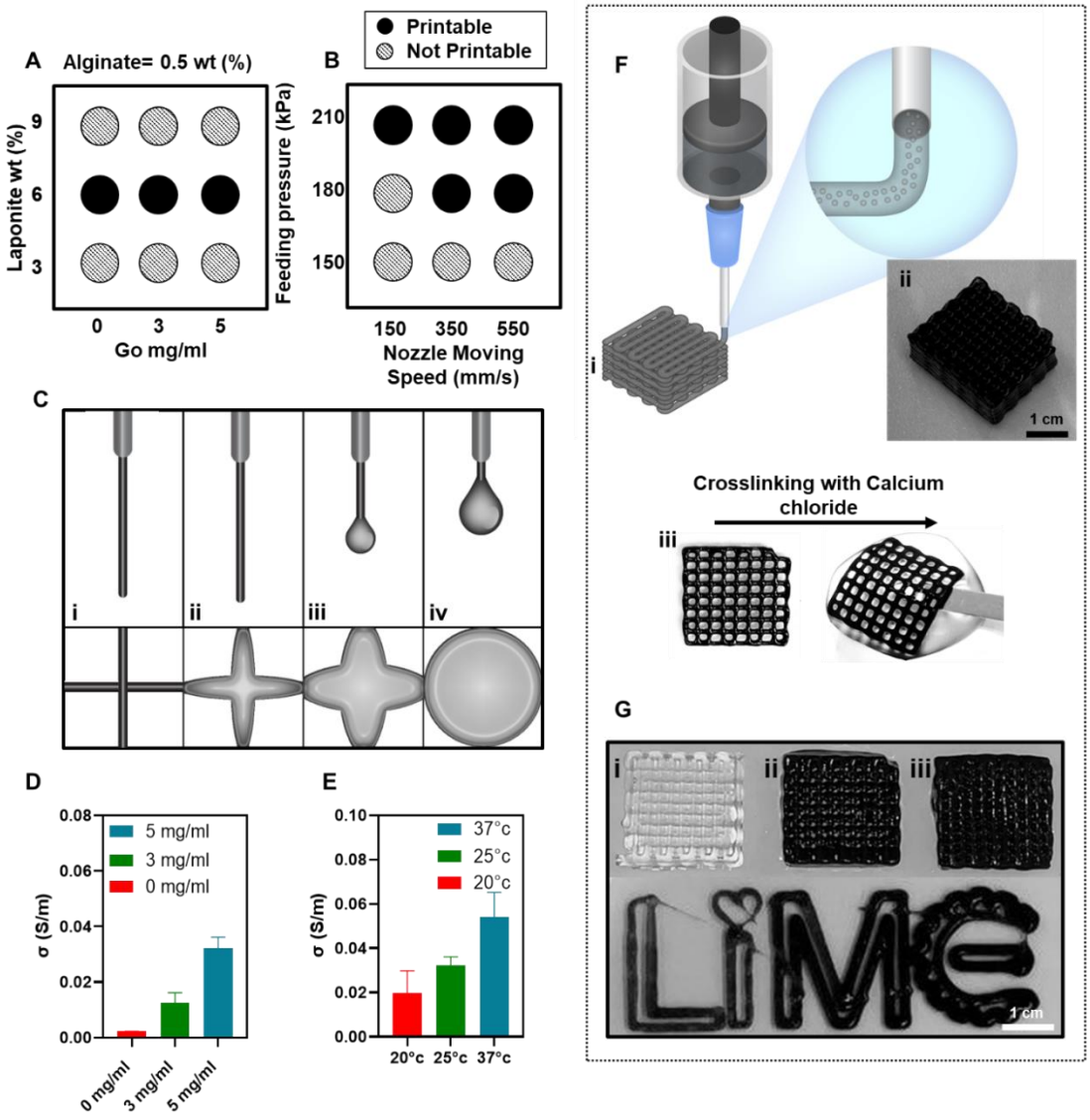

Figure 4.3. Printability and electrical conductivity characterization. A) Printability of 0.5%(w/v) alginate, with 3, 6, and 9%(w/v) Laponite and 0, 3, and 5 mg/ml graphene oxide were measured and 6%(w/v) Laponite and 5mg/ml graphene oxide were chosen as an optimum concentration. B) Optimum printing conditions were evaluated and were investigated as a function of feeding pressure and nozzle moving speed from 150 to 210 kPa and from 150 to 550 mm/s respectively, for the optimum formulation of the bio-ink. 180kPa feeding pressure and 350 mm/s nozzles moving speed were chosen to print the bio-ink at room temperature. C) Extrusion printing schematic of different formulations of the 0.5%(w/v) alginate and 3 mg/ml graphene oxide (Go) with 3, 6, and 9% (w/v) Laponite and the optimized formulation of the bio-ink with 0.5%(w/v) alginate, 6%(w/v) Laponite, and 5 mg/ml graphene oxide illustrated in order from right to the left. D) The electrical

conductivity of alginate/Laponite bio-ink with various concentrations of graphene oxide was measured at room temperature. E) Electrical conductivity of the alginate/Laponite with 5 mg/ml graphene oxide was measured at 20, 25, and 37 degrees Celsius. F) (i) Schematic of extrusion printing, (ii) Electro-conductive 3D scaffold was printed with alginate/Laponite and 5 mg/ml of graphene oxide, (iii) Rectangular single-layer scaffold was crosslinked with 4% $CaCl_2$ over 30 minutes. G) Alginate/Laponite was printed with 0, 3, and 5 mg/ml graphene oxide, the colour of the 5mg/ml graphene oxide was observed to be slightly darker than graphene oxide 3 mg/ml.

Figure 4.3 B illustrates printability with various feeding pressures and nozzle moving speeds. As shown in Figure 4.3 B a feeding pressure of 180 kPa and a 350 (mm/s) nozzle moving speed were chosen as the optimum conditions for extrusion printing in this work. These formulations were unsuitable for extrusion printing due to their low mechanical integrity, the deformation of the stacked-layer or the formation of a droplet instead of the desired, cylindrical filaments following extrusion, as shown in Figure 4.3 C (i). The electrical conductivity of the alginate/Laponite hydrogel with various concentrations of graphene oxide is presented in Figure 4.3 D. By increasing the concentration of the graphene oxide from 0 to 5 mg/ml, the conductivity of the bio-ink increased to 0.03 (s/m). Additionally, the effect of temperature on the electrical conductivity of the bio-ink with 5mg/ml graphene oxide is investigated in Figure 4.3 E. The experiment was conducted in the range of 25 ºC to 37 ºC, which is relevant to the biological applications of these nanocomposite hydrogels as an electro-conductive scaffold. The electrical conductivity of the bio-ink increased with temperature, which is the result of faster electron mobility, ion-migration and consequently charges transfer at 37°C [178]. Figure 4.3F shows a schematic (i) and optical image (ii) of an extrusion 3D printed cubical pattern with the optimum formulation of the bio-ink. As shown in Figure 4.3 F (iii), the printed pattern was crosslinked with 4% (w/v) $CaCl_2$. In order to form a flexible hydrogel structure, suitable for both tissue engineering and electrical conductor

applications, printed samples were immersed in $CaCl_2$ solution for 30 minutes and then washed with deionized water to remove excess amounts of $CaCl_2$ and to forestall over crosslinking of the printed pattern. Optical images of the 3D printed cubic patterns from 0.5 (w/v) alginate, 6 (w/v) Laponite and 0 (i), 3 (ii), and 5 (iii) mg/ml graphene oxide show the printability of different formulations of the bio-ink, Figure 4.3 G.

A polystyrene mould was designed and fabricated to maintain the consistency of measuring the electrical resistance of the printed patterns. Four copper rods were fixed inside the nonconductive lid and were connected to a multimeter. Patterns were crosslinked and placed inside the mould to measure the resistance of the samples. Figure 4.4A shows a rectangular printed pattern inside the mould. Rectangular patterns were printed with various fibre diameters including, 0.5, 1, and 2 mm with different spacing between fibres, including, 1, 3, and 5 mm, to compare the effect of geometry on the electrical resistance of the printed patterns. Figure 4.4 A shows a rectangular pattern with 2 mm (ii), 1 mm (iii), and 0.5 mm fibre diameters (iv), and 3 mm spacing between fibres. 1 mm, 2 mm, and 3 mm spacing between fibres, and 1 mm fibre diameters are shown in Figure 4.4 A (v), (iii), and (vi) respectively.

Various fibre dimeters were printed in order to show the adaptability of the bio-ink for printing and demonstrate the possibility of extrusion printing of narrow lines. This was accomplished by adjusting the feeding pressure. As shown in Figure 4.4 B, by decreasing the feeding pressure from 210 to 150 kPa the diameter of the fibres was reduced to an average of 200 µm. However, decreasing the nozzle moving speed results in an increase of the fibre's diameter to 900 µm, as shown in Figure 4.4 C. A wide range of fibre diameters

was achieved by changing the printing parameter which shows rebut control and adaptability of the printing process with this bio-ink.

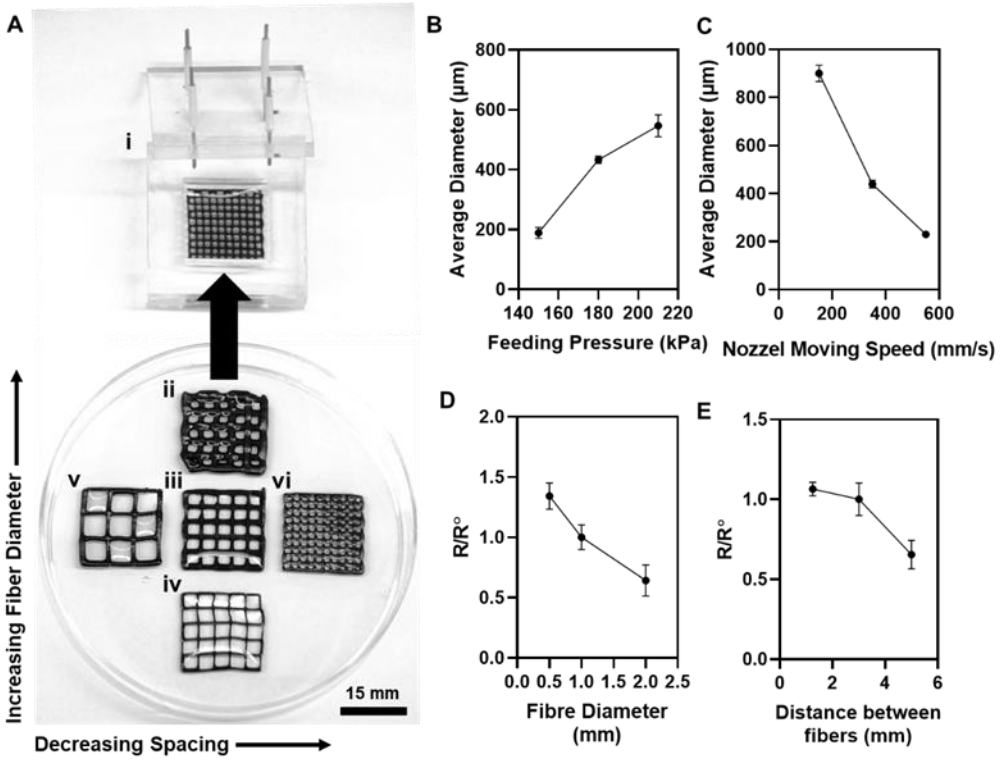

Figure 4.4. Reproducibility of stacked-layer of printed filaments. A) Optical images of crosslinked rectangular patterns and (i) a polystyrene mould with four cuppers rode which was used to measure the electrical resistance of the printed pattern. Optical images of printed rectangular patterns with 2mm (ii), 1mm (iii), and 0.5 mm (iv) fiber diameter, with 5 mm (v), 3 mm (iii), and 1 mm (vi) distance between fibers. The average diameter of alginate/Laponite bio-ink with 5 mg/ml graphene oxide was investigated as a function of B) feeding pressure and C) nozzle moving speed. The average diameter of the pattern illustrated an increasing trend by increasing the feeding pressure and reducing nozzle speed. The electrical conductivity of the printed pattern was measured as a function of D) fibre diameter, and E) spacing between fibres. The electrical resistance of the rectangular printed patterns with 0.5 and 2 mm fibre diameter and 1 and 5 mm distance between fibres (R) was monitored and compared with the electrical resistance of a sample with 1mm fibre diameter and 3mm distance between fibres (R_0). By increasing fibre diameter and distance between fibres electrical conductivity of the printed patterns decreased.

The electrical resistance of the various patterns was measured (R) and compared with the initial pattern, which was chosen to be a rectangular pattern with a 1 mm fibre diameter and a 3 mm fibre distancing (R_0). The electrical resistance of different fibre diameters and spacing between fibres were measured and compared with the electrical

resistance of the initial sample. As shown in Figure 4.4 D, increasing the fibre diameter from 0.5 to 2 mm results in a decrease in the electrical resistance and an increase in the conductivity of the pattern, which is due to the existence of a wider channel for transferring ions and electrons in a rectangular pattern. On the other hand, reducing fibre spacing leads to an increase in the electrical resistance and a decrease in the electrical conductivity of the pattern. Ions are responsible for transferring the electrical current and introducing more branches to the rectangular pattern results in spreading ions into more channels and weaken the current in each filament. Consequently, the adaptability of the bio-ink for printing provides more control over the electrical characteristics.

4.3.7. Design and fabrication of the flexible conductor on alginate substrate

In this work, a new technique was developed for ensuring the adhesion of the printed conductor to the surface of the alginate sheet. The alginate was employed to fabricate a flexible, biodegradable, and biocompatible substrate. Alginate is an anionic polymer that is naturally extracted from brown seaweed [121]. Alginate has found various applications in wound healing, controlled release, targeted drug delivery, and tissue engineering due to its biocompatibility, swelling capacity, sol-gel transition, mechanical stability, and viscoelastic properties [179].

Due to its favourable properties, alginate was chosen to produce a flexible substrate. Fabrication of the alginate substrate improves the mechanical stability of the conductor and extends the bioinks use to targeted drug delivery and wound healing applications. The fabrication ease and repeatability of the process contrasts with the challenges associated with other techniques. Extrusion printing is the strategy we employed to print a 3D complex

conductor on the alginate substrate. An electro-conductive bio-ink has been employed to print patterns on the alginate substrate.

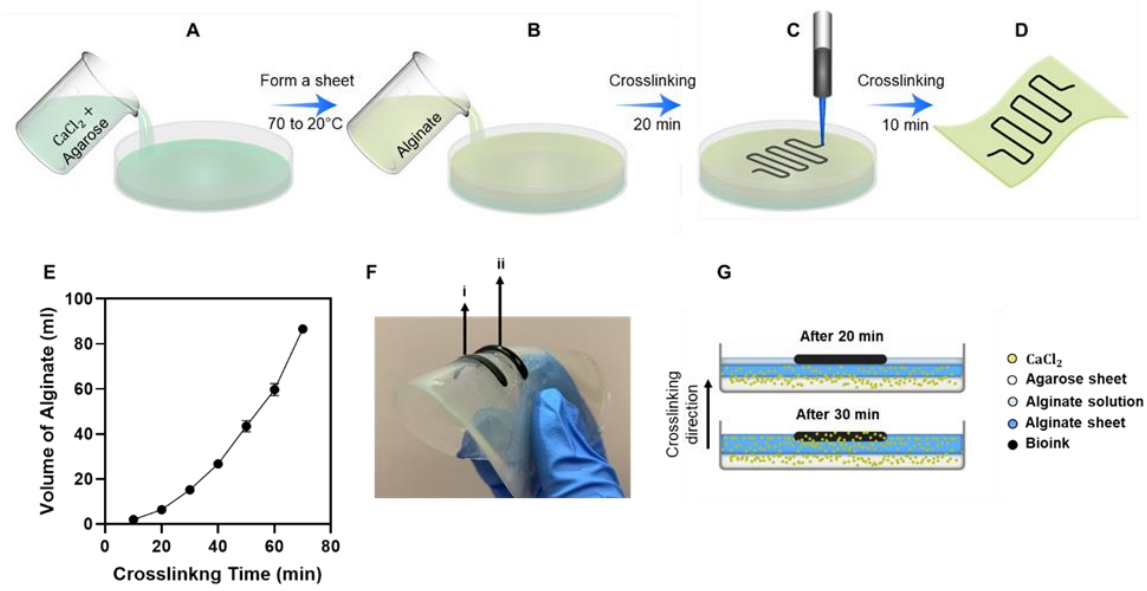

Figure 4.5. Schematic of the fabrication process. A) Preparation of agarose sheet with 4% (w/v) $CaCl_2$. B) Spreading alginate solution at the top of the agarose sheet for the slow diffusion of $CaCl_2$ from the agarose sheet into the alginate for 20 minutes. C) Printing electrical conductive pattern on alginate sheet which was formed inside the alginate solution during the 20 minutes of crosslinking. D) Parallel crosslinking of the alginate solution and bio-ink for 10 minutes to form the final substrate. E) Crosslinking profile of various volumes of alginate solution was measured to find the optimum time for crosslinking of the alginate substrate in a 100 mm petri dish. F) Optical image of printed bio-ink on alginate substrate after 20 minutes (i), and 30 minutes (ii) of crosslinking. G) Schematic of crosslinking process of the alginate substrate and bio-ink from bottom to the top illustrates the migration of Ca^{2+} ions from agarose sheet to different levels of alginate over time.

This conductive bio-ink consists of Laponite, alginate, and graphene oxide to maintain the mechanical integrity of bio-ink after printing, improve viscoelasticity, and create electrical conductivity. This nanocomposite hydrogel is biocompatible and has the requisite swelling capacity, good electrical conductivity, and viscoelastic properties necessary for practical applications. In order to fabricate the alginate substrate, 1.5% (w/v) agarose solution was added to 4% (w/v) of $CaCl_2$ and heated to 70°C to dissolve the agarose. The solution was subsequently cooled to room temperature to form a sheet in a 100 mm

petri dish, Figure 4.5 A. 4% (w/v) alginate solution was added to the top of the agarose sheet, as shown in Figure 4.5 B and crosslinked for 20 minutes. Bio-ink was printed on the alginate solution and on top of the crosslinked alginate layer to support and fix the printed pattern, as shown in Figure 4.5 C. Crosslinking continued for 10 minutes to fully ensure the attachment of the printed pattern to the alginate sheet by forming covalent bonds between calcium ions and alginate, [180] Figure 4.5 D. The optimum crosslinking time of 15 ml, alginate 4% (w/v) with 4% (w/v) of $CaCl_2$ was calculated using Figure 4.5 E. As observed in Figure 4.5 F, bio-ink was printed on the alginate solution after 20 (i) and 30 (ii) minutes of crosslinking of the alginate sheet. Samples (ii) did not show sufficient attachments between the bio-ink and alginate sheet and the pattern piled off after the first round of stretching. As shown in Figure 4.5 G the flexible fibre was printed on the solid surface of the half-crosslinked alginate solution. The fibre was trapped inside the alginate solution and crosslinked in parallel with the solution. This method provided a strong attachment between the alginate sheet and the flexible fibre. This flexible pattern remained stable on the alginate sheet even after 10 rounds of stretching.

The functionality of an elastic conductor relies on its ability to maintain its electrical conductivity under various loading conditions such as: stretching, as shown in Figure 4.6 A and bending Figure 4.6 F. The elastic printed conductor on the alginate sheet illustrated outstanding mechanical stretchability without any observable cracking or detachments from the thin alginate substrate, observed in Figure 4.6 B. As illustrated in Figure 4.6 C, the negligible increases in electrical resistance of the printed pattern after each cycle of force application and removal indicate the exceptional electrical conductivity recovery of the material. The electrical resistance of the flexible conductor was monitored over the first

one-minute cycle of applying 10% strain. Results indicate a steady increase and recovery of the electrical resistance by reducing the strain to 0%. Results from Figure 4.6 D indicate the significant elastic recovery and sustainable electrical conductivity of the printed conductor and illustrate the strong adhesion of the conductor to the alginate substrate. Such unique structural features of the flexible conductor result in developing durable elastic conductors for biomedical application. To further characterize the physical properties and realize the excellent performance of the flexible conductor, electrical resistance was observed at different loading conditions.

As shown in the schematic, Figure 4.6 A, sheets of alginate were glued to two-piece of garnet sandpapers from two ends and the sandpapers were fixed inside two grips of the tensile machine. This platform eliminated any direct contact between the alginate sheets and grips to forestall unwanted breakage of the substrate. A 10 kN% load was applied to each sample to stretch them by 10 % of their original length. This experiment was repeated for 7 cycles with a rate of 1 cycle/min to investigate the elastic recovery of the conductor, Figure 4.6 B. The stress-strain curves indicated slight variations after the second cycle; however, elastic recovery remained intact after 7 cycles. We also measured the electrical resistance after each cycle to illustrate the durability of the conductor. Results from Figure 4.6 C indicated no significant differences in the electrical resistance of a sample after each cycle. Figure 4.6 D reveals the variations in electrical resistance during and after each cycle, which were measured to illustrate the full recovery of the electrical conductivity of each sample at the end of the cycle. After removing the force from each sample, no significant deformation was observed, and the electrical resistance of the stretched sample recovered to the resistance of the unstretched sample.

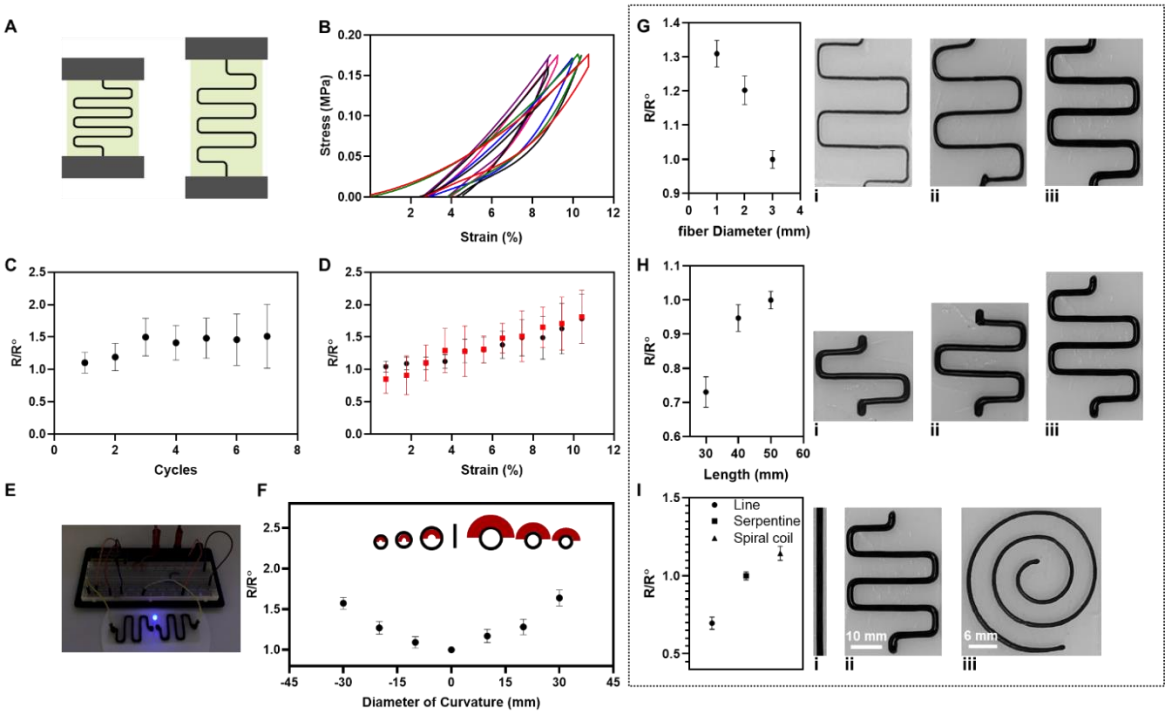

Figure 4.6. Elasticity, flexibility, and electrical resistance. A) Schematic of the setup used for stretching the sample, measuring electrical resistance, and monitoring stress as a function of strain to measure the tensile properties and electrical conductivity of the sample at different cycles. B) The sample was stretched by a maximum of 10% of its original length and recovered with a rate of 1 cycle/minute and then released to its original length, this process repeated over seven cycles to report more than 70% stress recovery after each stretch. C) The effect of the cyclic load was monitored by measuring the electrical resistance of seven cycles after each stretch (R) was compared to the electrical resistance of the upstretched sample (R_0), cyclic resistance measurement shows an insignificant increase in electrical resistivity. D) The sample was stretched by 10% of the original length in a cycle and the electrical residence was measured by exposing the sample to 1-10% strain to monitor a complete recovery of the sample after removing the load (Red: applying the strain, black: removing the strain). E) The optical image of conductivity properties of the flexible conductor was tested by a 3V LED bulb experiment. F) Schematic and diagram of a printed pattern of the bio-ink on alginate sheets, samples were wrapped around a cylindrical mould with various curvature diameter to measure the electrical resistance of the printed bio-ink after cyclic load (R) to initial electrical resistance (R_0), reducing the curvature diameter results in increasing the resistivity, and, consequently, decreasing the electrical conductivity of the printed samples. The electrical resistance of the serpentine pattern was investigated as a function of various G) fibre diameter, and H) fibre lengths, variations of the resistance indicate an increasing trend by decreasing the fibre diameter and shows an increase by shortening the serpentine pattern. I) switching the printed pattern to a straight line and a spiral design introduces a change in the resistivity of the samples and reveals repeatability of the fabrication process.

The elasticity and durability of the conductor were confirmed by no significant changes in the electrical resistance within the seven cycles. In addition, the conductivity of flexible conductors is shown in Figure 4.6 E. We also studied the repeatability of the fabrication process by investigating the electrical resistance of the triplicated samples. In order to investigate the durability of the conductor, alginate sheet samples were bent to a maximum curvature diameter of 30 mm. These results represent the ability of this flexible conductor to provide conformal contact with skin and accommodate natural motions without significant restraint in mechanical properties and electro-conductivity [181]. Figure 4.6 F illustrates the flexibility and durability of the conductor on the alginate sheet. Samples were wrapped around a curved shape and the electrical resistance of the sample was investigated at that position. Data from Figure 4.6 F shows a slight increase of the electrical resistance after bending each sample with various diameters including 10, 20, and 30 mm. Although results showed a slight increase of the electrical resistance by increasing the curvature diameter, bending did not have a noticeable effect on the electrical conductivity of the samples. Variations in electrical resistance were measured for various fibre diameters, lengths, and patterns. The electrical resistance of a serpentine pattern with 50 mm length and 3mm fibre diameter was measured as an initial value (R_0) and the electrical resistance of samples with 30, 40 mm length and 1, 2 mm fibre diameter were measured as (R) and compared with the initial value. Figure 4.6 G shows that due to the wide channel for transferring the ions from one end to the other side of the pattern, electrical resistance was reduced when the fibre diameter increased from 1 to 3 mm. Similarly, the electrical resistance of the printed pattern decreasing when the length of the pattern was also decreased, Figure 4.6 H. The Repeatability of the fabrication process was

also investigated by printing various printed patterns including a straight line, a serpentine, and a spiral pattern, Figure 4.6 I.

4.5.Conclusion

We have successfully fabricated a novel electro-conductive bio-ink for developing soft hydrogel-based electronics. The novel bio-ink is composed of alginate as the base material loaded with Laponite nanoplatelets and graphene oxide. The resulting bio-ink exhibited superior electrical conductivity and viscoelastic properties as compared to pristine alginate. Injectability and shear thinning properties of the bio-ink were evaluated using rheological tests, while the stretchability and durability of the flexible electronics were examined under significant stretching and bending at room temperature. Our results suggest that the addition of graphene oxide to alginate/Laponite bio-ink did not compromise the shear-thinning properties of the bio-ink. As such, the bio-ink was successfully used for creating complex conductive patterns on a hydrogel substrate. The conductive patterns showed consistent electro-conductive properties under 7 cycles of stretching and the reproducibility of the manufacturing process was examined by printing various patterns with different fibre diameters. Overall, the proposed novel bio-ink holds promise for designing implantable microelectronics with mechanical properties that match those of the host tissue and are suitable for accommodating body movement.

Chapter 5

5. Doxorubicin Loaded Shear-thinning Biomaterial for Minimally Invasive Treatment of Brain Tumors

Permeable

The objective of this research is to fabricate and characterize an injectable silicate-based nanocomposite hydrogel for localized drug delivery over an extended period of time. This nanocomposite hydrogel allows for direct injection of the drug into the site of interest followed by prolonged and continuous drug release. This shear-thinning hydrogel prevents premature leakage of the drug or degradation in biological environments and provides a sustainable release. The physical, chemical and rheological properties of this hydrogel are investigated by various experiments to examine the shear-thinning properties and the release behaviour. The results from the previously mentioned analysis indicate the significant effect of varying concentrations of Laponite and the optimized formulation of the nanocomposite hydrogel.

Abstract

Understanding the chemical and morphological characteristics of biomaterials plays a significant role in evaluating their potentials for biomedical applications. Silicate-based nanocomposite hydrogels have gained significant attention due to their unique rheological and morphological properties. Laponite is known for its shear-thinning properties, while gelatin is biocompatible and has a high water-retention capacity. Accordingly, combining these materials results in producing a shear-thinning nanocomposite hydrogel with an outstanding capacity for loading and releasing drugs. The

in situ mechanical strength of this composition, which is a function of the shear-thinning properties of Laponite, prevents degradation after injection and allows for the gradual releases of drugs. However, achieving the optimum formulation of this nanocomposite with high shear-thinning and drug loading capacity is a challenge. Accordingly, various mechanical, chemical and rheological experiments were employed to engineer a high drug loading capacity and constant release profile while maintaining high shear-thinning properties.

5.1.Introduction

Considering the current challenges with the systemic delivery of chemotherapeutic drugs to tumours and the lack of minimally/less invasive local treatment options, there is a pressing need for an effective delivery system that can be injected intratumorally [87]. We aimed to develop an injectable Doxorubicin (DOX) drug delivery system that (i) is safe and biodegradable; (ii) is injectable and contains an embolic agent; and (iii) effectively loads DOX and releases the drug over a prolonged period with predictable release kinetics. Shear-thinning or in-situ gelling hydrogels fulfill the criteria listed above as they are injectable and can readily fill and take the shape of a cavity and provides a good interface between the gel and the cancerous tissue [182]. Additionally, they often have tunable porosity and rheological properties, which allows further control over the release kinetics of drug delivery.

Gelatin is denatured collagen that can be inexpensively obtained from a variety of animal sources. Gelatin retains natural cell-binding motifs, such as RGD, as well as MMP-sensitive degradation sites, which make it suitable for clinical applications [158]. However, unmodified gelatin does not have the necessary shear-thinning properties to serve as an

injectable platform for drug delivery. Accordingly, it needs to be modified with other materials to gain the requisite shear-thinning characteristics that are essential for minimally invasive applications.

Laponite, an electrostatically charged, layered aluminosilicate, has shown efficient loading of ionic molecules and can act as a drug reservoir because of its layered structure [183]. It is an efficient platform for carrying and releasing DOX. Additionally, Laponite can be combined with gelatin to form a stable shear-thinning biomaterial (STB) nanocomposite hydrogel capable of treating hemorrhage and endovascular embolization [184-189]. This STB nanocomposite composed of Laponite and gelatin, first investigated by Gaharwar et al., is an injectable material that recovers its original gel-like consistency after experiencing shear stress similar to the shear stress experienced during injection and is capable of blood clot formation [188-189]. When the Laponite is mixed with gelatin, strong electrostatic interaction between the polymer and Laponite nanoparticle leads to the formation of this robust physically crosslinked hydrogel [190]. If sufficient stress is applied to the material, the bonds between Laponite and gelatin are broken and the material loses its physical strength and becomes viscous and liquidlike, which explains the shear-thinning behaviour mentioned previously.

Here, we developed and tested the previously researched gelatin-Laponite STB as a controlled DOX delivery system for the treatment of glioblastoma multiforme. Developing the STB as a DOX delivery system involved the characterization of its molecular interactions, microstructure, rheological properties, swelling and degradation, and DOX loading and release kinetics.

5.2. Materials and Methods

5.2.1. Materials and Hydrogel Fabrication

STB Formulation: An 18% (w/v) stock solution of type A gelatin from porcine skin (Sigma Aldrich, 300 Bloom, St. Louis, MI) was made in Milli-Q ultrapure water at 40°C, and vortexed to achieve a homogenous solution. A 6% or 9% (w/v) solution of Laponite XLG (BYK Performance Additives) was made in Milli-Q ultrapure water pre-cooled to 4°C to delay gelation while vortexing to produce a homogenous solution. The separate composites were then mixed in their corresponding ratios, diluting the gelatin by a factor of 2 with Milli-Q ultrapure water, and vortexed to make various compositions of the STB. For STBs containing DOX (Sigma Aldrich, St. Louis, MI), a solution of DOX HCl is used to dilute the gelatin solution when mixing the gels and the gels were stored at 37°C for at least 48hr to allow for DOX intercalation within the hydrogel.

5.2.2. Zeta Potential

The STB samples for this test were prepared as previously stated, and reduced in concentration to 0.2 wt% to have a less viscous solution. A Brookehaven BI-ZR3 Zeta Potential Analyzer with a 660nm wavelength laser was used to determine the zeta potential of the samples at room temperature.

5.2.3. X-Ray Diffraction

Nanocomposites were prepared as previously stated. The final concentration of DOX in DOX loaded nanocomposites was 300 µg/g of gel. All samples were freeze-dried in a -80^{o}C freezer for 24 hours and lyophilized for 2 days. The samples were then ground into a powder and analyzed on a PANalytical Empyrean X-Ray Diffractometer at room

temperature with a current of 40 mA and a voltage of 45 kV over the diffraction angle range of 10-90^{o} (2θ).

5.2.4. Scanning Electron Microscopy

Nanocomposites were prepared with varying compositions of gelatin and Laponite, as well as varying concentrations of DOX, and freeze-dried using the method previously stated. The samples were imaged using a Hitachi S-4800 FESEM.

5.2.5. Loading Efficiency

Varying compositions of STB were made in 0.7 g aliquots without DOX and immersed in 7 mL of a 300 µg/mL solution of DOX in 0.1M PBS at pH of 7.4. All samples were stored at 37 ^{o}C and agitated by gentle vortexing at the time of supernatant removal. The encapsulation of DOX by the STB was quantified by analyzing the supernatant DOX concentration with fluorescence spectroscopy. A 480 nm wavelength excitation and a 598 nm emission were used.

5.2.6. Release Study

Varying compositions of STB were made in 0.25g aliquots with 150µg/g DOX and immersed in 1mL of 0.1M phosphate-buffered saline (PBS) at a pH of 7.4. All samples were stored at 37 ^{o}C and agitated by gentle vortexing at the time of supernatant removal. The samples were centrifuged on a mini centrifuge at 2000G for 5 minutes before removing the supernatant. The release of DOX by the STB was quantified by removing the full 1mL of supernatant and analyzing the supernatant with fluorescence spectroscopy. A 480nm wavelength excitation and a 598nm emission were used.

5.2.7. *In Vitro* Anti-Tumor Activity of DOX-Loaded STBs

5.2.7.1. Cell Culture

U87 Human glioblastoma cells were cultured in 25cm^2 (surface area) flasks. High glucose Dulbecco's Modified Eagle Medium (DMEM) supplemented with 10% fetal bovine serum (FBS), 1% penicillin/streptomycin, and 4 µg/mL puromycin was used as the cell media and was changed every other day. The culture was stored at 37 °C with 95% relative humidity and 5% CO_2.

5.2.7.2. Free DOX Cell Viability

96-Well plates (VWR, Radnor, PA) were seeded with 10,000 cells per well and cultured in 0.2mL of media for 24hr. The media was changed and supplemented with 0.1, 1, 10 and 100µg/mL DOX in media. The plates were stored under the same conditions stated above for the cell culture. The cell viability of each condition was determined by using a Presto Blue assay at 24h, 48h, 72h, and 96h.

5.2.7.3. DOX-Loaded STB Treated Cell Viability

24-Well plates (Sarstedt, Numbrecht, Germany) were seeded with 25,000 cells per well and cultured in 1mL of media for 24hr. The cells were then treated with 0.1g samples of DOX-loaded STBs in a 12mm, 12µm pore size cell-culture insert (Millipore Sigma, 12mm diameter, 12µm pore size, Burlington, MA) and the wells were replaced with 0.6mL of fresh media in the well and 0.4mL of fresh media in the insert containing the DOX-loaded STB. The plates were stored under the same conditions stated above for the cell culture. The cell viability of each condition was determined by using a Presto Blue assay at 24h, 48h, 72h, and 96h.

5.2.8. *In Vitro* 3D Anti-Tumor Activity of DOX-Loaded STBs Brain-Tumor-on-a-Chip

5.2.8.1. Materials and Chip Fabrication

5.2.8.1.1. Materials

Polydimethylsiloxane (PDMS) elastomer kits were bought from Ellsworth Adhesives Co., SU-8 100 while its developers were purchased from MicroChem Corp. High glucose Dulbecco's modified eagle medium (DMEM) with L-glutamine, live/dead staining viability kits, fetal bovine serum (FBS), 0.5% trypsin-EDTA, temozolomide, penicillin-streptomycin (Pen Strep, 10000 units/mL penicillin and 10000 µg/mL streptomycin), simvastatin, puromycin dihydrochloride, Dulbecco's phosphate-buffered saline (DPBS), and poly-D-lysine were obtained from Millipore Sigma. Additionally, bovine collagen type 1 (10 mg/mL) and, 10x PBS, 0.5 N NaOH were purchased from Advanced BioMatrix Inc. All the other reagents in this section were of analytical grade.

5.2.8.1.2. Microfluidic device

Glioblastoma-on-chip was previously developed in our lab. A microfluidic device was fabricated using polydimethylsiloxane (PDMS) and bonding it on 25 mm coverslips. The microchannel architecture of the tumour compartment and the delivery side channels were formed by casting PDMS on a SU-8 master mould and baking in an oven at 80°C for 2 hours. Following that, the 5 mm media wells and the 1mm inlets for injecting hydrogel in the tumour compartment were made using biopsy punches. The PDMS piece and the cover slip were plasma treated for the 60s and bonded, followed by baking at 80°C for 30 min. To assure the sterility of the devices and removal of possible PDMS debris, they were rinsed with 70% ethanol twice and 100% ethanol once. The devices were then baked at 80°C for 4 hours in a sterile container to completely remove the ethanol. For the

enhancement of the hydrogel attachment to the microfluidic device, the surface of the tumour compartment was coated with Poly-D-lysine (PDL). A 1mg/mL solution of PDL in DI water was pipetted into the tumour compartment and incubated in a humid incubator at 37°C for 1 hour. The PDL solution was then removed and the microchannels were rinsed with DI water 3 times. To recover PDMS hydrophobicity, the devices were baked at 80°C for 4 hours.

5.2.8.1.3. Glioblastoma-on-a-chip

U87 cells were cultured on a culture plate until they reach 80% confluency. The cells were then trypsinized, centrifuged, and resuspended in fresh culture media at 4°C. The preparation of hydrogel and cell suspension was performed at 4°C. NaOH and 10X PBS were added to a 10mg/mL solution of acidic collagen type 1 to obtain a buffered 8 mg/mL collagen solution. The cell suspension and collagen solutions were mixed and the volume was adjusted by culture media to achieve a solution with a final concentration of 4 mg/mL collagen and a cell density of 1 M cells/mL. The cell/collagen solution was pipetted into the tumour compartment of the microfluidic device and incubated in a humid incubator at 37°C for 45-60 min until full gelation of collagen. Culture media was then added to the wells and the model was incubated overnight until the drug experiments.

5.2.8.1.4. Injection of STB

Injection of STB into the delivery channel of the glioblastoma-on-chip model was performed using a syringe pump at a constant flow rate to assure consistency in the delivery between different devices. STB was loaded in a 3mL syringe and the outlet was connected to a 0.8mm diameter Tygon tube. The flow rate in the syringe pump was set to 100µL/min and pumping was started until a steady flow of STB was observed. The media from one of

the 2 delivery channels was removed and the outlet of the tube was held at the inlet of the microchannel. The flow of STB was continued until the microchannel was uniformly filled and the two side wells were partially loaded with STB. The remaining space in the wells was filled with culture media to maintain the STB hydrated over the period of the experiment.

5.2.8.1.5. Diffusion tests

Diffusion of DOX into the tumour compartment of the glioblastoma-on-chip model was analyzed using free DOX dissolved in DPBS as well as DOX-loaded STB. The model was prepared with cell-free collagen and maintained hydrated with DPBS. For the case of free drugs, a 150mg/mL solution of DOX in DPBS was prepared. The DPBS from one of the delivery channels in the model was removed and replaced with the DOX solution, and live imaging was started immediately using the red channel of a Zeiss microscope. The exposure was set to 20ms, and images were taken every 60s for a period of 100min. The fluorescence intensity was measure in an axis covering a part of the delivery channel and the entire width of the tumour compartment. The measured fluorescence intensity was normalized with the average value in the delivery channel. For the case of DOX-loaded STB, the DPBS was removed from the delivery channel and STB was injected as explained in the previous section. Imaging with the red channel was performed every 4 hours for a total period of 4 days. Fluorescence intensity was measured across the width of the tumour compartment and a part of the delivery channel and it was normalized with the average intensity in the delivery channel.

5.3.Results & Discussion

5.3.1. Hydrogel Fabrication and Chemical Characterization

5.3.1.1. Naming and Formulation

In the present study, a nanocomposite system composed of gelatin and Laponite for the delivery of DOX is developed. Gelatin and Laponite solutions are mixed together to produce a final combined concentration (wt%) with carrying ratios of gelatin: Laponite. The formulations are named based on their final combined concentration, X, and their ratio of Laponite solution, Y, in the NC to produce a name in the form of XNCY, with NC standing for nanocomposite. For example, an STB with 25 parts 9% Laponite solution and 75 parts 9% gelatin solution would be named 9NC25. DOX is loaded into the STB by diluting a higher concentration solution of gelatin down to the desired final concentration with a solution of DOX. Samples containing DOX are named with the mass of loaded drug per gram of STB. For example, 9NC25 loaded with 150µg of DOX per gram of STB is named 9NC25-150. Laponite is a platelet with a negative overall charge and a diameter of 25 nm a height of 1nm. Despite having a negative overall charge, it has positive charges on its edges and negative charges on its surface[150]. The negative charge density on the surface of Laponite is due to the isomorphic substitution of Mg^{2+} by Li^{+}in the crystal lattice [151-152]. The unique replacement reaction of the laponite platelets and the charge distribution gives laponite the ability to interact electrostatically with both anionic and cationic polymers and modify the rheological properties of biomaterials. This charge distribution gives Laponite the ability to interact electrostatically with gelatin and DOX. DOX has a positive charge as illustrated in Figure 5.1 D and readily loads onto the Laponite platelets as illustrated in Figure 5.1 A. The Laponite nanoparticles act as cross-linkers and the gelatin polymer chains attach themselves to the surfaces of the Laponite through ionic

or polar interactions, resulting in a unique organic/inorganic network as illustrated in Figure 5.1A. It is this interaction that gives the STB its unique shear thinning ability and makes the STB injectables as illustrated in Figure 5.1 B.

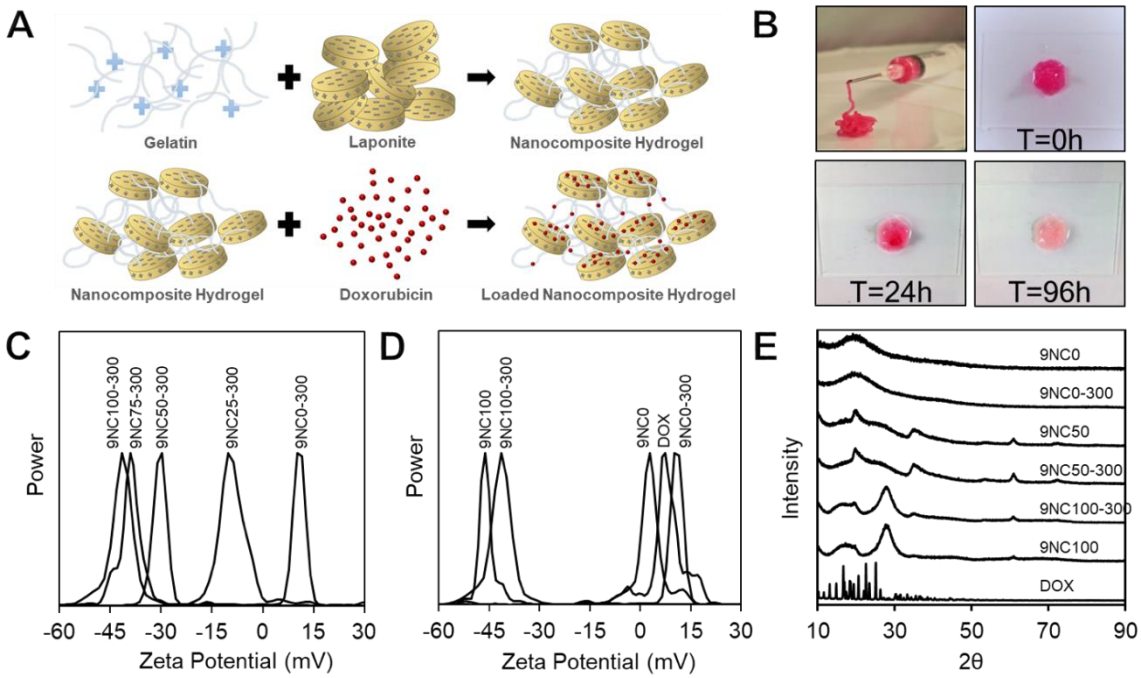

Figure 5.1. Fabrication and chemical characterization. These interactions allow the nanocomposite to have the shear-thinning capability and the drug to load efficiently and amorphously. A) Schematic of drug-loaded nanocomposite formulation. B) Images of 9NC50 being injected through an 18G needle and releasing red food dye over 96h. C) Zeta potential of drug-loaded nanocomposite hydrogels indicates the overall charge of the gel at varying compositions. D) Effect of doxorubicin on the zeta potential of nanocomposite components proposes a strong electrostatic interaction between Laponite and doxorubicin and weak interaction between gelatin and doxorubicin. E) XRD of nanocomposite components and 9NC50 with and without doxorubicin shows that doxorubicin loads amorphously into the nanocomposite hydrogels.

Furthermore, it's clear why changing the ratio of Laponite and gelatin leads to changes in this electrostatic interaction between the two materials and would result in changes to the material's physical characteristics. These interactions also explain why the STB is physically robust and does not lose its shape as shown in Figure 5.1 B. It's important to note that the STB maintains its shape even when DOX is released from the gel as is

illustrated in Figure 5.1 B. The loss of red colouring observed in that figure is the result of DOX release as DOX is red in colour.

5.3.1.2. Zeta Potential

The zeta potential of Laponite, gelatin, and DOX hydrochloride was measured to be -46.22, 2.73, and 7.44mV, respectively. Incorporating DOX into either STB component results in a positive shift of the zeta potential, which correlates with its positive charge. When combining all three components to make a DOX-loaded STB, the overall charge is governed by altering the ratio of gelatin to Laponite. By increasing the ratio of Laponite to 25, 50, and 75%, the overall charge of the DOX-loaded STB is reduced to -10.15, -29.74, and -39.14mV, respectively. The overall charges of DOX-loaded STBs and the individual components of the system are representative of electrostatic interactions that occur within the STB. Additionally, as shown in Figure 5.1 D hydrogels that are loaded with DOX have a more positive zeta potential compared to the equivalent blank hydrogels. Since DOX is positively charged, an increase in the zeta potential is expected.

In the Laponite-Gelatin STB, it is probable that the negatively charged Laponite platelets and the positively charged gelatin interact electrostatically to form a stable hydrogel with a house of card structure that is a characteristic of Laponite. When this material is subjected to shear stress, the bonds between Laponite and gelatin are broken and the material loses its gel-like consistency and becomes more liquid, thus showing shear-thinning behaviour. Accordingly, it is reasonable to expect that changing the ratio of Laponite to gelatin, which would change the zeta potential and electrostatic interactions of the STB, would lead to changes in the rheological properties of the nanocomposite. Indeed, according to Figure 5.1 C, the nanocomposites with greater levels of Laponite,

9NC50 and 9NC75 have more negative zeta potential than 9NC25 and also show different rheological properties. Specifically, the high Laponite nanocomposites have a greater G′ value as shown in Figure 5.3 C-D, which indicates greater shear-thinning ability. In addition, having a negatively charged STB drug carrier allows for control over the affinity and loading capacity of the hydrogel with the positively charged drug DOX.

5.3.1.3.Powder X-Ray Diffraction

In order to determine the state in which DOX loads into the STB, an X-ray diffraction (XRD) analysis was employed. DOX in its dry form exists in a crystalline state, as shown by the existence of several sharp peaks between 10-30° for the DOX sample in Figure 5.1 E. Both 9NC0 and 9NC100 display mostly amorphous structure, with the appearance of a single broad peak at 20.5° for 9NC0 and three broad peaks at 18.2°, 28.5°, and 62.5° for 9NC100. The 50/50 composite of 9% gelatin and 9% Laponite, 9NC50, contained the amorphous broad peak characteristic of gelatin with the addition of two broad peaks at 20.3° and 36.3°. The addition of these peaks in the 9NC50 spectra is likely due to an increase in the basal plane spacing of Laponite caused by gelatin[191]. The addition of DOX into 9NC0, 9NC50, and 9NC100 results in a disappearance of DOX's sharp peaks between 10-30° suggesting that DOX intercalates into the STB and its individual components in an amorphous state via electrostatic interactions [183,192].

The ability of STB formulations to intercalate DOX was further confirmed by XRD, the loading capacity, and quantification of the pore size of lyophilized formulations with and without DOX loading. Laponite has been highlighted as an efficient platform for loading doxorubicin in several other studies [187,192-195]. However, maintaining the shear-thinning and amorphous structure of the gel is important for rendering the

formulation as a useful, injectable drug delivery vehicle. As demonstrated in Figure 5.2 J, the doxorubicin loading capacity of STB was directly dependent on the ratio of Laponite used in the formulation.

Despite the decrease in the hydrogel's pore size with increasing ratios of Laponite (Figure 5.2 A-D), Dox was able to intercalate between the Laponite nanoplatelets without disrupting the electrostatic interactions between gelatin and Laponite. The electrostatic interactions between negatively charged Laponite and DOX, which both have positive charges results in a decrease in the pore size and a slower release profile. A combination of the loading capacity, the control over porosity, and electrostatic interactions during formulation provided predictable release kinetics by altering the overall STB density, Laponite ratio, and DOX loading concentration (Figure 5.2 A-J).

5.3.2. Morphological Characterization

5.3.2.1.Scanning Electron Microscopy

Scanning electron microscope (SEM) images of STBs with varying ratios of gelatin and Laponite as well as a varying concentration of DOX were taken to determine the effect of these parameters on the pore size of the STB, the results of which can be observed in Figure 5.2 A-H. As observed in Figures 5.2 I, increasing the ratio of Laponite resulted in a near-linear reduction in pore size from 97.76μm for STBs with 0% Laponite to 21.17μm for STBs with 75% Laponite. The pore size of the 9NC100 sample was immeasurable with ImageJ. The decrease in pore size with the increase in Laponite concentration may be due to the electrostatic interactions between Laponite and gelatin. Since the Laponite nanoparticles act as a multifunctional crosslinker, increasing their concentration would lead to more crosslinking and a reduction in pore size.

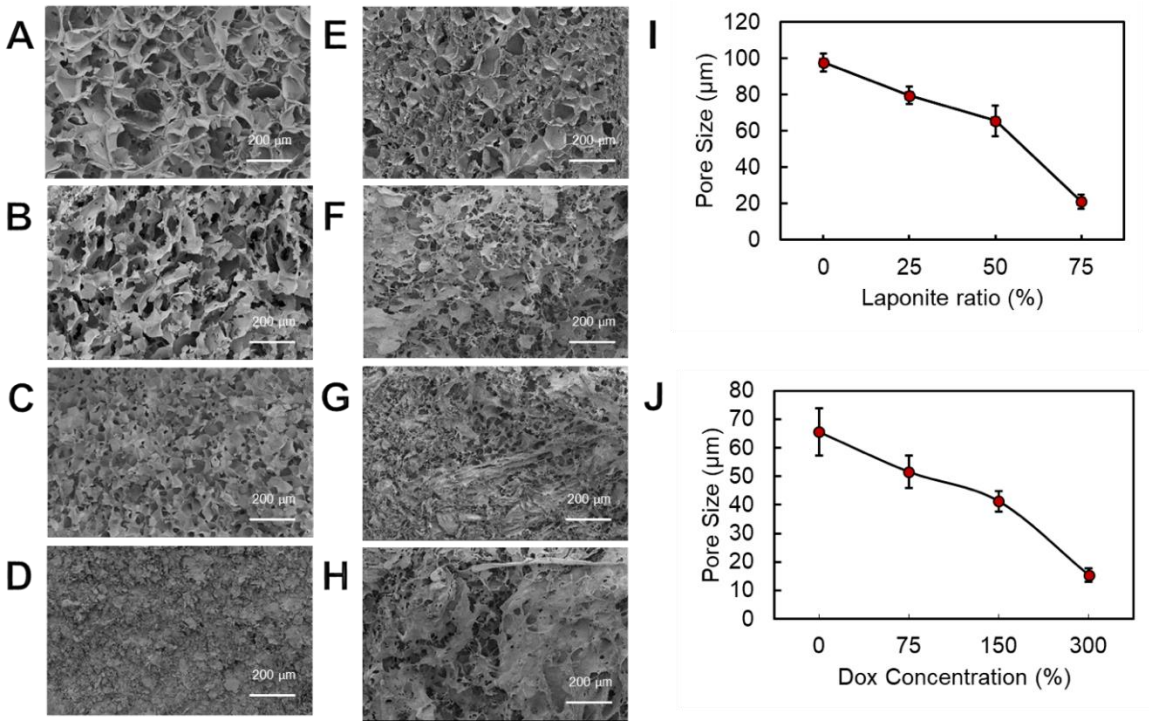

Figure 5.2. Morphological characterization. Altering the composition gives control over the microstructure of the STB. SEM images of A) 9NC0 B) 9NC25 C) 9NC75 D) 9NC100 E) 9NC50 F) 9NC50-75 G) 9NC50-150 and H) 9NC50-300. I) Pore size of the hydrogels decreases with an increasing ratio of Laponite. J) Pore size of the hydrogels decreases with an increasing concentration of doxorubicin-loaded into the nanocomposite.

A similar effect was seen by increasing the concentration of DOX loaded into the STBs. A near-linear reduction in pore size was observed when increasing the DOX concentration from 0 to 300µg of DOX per gram of STB. This reduction in pore size may initially appear counterintuitive as DOX has a positive charge as observed in Figure 5.1 D, in contrast to Laponite's negative charge. However, increasing the concentration of loaded DOX in the STB increases means there are more ions for crosslinking in the STB(DOX is positively charged and can act as a crosslinker), which leads to a greater level of crosslinking. The greater level of crosslinking explains why the increase in DOX concentration leads to a decrease in the pore size, similar to the effect observed by the increase in the negatively charged Laponite.

5.3.3. Physical and Rheological Characterization

5.3.3.1.Enzymatic Degradation and Swelling

A degradation study of the STBs was conducted at 37°C in the presence of collagenase, a naturally occurring enzyme that degrades gelatin, to demonstrate the STB's ability to degrade after implantation in the body. The degradation study was conducted over a period of 19 days, resulting in an increased degradation rate for samples containing larger ratios of gelatin and smaller ratios of Laponite. As seen in Figure 5.3 A, 9NC25, 9NC50, and 9NC75 had 45%, 72%, and 85% remaining after 19 days, respectively.

Samples containing higher ratios of gelatin and lower concentrations of Laponite also have larger pores, as seen in Figure 5.2, which allows for more interaction with the supernatant and thus more exposure to collagenase. This greater degree of exposure to collagenase due to the larger pores partially explains why the samples with more gelatin and less Laponite degrade quicker.

A swelling test also determined that the hydrogels with higher ratios of gelatin were subject to a higher degree of swelling. As observed in Figure 5.3 B, the degree of swelling was 1096%, 1461%, and 1876% for 9NC75, 9NC50, and 9NC25, respectively. Similar to the degradation rate, the difference in swelling can be explained by the differences in pore size. The larger the pores, the greater the available volume for water to permeate into.

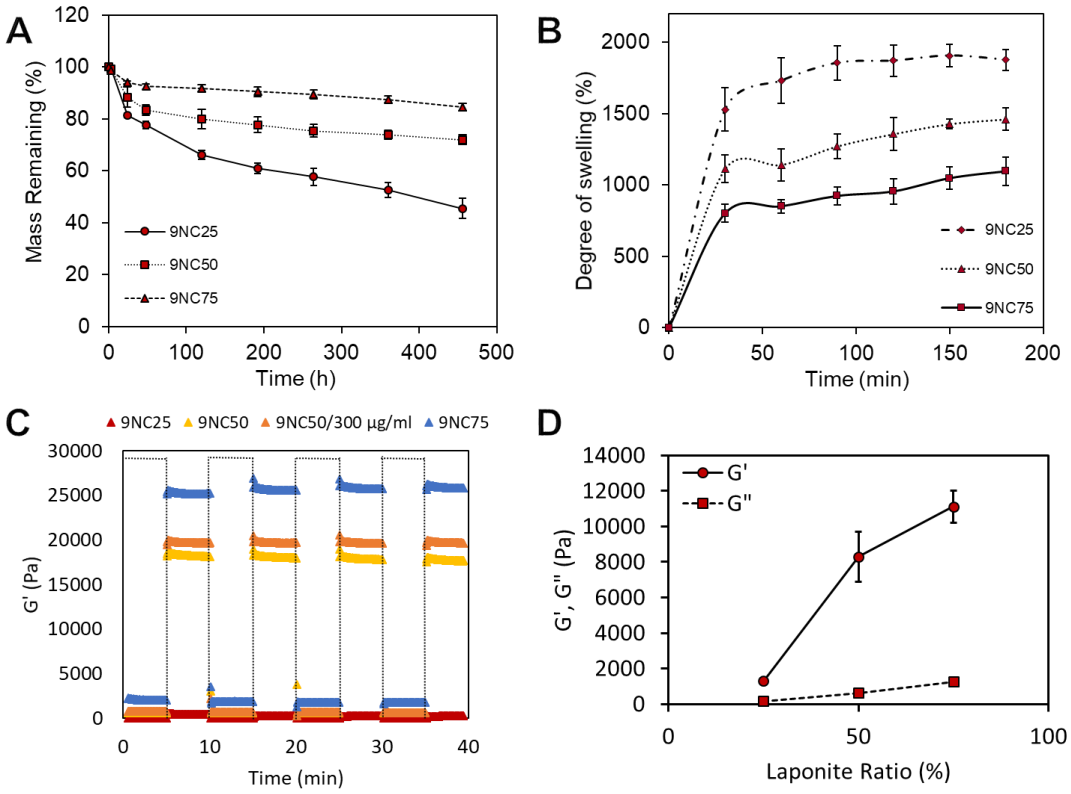

Figure 5.3. Physical and rheological characterization. A) Degradation of STBs in the presence of collagenase and B) swelling of STBs show increase with a decreased ratio of Laponite. C) STBs show full recovery after repeated exposure to high and low strain. D) Storage and loss modulus increase with increasing Laponite ratio.

5.3.3.2. Viscoelasticity and Shear-thinning Analysis

The storage (G') and loss (G") moduli were determined at 37°C using an ElastoSens™ Bio2 (Rheolution Instruments), a non-destructive method of monitoring mechanical properties of viscoelastic materials. As illustrated in Figures 5.3 C and D, 9NC25 exhibited the lowest G' and G" at 1300Pa and 176Pa, respectively, which corresponds with the largest gelatin ratio and lowest Laponite ratio in this sample at 37°C. 9NC50 and 9NC75 exhibited G' and G" values of 8294Pa and 639Pa, and 11118Pa and 1252Pa, respectively. The increased G' and G" with increasing Laponite is due to the

increased physical crosslinking from the increased electrostatic interactions between Laponite and gelatin.[188]

All three STBs had a higher storage modulus than loss modulus, which demonstrates the elastic nature of the STBs and their ability to maintain their solid structure after being exposed to stress [189]. This property was further characterized by employing a recovery analysis in which the STBs were subjected to oscillatory strain conditions with high (100%) and low (1%) strain amplitudes. All samples were shown to rapidly recover their solid-like behaviour after application of high strain, and the intercalation of DOX into 9NC50 led to a slight increase in the storage modulus of the STB. This was likely due to an increase in the electrostatic attraction between Laponite and DOX, as is evident in the zeta potential analysis and has been discussed at length previously.

5.3.4. Loading Efficiency and Release Characterization

5.3.4.1.Loading Efficiency

The loading efficiency of DOX was determined by immersing STBs and their individual components in PBS containing 300µg/mL DOX at 37°C. As can be seen in Figure 5.4 A, samples containing higher ratios of Laponite displayed higher loading efficiency. This increase in loading efficiency can be explained by the central role of Laponite in DOX loading. Laponite, with its negative charge and high aspect ratio, is ideally suited for interacting with the positively charged DOX. Accordingly, an increase in Laponite concertation leads to an increase in the hydrogel's DOX loading capacity. The STBs' ability to maintain their loading capacity was demonstrated for a period of 29 days, and samples containing higher ratios of gelatin show fluctuations with a slight decrease in

loading efficiency, which is likely due to their larger pore size and the degradation of gelatin.

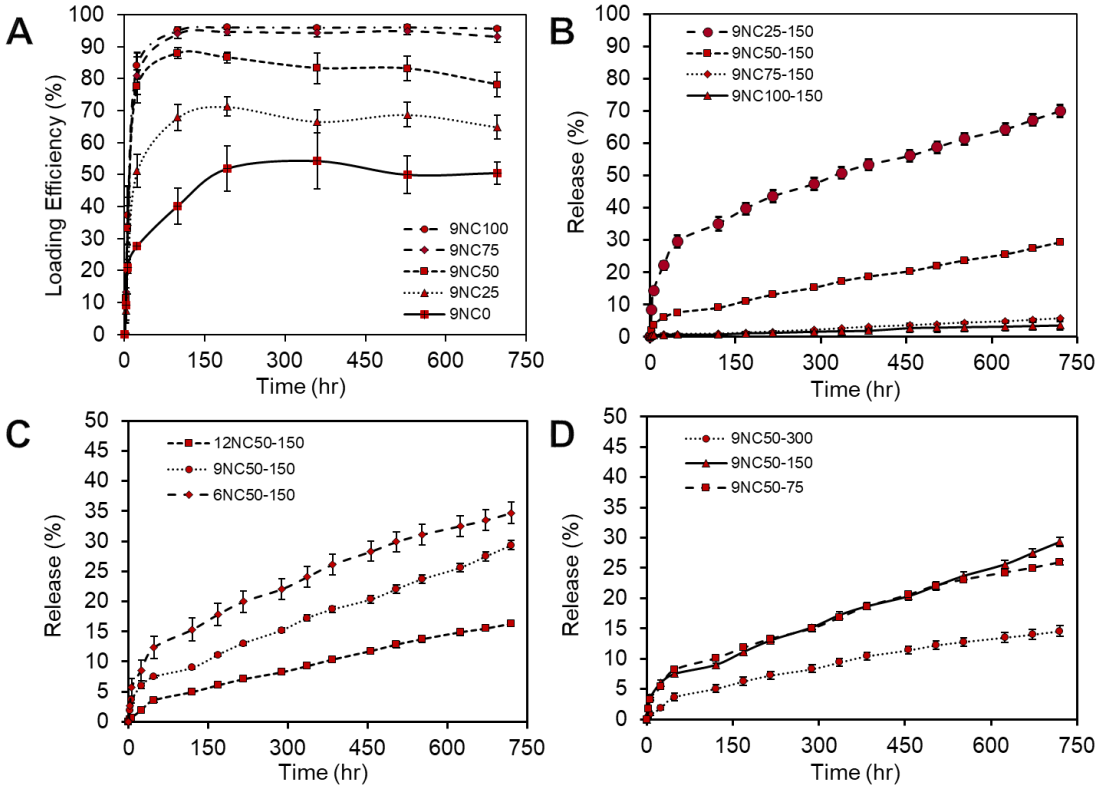

Figure 5.4. Loading efficiency and release characterization. Varying the STB composition offers control over the loading efficiency and release of DOX. A) Loading efficiency of DOX increases with increasing ratio of Laponite. B) Release of DOX decreases with increasing ratio of Laponite. C) Decreasing the overall STB concentration results in an increased release of DOX. D) Increasing the amount of DOX loaded into STBs demonstrates the concentration dependence of diffusion-based release of DOX.

5.3.4.2.Release Studies

For effective clinical treatment, DOX should be released over a sustained period of time at a constant rate of release. The release kinetics of DOX from the STBs was investigated by varying the ratios of gelatin to Laponite, varying the overall STB concentration, and varying DOX concentration loaded into the STB.

As anticipated, a high degree of control over the release kinetics was obtained by varying the ratio of Laponite in the STBs. As observed in Figure 5.4 B 9NC25 showed an initial burst release of 29.5% after 48 hours and a total release of 69.9% after 29 days. After the initial burst release, the release rate was fairly constant with an average release rate of 1.5% of the loaded drug per day. As shown in Figure 5.4 B similar release kinetics were observed for 9NC50 with a burst release of 7.5%, a total release of 29.3%, and an average release rate of 0.81% per day after the initial burst release. Samples containing higher ratios of Laponite than 9NC50, so 9NC75 and 9C100, showed very little release over 29 days as observed in Figure 5.4 B. In general, a decreasing release was observed in samples with higher concentrations of Laponite, which follows similar decreasing trends in pore size, degradation rate, and swelling characteristics that are observed with an increase in Laponite.

As observed in Figure 5.4 C another control parameter included varying overall STB concentration, which decreased the release rate for higher STB concentrations. Increasing the overall concentration of the STB leads to a corresponding increase in the concentration of Laponite. This increase in Laponite concertation translates to greater electrostatic bonding with DOX, which translates to reduced DOX release.

However, as observed in Figure 5.4 D, varying DOX concentration led to a counterintuitive decrease in release rate when DOX concentration was increased. This counterinitiative result was hypothesized to be the result of over-crosslinking in the hydrogel and the corresponding decrease in pore size that was observed with increasing concentrations of DOX. This over-crosslinked hydrogel with small pores is poorly

permeable and would have a slower release rate compared to hydrogels with larger pore sizes.

5.3.5. *In Vitro* Anti-Tumor Activity of DOX-Loaded STBs; 2D Model

5.3.5.1.U87 Human Glioblastoma Cell Viability

To examine the anti-proliferative effect of DOX loaded STBs on brain tumour cells, U87 human glioblastoma multiforme cells were cultured and exposed to varying concentrations of free DOX and DOX loaded 9NC25. Cells viability was determined using a Presto-Blue assay.

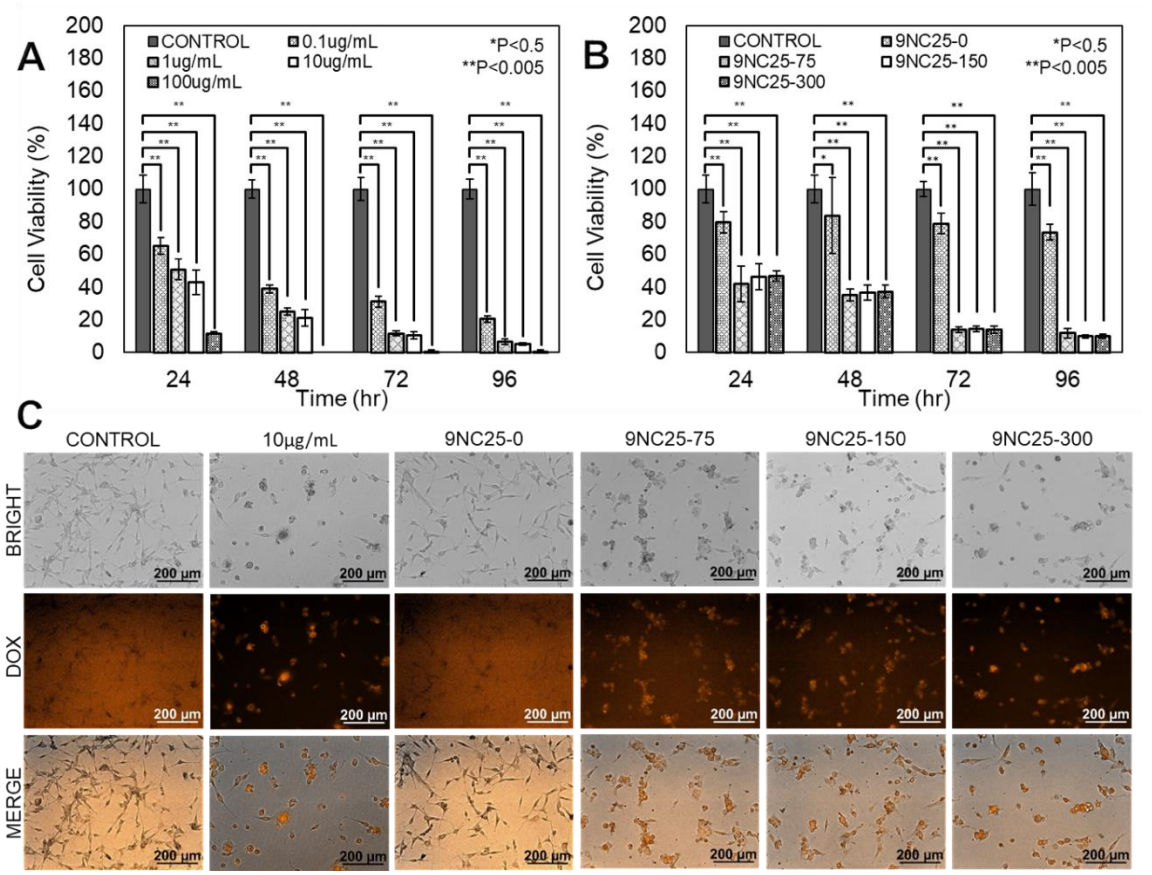

Figure 5.5. *In vitro* anti-tumour activity of DOX-loaded STBs. DOX-loaded STBs effectively kill U87 cells with similar efficacy to free DOX. A) Free DOX treatment over 96 hours. B) Treatment with DOX-loaded STBs over 96 hours. C) 10X Magnification images of cell morphology and infiltration of DOX into cells 48 hours after treatment.

The IC50 for free dox after 48 hours was extrapolated to be ~0.2µg/mL, and the U87 cells exhibited dose-dependent viability over 4 days (Figure 5.5). U87 cells were treated with 9NC25 loaded with three different concentrations of DOX. This STB was chosen for its release profile, and 0.1g samples were weighed to release approximately 0.23, 0.45, and 0.90µg/mL DOX after 48hr of treatment with 9NC25-75, 9NC25-150, and 9NC25-300, respectively.

All three DOX-loaded STBs were effective in reducing the viability of the U87 cells, however, no statistical difference was seen between the samples containing different DOX concentrations. This was likely due to the small well plate volume and the concentration-dependent release of the STBs. The DOX-loaded STBs' ability to effectively reduce the viability of U87 cells was also evident in the morphology of the cells. The healthy, adhered star-shaped morphology seen in the control and unloaded STB samples were lost with the treatment of DOX, showing a rounded morphology. DOX infiltration was also imaged by fluorescent microscopy and showed that DOX successfully entered cells where it forces a cell to commit apoptosis [11]. The unloaded STBs exhibited a slightly reduced viability when compared to the control, however, the morphology of the cells looked healthy. This suggests that the unloaded STB may not kill cells, but rather reduce their ability to proliferate. Cell viability for all three DOX-loaded samples on day 4 was ~10%, which suggests that the average concentration of DOX in the media was between 0.1 and 1µg/mL when comparing with the free DOX treatment results. This agrees with the prediction calculation based on the release data.

5.3.6. *In Vitro* Anti-Tumor Activity of DOX-Loaded STBs Brain-Tumor-on-a-Chip; 3D Model

5.3.6.1.U87 Human Glioblastoma Cell Viability Brain-Tumor-on-a-Chip

In order to bridge the gap between *in vitro* and *in vivo* studies, an *in vitro* brain tumour on a chip was used to further investigate the anti-tumour activity of the DOX-loaded STB. The aim was to obtain more accurate data on DOX release from DOX-loaded STB and DOX penetration into dense tumour tissue to effectively kill tumour cells. 3D Tumor tissues were first grown and then treated with free DOX and DOX-loaded STBs, then imaged with live-dead staining to determine cell viability and to display cell morphology. As seen in Figure 5.6 A, the ability of free DOX to effectively kill U87 cells was significantly reduced when compared to the 2D *in vitro* study, with the 100µg/mL concentration reaching 36.5% cell viability after 96 hours (compared to ~0% viability in the 2D study after 72 hours). This effect is likely due to the reduced ability of DOX to diffuse through collagen and penetrate into the cells compared to the 2D study.

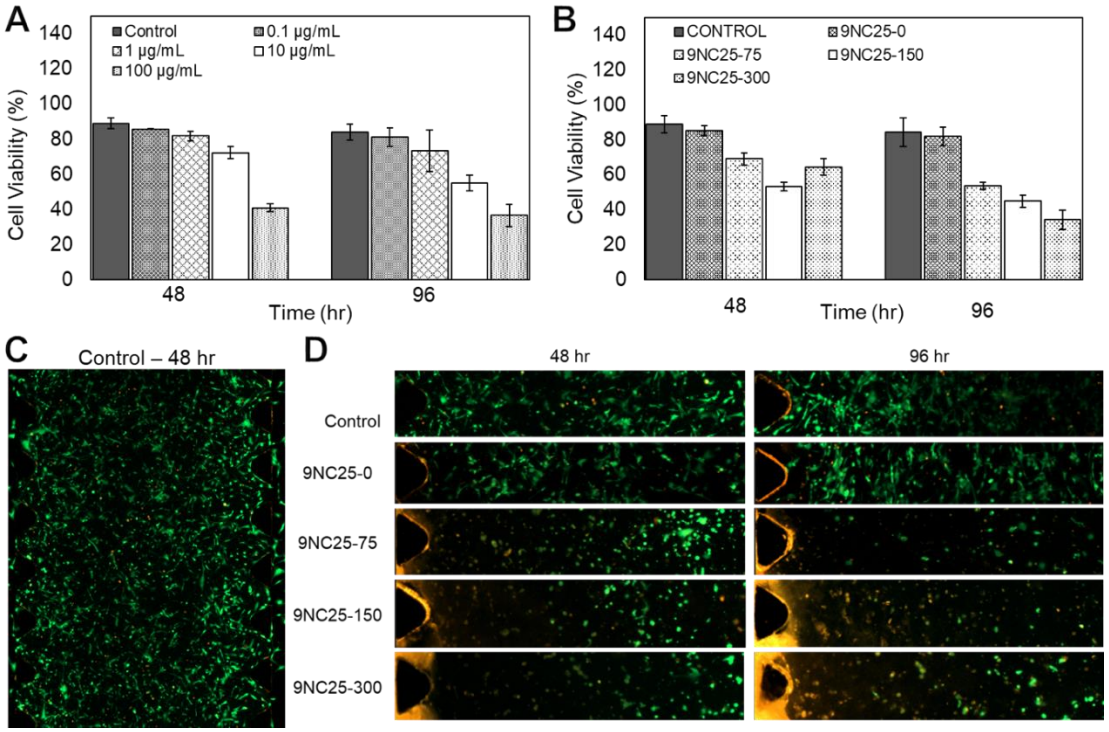

Figure 5.6. *In vitro* anti-tumour activity of DOX-loaded STBs brain-tumour-on-a-chip. DOX-loaded STBs show effective DOX penetration of 3D tumour tissue and improved anti-tumour activity. A) Free DOX treatment of 3D tumour tissue is less effective than in a 2D study. B) DOX-loaded STBs effectively treat 3D tumour tissue and show dependence on the amount of loaded DOX. C) An untreated, live-dead stained 3D tumour tissue has spindle-shaped cell morphology and high cell density. D) Live-dead stained cross-sections of unloaded and DOX-loaded STB treated tissues show changes in cell morphology and viability with varying treatment.

A similar effect is seen for treatment with DOX-loaded 9NC25. All three samples with varying concentrations of DOX showed a reduced ability to kill U87 cells in the 3D tissue. However, unlike the 2D study, DOX saturation was not reached. Increasing the DOX loaded into the STBs resulted in a decreased cell viability over 96 hours, with final viability of 53.7%, 44.9%, and 34.2% for 9NC25-75, 9NC25-150, and 9NC25-300, respectively.

The efficacy of the DOX-loaded STBs is further exemplified by the rounded morphology of the live and dead cells seen in Figure 5.6 D. The number of dead cells decreases with increasing distance from the STBs. This is likely due to the gradual release of DOX, which creates a concentration gradient across the full length of the device. The unloaded 9NC25-0 sample showed a slightly reduced cell viability when compared to the control, however, the control viability was not 100% due to shear forces experienced by the cells within the device. The morphology of the cells for both the control and the 9NC25-0 treated samples looks healthy and spindle-shaped and the distribution of dead cells appeared random and was not a function of distance from the unloaded STB. An increased cell density is also observed between the 48 and 96-hour control and 9NC25-0 samples demonstrating that the cells are proliferating within the device.

5.4.Conclusion

The present study demonstrates the potential use of a Laponite, gelatin, doxorubicin nanocomposite STB as an effective drug delivery tool. The use of these materials in a nanocomposite allowed for a great degree of control over the drug loading and the release of doxorubicin. Control over the electrostatic interactions between DOX and the STB, pore size, swelling, and degradation by varying the ratio of gelatin and Laponite allows for great control over the release kinetics of DOX from the STB, as shown in the release study. In addition, the STBs' rheological properties make the material suitable for use as a local treatment for glioblastoma multiform. In addition, this research may include long-term *in vivo* studies to determine any potential long-term cytotoxic effects as well as further formulation optimization of and drug dosage.

Chapter 6

6. Conclusions and Future Work

This chapter links the contributions of three studies presented in Chapter 3 to Chapter 5 and summarizes the final results. This chapter is then followed by discussion and suggestions for future work.

6.1.Conclusions and Contributions

This dissertation presents the fabrication and characterization of silicate-based nanocomposite hydrogels for biomedical applications. The motivation for carrying out this research was to produce highly viscoelastic and shear-thinning biomaterials which can be utilized for minimally invasive drug delivery and tissue engineering applications. Laponite is known for its ability to form a stable gel, enhancing the rheological properties of various hydrogels, such as shear-thinning and viscoelastic properties. In this research, Laponite was combined with various organic and inorganic materials for developing multifunctional nanocomposite hydrogels. However, optimizing the formulation of this nanocomposite to produce hydrogels that maintain their favourable rheological and chemical properties was challenging. The challenges of acquiring an optimal formulation for these nanocomposite hydrogels are addressed in Chapters 4 through 6 of this dissertation.

Specifically, Chapter 4 presents the process of obtaining the optimum formulation for a stimuli-responsive yet injectable drug carrier. In addition, Chapter 5 describes methods for optimizing the composition of a bioink to maintain the flexibility and electroconductivity necessary for developing printable conductors. Finally, Chapter 6

investigates the optimum formulation of a drug carrier that provides prolonged and sustained drug release for minimally invasive cancer treatment.

6.1.1. Smart Shear-thinning Hydrogels as Injectable Drug Delivery Systems

In the first study of this dissertation, a smart nanocomposite hydrogel was developed for an on-demand drug delivery application. The main objective of this study was to employ pH-sensitive chitosan or PNIPAM microgels to engineer silicate-based, injectable, and stimuli-responsive drug carriers using gelatin and Laponite. Various experiments were performed to determine the optimal formulations of these multifunctional biomaterials with shear-thinning and pH-responsivity properties. The shear-thinning characteristic is essential for depositing the drug at the site of interest and preventing early exposure of the drug to the biological environment and removal via blood circulation. Accordingly, rheological analysis was employed to evaluate the effect of various components on the shear-thinning properties of the hydrogels. The results from the rheological analysis elucidated the effects of adding chitosan and PNIPAM microgels to the Laponite/gelatin nanocomposite hydrogel. For instance, these experiments showed a decrease in the shear-thinning properties of the gel as chitosan microgels were introduced to the Laponite/gelatin. However, the addition of PNIPAM had a negligible effect on the hydrogel's shear-thinning properties. These results may be associated with the electrostatic interactions of PNIPAM and chitosan with Laponite/gelatin, which also affects the morphological properties of these nanocomposite hydrogels. In fact, the addition of PNIPAM decreased the pore size of the nanocomposite hydrogel, while notably larger pores were observed in SEM images as chitosan was incorporated into the hydrogel. These electrostatic interactions were highly influenced by the various pH values of the

surrounding environment and resulted in pH-sensitive swelling and degradation. In addition, the results from the release study showed that the highest degrees of swelling and degradation occurred in a pH 9 buffer. Therefore, the proposed nanocomposite hydrogels displayed good potential for localized drug delivery in which the release is triggered by a localized basic pH.

6.1.2. Multifunctional Silicate-Based Electroconductive Bioinks for Fabricating Soft Electronics

In the second study of this dissertation, an electroconductive bioink was developed for extrusion-based 3D printing of a flexible conductor on an alginate substrate. The main objective of this study was to utilize graphene oxide for its electrically conductive properties while maintaining the shear-thinning properties of the Lapointe/alginate nanocomposite hydrogel. Various experiments were employed to optimize the concentration of the graphene oxide to develop a highly electroconductive bioink with the appropriate shear-thinning and viscoelastic behaviour. The shear-thinning properties were essential for maintaining the cylindrical geometry of the stacked layers of filaments post-extrusion while providing a high degree of control over the printing process. Flexible conductors were printed onto alginate substrates with complex pattern geometries and various fibre diameters. After evaluating the reproducibility of the 3D printed flexible conductors, the durability of the conductors under bending and stretching conditions were investigated by various mechanical analyses. The results from a rheological analysis highlighted the shear-thinning properties of the silicate-based bioink are essential for the reproducibility of the printed conductor on alginate substrates. In addition, the results from mechanical and electrical experiments demonstrate the viscoelastic and electroconductive

behaviour of this flexible conductor, which are necessary for potential electrically stimulated tissue engineering applications.

6.1.3. Doxorubicin Loaded Shear-thinning Biomaterial for Minimally Invasive Treatment of Brain Tumors

In the last study of this dissertation, an injectable nanocomposite hydrogel with the requisite *in situ* mechanical stiffness for depositing the drug and maintaining a dosage at the site of interest was developed. The main objective of this study was to optimize the formulation of Laponite and gelatin concentrations to produce a highly shear-thinning drug (doxorubicin) carrier that would provide a sustainable release in localized tissue. Various experiments were developed to study the effect of total solid weight and Laponite concentration on the chemical and rheological properties of the nanocomposite hydrogels. Optimizing the formulation not only affected the shear-thinning properties of the hydrogel but is also essential for providing greater control over drug release. Drug release occurs as a function of swelling, degradation, and electrostatic interactions between Laponite, gelatin, and doxorubicin. Additionally, the highest level and the fastest rate of drug release occurred at the lowest concentration of Laponite which also demonstrated the greatest swelling and degradation rate. Therefore, the optimized formulation of the nanocomposite hydrogel can be potentially utilized for depositing the drug into the site of interest and for providing sustainable release over an extended period of time.

6.1.4. Conclusions

This work presents the fabrication and characterization of silicate-based nanocomposite hydrogels with noteworthy shear-thinning properties, viscoelastic behaviour, and high water retention capacities. The high surface area of the Laponite

nanoparticle component allowed for the addition of a wide range of organic and inorganic materials within the stable Laponite colloid, important for developing multifunctional biomaterials. A considerable challenge was the development of biomaterials with multiple properties that did not sacrifice the shear-thinning properties of the nanocomposite hydrogel. Accordingly, the chemical, rheological, and morphological properties of these nanocomposite hydrogels were experimentally assessed to determine the optimum formulation for each hydrogel.

6.2.Future Work

The initial motivation for this research was to fabricate silicate-based nanocomposite hydrogels for biomedical applications. The chemical, physical, and rheological properties of these biomaterials were experimentally examined in order to determine the optimum formulation based on particular property requirements. After the characterization of these nanocomposite hydrogels, future investigations are essential for validating the aforementioned properties within a physiologically relevant environment. Future research should consider the potential effects of biological environments on the microstructural characteristics of these nanocomposite hydrogels. Therefore, *in vitro* and *in vivo* studies will be key components in future attempts to optimize the formulation of these nanocomposite hydrogels after exposure to physiological conditions.

References

[1] Y. Qiu and K. Park, "Environment-sensitive hydrogels for drug delivery," *Adv. Drug Deliv. Rev.*, vol. 53, no. 3, pp. 321–339, 2001.

[2] E. M. Ahmed, "Hydrogel: Preparation, characterization, and applications: A review," *J. Adv. Res.*, vol. 6, no. 2, pp. 105–121, 2015.

[3] A. S. Hoffman, "Hydrogels for biomedical applications," *Adv. Drug Deliv. Rev.*, vol. 64, pp. 18–23, 2012.

[4] N. A. Peppas, J. Z. Hilt, A. Khademhosseini, and R. Langer, "Hydrogels in Biology and Medicine: From Molecular Principles to Bionanotechnology," *Adv. Mater.*, vol. 18, no. 11, pp. 1345–1360, 2006.

[5] N. Annabi *et al.*, "25th Anniversary Article: Rational Design and Applications of Hydrogels in Regenerative Medicine," *Adv. Mater.*, vol. 26, no. 1, pp. 85–124, 2014.

[6] D. K. Ho, D. T. Nguyen, T. Thambi, D. S. Lee, and D. P. Huynh, "Polyamide-based pH and temperature-responsive hydrogels: Synthesis and physicochemical characterization," *J. Polym. Res.*, vol. 26, no. 1, pp. 1–9, 2019.

[7] S. R. Caliari and J. A. Burdick, "A practical guide to hydrogels for cell culture," *Nat. Metho.*, vol. 13, no. 5, pp. 405–414, 2016.

[8] H. G. Im *et al.*, "Flexible transparent conducting hybrid film using a surface-embedded copper nanowire network: A highly oxidation-resistant copper nanowire electrode for flexible optoelectronics," *ACS Nano*, vol. 8, no. 10, pp. 10973–10979, 2014.

[9] K. S. Anseth, C. N. Bowman, and L. Brannon-Peppas, "Mechanical properties of hydrogels and their experimental determination," *Bio.*, vol. 17, no. 17, pp. 1647–

1657, 1996.

[10] D. T. Eddington and D. J. Beebe, “Flow control with hydrogels,” *Adv. Drug Deliv. Rev.*, vol. 56, no. 2, pp. 199–210, 2004.

[11] H. Y. Zhang Jianyong, “Gel Chemistry: Interactions, Structures and Properties,” *Spr. Nature Sin.*, 2018. [Online]. Available: https://doi.org/10.1007/978-981-10-6881-2_1. [Accessed: 06-Feb-2021].

[12] S. K. De, N. R. Aluru, B. Johnson, W. C. Crone, D. J. Beebe, and J. Moore, “Equilibrium swelling and kinetics of pH-responsive hydrogels: models, experiments, and simulations,” *J. Microelec. Syst.*, vol. 11, no. 5, pp. 544–555, 2002.

[13] H. Sung, Y. Chang, I. Liang, W. Chang, and Y. Chen, “Fixation of biological tissues with a naturally occurring crosslinking agent: Fixation rate and effects of pH, temperature, and initial fixative concentration,” *J. Biomed. Mater. Res.*, vol. 52, no. 1, pp. 77–87, 2000.

[14] M. F. Akhtar, M. Hanif, and N. M. Ranjha, “Methods of synthesis of hydrogels: A review,” *Saudi Pharm J SAUDI PHARM J*, vol. 24, no. 5., pp. 554–559, 2016.

[15] D. A. Gyles, L. D. Castro, J. O. C. Silva, and R. M. Ribeiro-Costa, “A review of the designs and prominent biomedical advances of natural and synthetic hydrogel formulations,” *Eur. Polymer J.*, vol. 88, pp. 373–392, 2017.

[16] M. M. Khansari *et al.*, “Classification of Hydrogels Based on Their Source: A Review and Application in Stem Cell Regulation,” *Min. Met. and Materials Soc.*, vol. 69, no. 8., pp. 1340–1347, 2017.

[17] S. Rafieian, H. Mirzadeh, H. Mahdavi, and M. E. Masoumi, “A review on

nanocomposite hydrogels and their biomedical applications," *Sci. Eng. Compos. Mater.*, vol. 26, no. 1, pp. 154–174, 2019.

[18] A. Sionkowska, "Current research on the blends of natural and synthetic polymers as new biomaterials: Review," *Prog. Polym. Sci. (Oxford)*, vol. 36, no. 9, pp. 1254–1276, 2011.

[19] G. Sharma *et al.*, "Applications of nanocomposite hydrogels for biomedical engineering and environmental protection," *Environ. Chem. Lett.*, vol. 16, no. 1, pp. 113–146, 2018.

[20] R. Singhal and K. Gupta, "A Review: Tailor-made Hydrogel Structures (Classifications and Synthesis Parameters)," *Polym. Plast. Technol. Eng.*, vol. 55, no. 1, pp. 54–70, 2016.

[21] S. Utech and A. R. Boccaccini, "A review of hydrogel-based composites for biomedical applications: enhancement of hydrogel properties by addition of rigid inorganic fillers," *J. Mater. Sci.*, vol. 51, no. 1, pp. 271–310, 2016.

[22] V. A. Drits and A. Plançon, "Expert System for Structural Characterization of Phyllosilicates: II. Application to Mixed-Layer Minerals," *Clay Miner.*, vol. 29, no. 1, pp. 39–45, 1994.

[23] B. Velde, "Clays and Clay Minerals in Natural and Synthetic Systems, *Google Books*", vol. 21, no. 1, pp. 1–219, 1977.

[24] T. Britannica, "cyclosilicate | Structure & Facts | Britannica," *Encyclopaedia* , May-2018. [Online]. Available: https://www.britannica.com/science/cyclosilicate. [Accessed: 06-Feb-2021].

[25] P. Nimis, S. G. Tesalina, P. Omenetto, P. Tartarotti, and C. Lerouge,

"Phyllosilicate minerals in the hydrothermal mafic-ultramafic-hosted massive-sulfide deposit of Ivanovka (southern Urals): Comparison with modern ocean seafloor analogues," *Contrib. to Mineral. Petrol.*, vol. 147, no. 3, pp. 363–383, 2004.

[26] Q. Wang, C. Zhu, J. Yun, and G. Yang, "Isomorphic Substitutions in Clay Materials and Adsorption of Metal Ions onto External Surfaces: A DFT Investigation," *J. Phys. Chem. C*, vol. 121, no. 48, pp. 26722–26732, 2017.

[27] L. Benco, D. Tunega, J. Hafner, and H. Lischka, "Ab initio density functional theory applied to the structure and proton dynamics of clays," *Chem. Phys. Lett.*, vol. 333, no. 6, pp. 479–484, 2001.

[28] C. D. Barton and A. D. Karathanasis, "Clay minerals", *Lal, R., Ed., Encyc. of Soil Sci.*, vol. 9, no. 9, pp 187-192, 2002.

[29] C. Viseras, C. Aguzzi, P. Cerezo, and M. C. Bedmar, "Biopolymer–clay nanocomposites for controlled drug delivery," *Mater. Sci. Technol.*, vol. 24, no. 9, pp. 1020–1026, 2008.

[30] T. J. Dening *et al.*, "Montmorillonite and Laponite Clay Materials for the Solidification of Lipid-Based Formulations for the Basic Drug Blonanserin: In Vitro and in Vivo Investigations," *Mol. Pharm.*, vol. 15, no. 9, pp. 4148–4160, 2018.

[31] A. A. Adeyemo, I. O. Adeoye, and O. S. Bello, "Adsorption of dyes using different types of clay: a review," *Appl. Water Sci.*, vol. 7, no. 2, pp. 543–568, 2017.

[32] D. Zhang, C. H. Zhou, C. X. Lin, D. S. Tong, and W. H. Yu, "Synthesis of clay

minerals," *Appli. Clay Sci.*, vol. 50, no. 1, pp. 1–11, 2010.

[33] V. Mittal and V. Herle, "Physical adsorption of organic molecules on the surface of layered silicate clay platelets: A thermogravimetric study," *J. Colloid Inter. Sci.*, vol. 327, no. 2, pp. 295–301, 2008.

[34] P. Liu, "Polymer modified clay minerals: A review," *Appl. Clay Sci.*, vol. 38, no. 1–2, pp. 64–76, 2007.

[35] A. K. Gaharwar *et al.*, "Bioactive silicate nanoplatelets for osteogenic differentiation of human mesenchymal stem cells," *Adv. Mater.*, vol. 25, no. 24, pp. 3329–3336, 2013.

[36] A. K. Gaharwar, N. A. Peppas, and A. Khademhosseini, "Nanocomposite hydrogels for biomedical applications," *Biotechnol. Bioeng.*, vol. 111, no. 3, pp. 441–453, 2014.

[37] S. Jatav and Y. M. Joshi, "Chemical stability of Laponite in aqueous media," *Appl. Clay Sci.*, vol. 97–98, pp. 72–77, 2014.

[38] D. Chimene, D. L. Alge, and A. K. Gaharwar, "Two-Dimensional Nanomaterials for Biomedical Applications: Emerging Trends and Future Prospects," *Adv. Mater.*, vol. 27, no. 45, pp. 7261–7284, 2015.

[39] A. K. Gaharwar *et al.*, "Physically Crosslinked Nanocomposites from Silicate-Crosslinked PEO: Mechanical Properties and Osteogenic Differentiation of Human Mesenchymal Stem Cells," *Macromol. Biosci.*, vol. 12, no. 6, pp. 779–793, 2012.

[40] Q. Jin, P. Schexnailder, A. K. Gaharwar, and G. Schmidt, "Silicate Cross-Linked Bio-Nanocomposite Hydrogels from PEO and Chitosan," *Macromol. Biosci.*, vol. 9, no. 10, pp. 1028–1035, 2009.

[41] S. Samimi Gharaie, S. Dabiri, M. Akbari, S. Samimi Gharaie, S. M. H. Dabiri, and M. Akbari, “Smart Shear-Thinning Hydrogels as Injectable Drug Delivery Systems,” *Polym. (Basel).*, vol. 10, no. 12, pp. 1317-1332, 2018.

[42] V. Adibnia, S. M. Taghavi, and R. J. Hill, “Roles of chemical and physical crosslinking on the rheological properties of silica-doped polyacrylamide hydrogels,” *Rheol. Acta*, vol. 56, no. 2, pp. 123–134, 2017.

[43] F. Pignon, J.-M. Piau, and A. Magnin, “Structure and Pertinent Length Scale of a Discotic Clay Gel,” Phys. Rev. Lett., vol. 76, no. 25, pp 17-25, 1996.

[44] M. Manzano *et al.*, “Studies on MCM-41 mesoporous silica for drug delivery: Effect of particle morphology and amine functionalization,” *Chem. Eng. J.*, vol. 137, no. 1, pp. 30–37, 2008.

[45] M. M. Lübtow, T. Lorson, T. Finger, F. Gröber-Becker, and R. Luxenhofer, “Combining Ultra-High Drug-Loaded Micelles and Injectable Hydrogel Drug Depots for Prolonged Drug Release,” *Macromol. Chem. Phys.*, vol. 221, no. 1, p. 1900341–1900354, 2020.

[46] H. Maeda, G. Y. Bharate, and J. Daruwalla, “Polymeric drugs for efficient tumor-targeted drug delivery based on EPR-effect,” *Eur. J. of Pharm. and Bioph.*, vol. 71, no. 3, pp. 409–419, 2009.

[47] C. Viseras, C. Aguzzi, P. Cerezo, and M. C. Bedmar, “Biopolymer–clay nanocomposites for controlled drug delivery,” *Mat. Sci. and Tech.*, vol. 24, no. 9, pp. 1020-1026, 2008.

[48] P. F. Luckham and S. Rossi, “Colloidal and rheological properties of bentonite suspensions,” *Adv. Colloid Interface Sci.*, vol. 82, no. 1, pp. 43–92, 1999.

[49] S. Zhai, X. Hu, Y. Hu, B. Wu, and D. Xing, “Visible light-induced crosslinking and physiological stabilization of diselenide-rich nanoparticles for redox-responsive drug release and combination chemotherapy,” *Biomat.*, vol. 121, pp. 41–54, 2017.

[50] H. S. Kim, J. Yang, K. Kim, and U. S. Shin, “Biodegradable and injectable hydrogels as an immunosuppressive drug delivery system,” *Mater. Sci. Eng. C*, vol. 98, pp. 472–481, 2019.

[51] R. C. Cooper and H. Yang, “Hydrogel-based ocular drug delivery systems: Emerging fabrication strategies, applications, and bench-to-bedside manufacturing considerations,” *J Control Release*, vol. 306., pp. 29–39, 2019.

[52] M. M. Lübtow, T. Lorson, T. Finger, F. Gröber-Becker, and R. Luxenhofer, “Combining Ultra-High Drug-Loaded Micelles and Injectable Hydrogel Drug Depots for Prolonged Drug Release,” *Macromol. Chem. Phys.*, vol. 221, no. 1, p. 1900341–1900354, 2020.

[53] “Tissue Engineering - an overview | ScienceDirect Topics.” [Online]. Available: https://www.sciencedirect.com/topics/engineering/tissue-engineering. [Accessed: 05-Jun-2020].

[54] S. Caddeo, M. Boffito, and S. Sartori, “Tissue engineering approaches in the design of healthy and pathological in vitro tissue models,” *Frontiers in Bioengineering and Biotechnology*, vol. 5, no. 2 , pp. 1–40, 2017.

[55] Y. Ganji, Q. Li, E. S. Quabius, M. Böttner, C. Selhuber-Unkel, and M. Kasra, “Cardiomyocyte behavior on biodegradable polyurethane/gold nanocomposite scaffolds under electrical stimulation,” *Mater. Sci. Eng. C*, vol. 59, pp. 10–18,

2016.

[56] Q. Gu, “Functional tissues from intelligent materials, 3D printing and stem cells,” *Doctor of Philosophy thesis, Intelligent Polymer Research Institute, University of Wollongong*, p. 1–239, 2017.

[57] B. Liau, D. Zhang, and N. Bursac, “Functional cardiac tissue engineering,” *Regen. Med.*, vol. 7, no. 2, pp. 187–206, 2012.

[58] B. Maharjan *et al.*, “Synthesis and characterization of gold/silica hybrid nanoparticles incorporated gelatin methacrylate conductive hydrogels for H9C2 cardiac cell compatibility study,” *Compos. Part B Eng.*, vol. 177, no. 1, p. 107415–107424, 2019.

[59] K. Zhu *et al.*, “Gold Nanocomposite Bioink for Printing 3D Cardiac Constructs,” *Adv. Funct. Mater.*, vol. 27, no. 12, p. 1605352–1605364, 2017.

[60] N. Paxton, W. Smolan, T. Böck, F. Melchels, J. Groll, and T. Jungst, “Proposal to assess printability of bioinks for extrusion-based bioprinting and evaluation of rheological properties governing bioprintability,” *Biof.*, vol. 9, no. 4, p. 044107–044127, 2017.

[61] J. L. Dávila and M. A. d’Ávila, “Rheological evaluation of Laponite/alginate inks for 3D extrusion-based printing,” *Int. J. Adv. Manuf. Technol.*, vol. 101, no. 1–4, pp. 675–686, 2019.

[62] B. Dume, “Heart-on-a-chip’ process aims to speed up drug testing,” Biofabrication, vol. 10, no. 12, pp. 025004–025005, 2018.

[63] Q. He *et al.*, “Centimeter-long and large-scale micropatterns of reduced graphene oxide films: Fabrication and sensing applications,” *ACS Nano*, vol. 4, no. 6, pp.

3201–3208, 2010.

[64] X. Cui *et al.*, “Advances in Extrusion 3D Bioprinting: A Focus on Multicomponent Hydrogel-Based Bioinks,” *Adv. Healthc. Mater.*, vol. 9, no. 15, p. 1901648–1901675, 2020.

[65] A. Blaeser, D. F. Duarte Campos, U. Puster, W. Richtering, M. M. Stevens, and H. Fischer, “Controlling Shear Stress in 3D Bioprinting is a Key Factor to Balance Printing Resolution and Stem Cell Integrity,” *Adv. Healthc. Mater.*, vol. 5, no. 3, pp. 326–333, 2016.

[66] B. Mirani *et al.*, “An Advanced Multifunctional Hydrogel-Based Dressing for Wound Monitoring and Drug Delivery,” *Adv. Healthc. Mater.*, vol. 6, no. 19, pp. 1–26, 2017.

[67] B. V. Slaughter, S. S. Khurshid, O. Z. Fisher, A. Khademhosseini, and N. A. Peppas, “Hydrogels in Regenerative Medicine,” *Adv. Mater.*, vol. 21, no. 32–33, pp. 3307–3329, 2009.

[68] S. Khetan and J. A. Burdick, “Patterning hydrogels in three dimensions towards controlling cellular interactions.” *Soft Mat.*, vol. 7, no. 3, pp. 830–838, 2011.

[69] S. Y. Lee and G. Tae, “Formulation and in vitro characterization of an in situ gelable, photo-polymerizable Pluronic hydrogel suitable for injection,” *J. Contr. Rel.* vol. 119, no. 3, pp. 313–319, 2007.

[70] R. Jin, L. S. Moreira Teixeira, P. J. Dijkstra, C. A. van Blitterswijk, M. Karperien, and J. Feijen, “Enzymatically-crosslinked injectable hydrogels based on biomimetic dextran-hyaluronic acid conjugates for cartilage tissue engineering,” *Biom.*, vol. 31, no. 11, pp. 3103–3113, 2010.

[71] D. Jaikumar *et al.*, “Injectable alginate-O-carboxymethyl chitosan/nano fibrin composite hydrogels for adipose tissue engineering,” *Int. J. Biol. Macromol.*, vol. 74, pp. 318–326, 2015.

[72] A. Dubbini *et al.*, “Injectable hyaluronic acid/PEG-p(HPMAm-lac)-based hydrogels dually cross-linked by thermal gelling and Michael addition,” *Eur. Polym. J.*, vol. 72, pp. 423–437, 2015.

[73] L. Nair, C. Laurencin, and M. Tandon, Injectable hydrogels as biomaterials, Adv. Biom., vol. 1, no. 1, pp. 179-203, 2010.

[74] A. Sabnis, M. Rahimi, C. Chapman, and K. T. Nguyen, “Cytocompatibility studies of an in situ photopolymerized thermoresponsive hydrogel nanoparticle system using human aortic smooth muscle cells,” *J. Biomed. Mater. Res. - Part A*, vol. 91, no. 1, pp. 52–59, 2009.

[75] H. D. Lu, M. B. Charati, I. L. Kim, and J. A. Burdick, “Injectable shear-thinning hydrogels engineered with a self-assembling Dock-and-Lock mechanism,” *Biom.*, vol. 33, no. 7, pp. 2145–2153, 2012.

[76] C. Yan, A. Altunbas, T. Yucel, R. P. Nagarkar, J. P. Schneider, and D. J. Pochan, “Injectable solid hydrogel: Mechanism of shear-thinning and immediate recovery of injectable β-hairpin peptide hydrogels,” *Soft Mat.*, vol. 6, no. 20, pp. 5143–5156, 2010.

[77] M. Guvendiren, H. D. Lu, and J. A. Burdick, “Shear-thinning hydrogels for biomedical applications,” *Soft Mat.*, vol. 8, no. 2. pp. 260–272, 2012.

[78] R. K. Avery *et al.*, “An injectable shear-thinning biomaterial for endovascular embolization.,” *Sci. Transl. Med.*, vol. 8, no. 365, pp. 156-365, 2016.

[79] A. K. Gaharwar *et al.*, “Shear-thinning nanocomposite hydrogels for the treatment of hemorrhage,” *ACS Nano*, vol. 8, no. 10, pp. 9833–9842, 2014.

[80] X. Li, A. Liu, R. Ye, Y. Wang, and W. Wang, “Fabrication of gelatin–laponite composite films: Effect of the concentration of laponite on physical properties and the freshness of meat during storage,” *Food Hydr.*, vol. 44, pp. 390–398, 2015.

[81] N. Pawar and H. B. Bohidar, “Spinodal decomposition and phase separation kinetics in nanoclay-biopolymer solutions,” *J. Polym. Sci. Part B Polym. Phys.*, vol. 48, no. 5, pp. 555–565, 2010.

[82] J. Gu, F. Xia, Y. Wu, X. Qu, Z. Yang, and L. Jiang, “Programmable delivery of hydrophilic drug using dually responsive hydrogel cages,” *J. Contr. Rel.*, vol. 117, no. 3, pp. 396–402, 2007.

[83] T. Kureha, T. Shibamoto, S. Matsui, T. Sato, and D. Suzuki, “Investigation of changes in the microscopic structure of anionic poly(N-isopropylacrylamide-co-acrylic acid) microgels in the presence of cationic organic dyes toward precisely controlled uptake/release of low-molecular-weight chemical compound,” *Langm.*, vol. 32, no. 18, pp. 4575–4585, 2016.

[84] Q. Gan *et al.*, “A dual-delivery system of pH-responsive chitosan-functionalized mesoporous silica nanoparticles bearing BMP-2 and dexamethasone for enhanced bone regeneration,” *J. Mater. Chem. B*, vol. 3, no. 10, pp. 2056–2066, 2015.

[85] N. Ahmadi Nasab, H. Hassani Kumleh, M. Beygzadeh, S. Teimourian, and M. Kazemzad, “Delivery of curcumin by a pH-responsive chitosan mesoporous silica nanoparticles for cancer treatment,” *Artif. Cells, Nanom., Biot.*, vol. 46, no. 1, pp. 75–81, 2018.

[86] Q. Gan, T. Wang, C. Cochrane, and P. McCarron, “Modulation of surface charge, particle size and morphological properties of chitosan-TPP nanoparticles intended for gene delivery,” *Coll. Surf. B Bio.*, vol. 44, no. 2–3, pp. 65–73, 2005.

[87] L. Jin and R. Bai, “Mechanisms of lead adsorption on chitosan/PVA hydrogel beads,” *Lang.*, vol. 18, no. 25, pp. 9765–9770, 2002.

[88] P. Mazancová, V. Némethová, D. Treľová, L. Kleščíková, I. Lacík, and F. Rázga, “Dissociation of chitosan/tripolyphosphate complexes into separate components upon pH elevation,” *Carbohydr. Polym.*, vol. 192, pp. 104–110, 2018.

[89] H. Q. Mao *et al.*, “Chitosan-DNA nanoparticles as gene carriers: Synthesis, characterization and transfection efficiency,” *J. Contr. Rel.*, vol. 70, no. 3, pp. 399–421, 2001.

[90] X. Z. Shu, K. J. Zhu, and W. Song, “Novel pH-sensitive citrate cross-linked chitosan film for drug controlled release,” *Int. J. Pharm.*, vol. 212, no. 1, pp. 19–28, 2001.

[91] M. Karg, I. Pastoriza-Santos, B. Rodriguez-González, R. Von Klitzing, S. Wellert, and T. Hellweg, “Temperature, pH, and ionic strength induced changes of the swelling behavior of PNIPAM-poly(allylacetic acid) copolymer microgels,” *Lang.*, vol. 24, no. 12, pp. 6300–6306, 2008.

[92] C. Li, C. Mu, W. Lin, and T. Ngai, “Gelatin Effects on the Physicochemical and Hemocompatible Properties of Gelatin/PAAm/Laponite Nanocomposite Hydrogels,” *ACS Appl. Mater. Interfaces*, vol. 7, no. 33, pp. 18732–18741, 2015.

[93] X. Li, A. Liu, R. Ye, Y. Wang, and W. Wang, “Fabrication of gelatin-laponite composite films: Effect of the concentration of laponite on physical properties and

the freshness ofmeat during storage," *Food Hydrocoll.*, vol. 44, pp. 390–398, 2015.

[94] J. J. Chen, A. L. Ahmad, and B. S. Ooi, "Poly(N-isopropylacrylamide-co-acrylic acid) hydrogels for copper ion adsorption: Equilibrium isotherms, kinetic and thermodynamic studies," *J. Environ. Chem. Eng.*, vol. 1, no. 3, pp. 339–348, 2013.

[95] Z. Osman and A. K. Arof, "FTIR studies of chitosan acetate based polymer electrolytes," *Electrochim. Acta*, vol. 48, no. 8, pp. 993–999, 2003.

[96] A. Pawlak and M. Mucha, "Thermogravimetric and FTIR studies of chitosan blends," in *Thermochim. Acta*, vol. 396, no. 1–2, pp. 153–166, 2003.

[97] S. M. H. Dabiri, A. Lagazzo, F. Barberis, A. Shayganpour, E. Finocchio, and L. Pastorino, "New in-situ synthetized hydrogel composite based on alginate and brushite as a potential pH sensitive drug delivery system," *Carbohydr. Polym.*, vol. 177, pp. 324–333, 2017.

[98] J. Zhang, Q. Wang, and A. Wang, "In situ generation of sodium alginate/hydroxyapatite nanocomposite beads as drug-controlled release matrices," *Acta Biomater.*, vol. 6, no. 2, pp. 445–454, 2010.

[99] S. Bagherifard *et al.*, "Dermal Patch with Integrated Flexible Heater for on Demand Drug Delivery," *Adv. Healthc. Mater.*, vol. 5, no. 1, pp. 175–184, 2016.

[100] C. C. Lin and A. T. Metters, "Hydrogels in controlled release formulations: Network design and mathematical modeling," *Adv. Drug Del. Reviews*, vol. 58, no. 12–13, pp. 1379–1408, 2006.

[101] L. A. Schneider, A. Korber, S. Grabbe, and J. Dissemond, "InXuence of pH on

wound-healing: a new perspective for wound-therapy?," *Arch. Derm.l Res.*, vol. 298, no. 9, pp. 413–420, 2007.

[102] M. Sasaki, B. C. Karikkineth, K. Nagamine, H. Kaji, K. Torimitsu, and M. Nishizawa, "Highly Conductive Stretchable and Biocompatible Electrode-Hydrogel Hybrids for Advanced Tissue Engineering," *Adv. Healthc. Mater.*, vol. 3, no. 11, pp. 1919–1927, 2014.

[103] S. V. Murphy and A. Atala, "3D bioprinting of tissues and organs," *Nat. Biotechnol.*, vol. 32, no. 8, pp. 773–785, 2014.

[104] Y. S. Zhang *et al.*, "3D Bioprinting for Tissue and Organ Fabrication," *Ann. Biomed. Eng.*, vol. 45, no. 1, pp. 148–163, 2017.

[105] B. Zhang, L. Gao, L. Ma, Y. Luo, H. Yang, and Z. Cui, "3D Bioprinting: A Novel Avenue for Manufacturing Tissues and Organs," *Eng.*, vol. 5, no. 4, pp. 777–794, 2019.

[106] A. Saberi, F. Jabbari, P. Zarrintaj, M. R. Saeb, and M. Mozafari, "Electrically conductive materials: Opportunities and challenges in tissue engineering, " Biomo., vol. 9, no. 9. p. 448, 2019.

[107] J. Zhou *et al.*, "Engineering the heart: Evaluation of conductive nanomaterials for improving implant integration and cardiac function," *Sci. Rep.*, vol. 4, pp. 1–11, 2014.

[108] D. D. L. Chung, "Review Exfoliation of graphite," *J. of Mat. Sci.*, volume 51, pp. 554–568, 2016.

[109] S. R. Shin *et al.*, "A Bioactive Carbon Nanotube-Based Ink for Printing 2D and 3D Flexible Electronics," *Adv. Mater.*, vol. 28, no. 17, pp. 3280–3289, 2016.

[110] H. Li, C. Tan, and L. Li, “Review of 3D printable hydrogels and constructs,” *Mater. Des.*, vol. 159, no. 15, pp. 20–38, 2018.

[111] S. Kyle, Z. M. Jessop, A. Al-Sabah, and I. S. Whitaker, “‘Printability’’ of Candidate Biomaterials for Extrusion Based 3D Printing: State-of-the-Art,’” *Adv. Healthc. Mater.*, vol. 6, no. 16, pp. 1–16, 2017.

[112] S. Naahidi *et al.*, “Biocompatibility of hydrogel-based scaffolds for tissue engineering applications,” *Biotechnol. Adv.*, vol. 35, no. 5, pp. 530–544, 2017.

[113] L. Ouyang, C. B. Highley, C. B. Rodell, W. Sun, and J. A. Burdick, “3D Printing of Shear-Thinning Hyaluronic Acid Hydrogels with Secondary Cross-Linking,” *ACS Biomater. Sci. Eng.*, vol. 2, no. 10, pp. 1743–1751, 2016.

[114] G. R. López-Marcial, A. Y. Zeng, C. Osuna, J. Dennis, J. M. García, and G. D. O’Connell, “Agarose-Based Hydrogels as Suitable Bioprinting Materials for Tissue Engineering,” *ACS Biomater. Sci. Eng.*, vol. 4, no. 10, pp. 3610–3616, 2018.

[115] E. Axpe and M. L. Oyen, “Applications of alginate-based bioinks in 3D bioprinting,” *Int. J. Mol. Sci.*, vol. 17, no. 12, p. 1976, 2016.

[116] H. Ding, N. P. Illsley, and R. C. Chang, “3D Bioprinted GelMA Based Models for the Study of Trophoblast Cell Invasion,” *Sci. Rep.*, vol. 9, no. 1, pp. 1–13, 2019.

[117] Z. Zheng *et al.*, “3D Bioprinting of Self-Standing Silk-Based Bioink,” *Adv. Healthc. Mater.*, vol. 7, no. 6, pp. 1701026–1701038, 2018.

[118] S. Salinas-Fernández, M. Santos, M. Alonso, L. Quintanilla, and J. C. Rodríguez-Cabello, “Genetically engineered elastin-like recombinamers with sequence-based molecular stabilization as advanced bioinks for 3D bioprinting,” *Appl. Mater.*

Today, vol. 18, p. 100500–100513, 2020.

[119] N. Ashammakhi *et al.*, "Bioinks and bioprinting technologies to make heterogeneous and biomimetic tissue constructs," *Mater. Today Bio*, vol. 1,no. 1, pp. 100008–100031, 2019.

[120] J. Sun and H. Tan, "Alginate-based biomaterials for regenerative medicine applications," *Mater. (Basel).*, vol. 6, no. 4, pp. 1285–1309, 2013.

[121] K. Y. Lee and D. J. Mooney, "Alginate: Properties and biomedical applications," *Prog. in Polymer Sci. (Oxford)*, vol. 37, no. 1, pp. 106–126, 2012.

[122] J. L. Drury, R. G. Dennis, and D. J. Mooney, "The tensile properties of alginate hydrogels," *Biomat.*, vol. 25, no. 16, pp. 3187–3199, 2004.

[123] M. Ghadiri, W. Chrzanowski, W. H. Lee, A. Fathi, F. Dehghani, and R. Rohanizadeh, "Physico-chemical, mechanical and cytotoxicity characterizations of Laponite®/alginate nanocomposite," *Appl. Clay Sci.*, vol. 85, no. 1, pp. 64–73, 2013.

[124] D. W. Thompson and J. T. Butterworth, "The nature of laponite and its aqueous dispersions," *J. Coll. Interface Sci.*, vol. 151, no. 1, pp. 236–243, 1992.

[125] J. L. Dávila and M. A. d'Ávila, "Laponite as a rheology modifier of alginate solutions: Physical gelation and aging evolution," *Carbohydr. Polym.*, vol. 157, no. 1, pp. 1–8, 2017.

[126] T. Ahlfeld *et al.*, "Development of a clay based bioink for 3D cell printing for skeletal application," *Biof.*, vol. 9, no. 3, pp. 034103–034120, 2017.

[127] M. A. Habib and B. Khoda, "Development of clay based novel bio-ink for 3D bio-printing process," *Procedia Manuf.*, vol. 26, pp. 846–856, 2018.

[128] C. Tondera *et al.*, “Highly Conductive, Stretchable, and Cell-Adhesive Hydrogel by Nanoclay Doping,” *Small*, vol. 15, no. 27, pp. 1901406–1901414, 2019.

[129] K. Zhu *et al.*, “Gold Nanocomposite Bioink for Printing 3D Cardiac Constructs,” *Adv. Funct. Mater.*, vol. 27, no. 12, pp. 1605352–1605364, 2017.

[130] B. Y. Ahn and J. A. Lewis, “Amphiphilic silver particles for conductive inks with controlled wetting behavior,” *Mater. Chem. Phys.*, vol. 148, no. 3, pp. 686–691, 2014.

[131] G. M. Vlăsceanu, H. Iovu, and M. Ioniţă, “Graphene inks for the 3D printing of cell culture scaffolds and related molecular arrays,” *Compos. Part B Eng.*, vol. 162, no. 2018, pp. 712–723, 2019.

[132] C. T. Huang, L. Kumar Shrestha, K. Ariga, and S. H. Hsu, “A graphene-polyurethane composite hydrogel as a potential bioink for 3D bioprinting and differentiation of neural stem cells,” *J. Mater. Chem. B*, vol. 5, no. 44, pp. 8854–8864, 2017.

[133] Y. Zhu *et al.*, “Graphene and graphene oxide: Synthesis, properties, and applications,” *Adv. Mater.*, vol. 22, no. 35, pp. 3906–3924, 2010.

[134] S. Stankovich *et al.*, “Synthesis of graphene-based nanosheets via chemical reduction of exfoliated graphite oxide,” *Carbon N. Y.*, vol. 45, no. 7, pp. 1558–1565, 2007.

[135] K. Takei, W. Honda, S. Harada, T. Arie, and S. Akita, “Toward Flexible and Wearable Human-Interactive Health-Monitoring Devices,” *Adv. Healthc. Mater.*, vol. 4, no. 4, pp. 487–500, 2015.

[136] C. Yan *et al.*, “Highly Stretchable Piezoresistive Graphene-Nanocellulose

Nanopaper for Strain Sensors," *Adv. Mater.*, vol. 26, no. 13, pp. 2022–2027, 2014.

[137] H. Wu, W. Gao, and Z. Yin, "Materials, Devices and Systems of Soft Bioelectronics for Precision Therapy," *Adv. Healthc. Mater.*, vol. 6, no. 10, p. 1700017–1700026, 2017.

[138] S. Zhao *et al.*, "Layer-by-layer assembly of multifunctional porous N-doped carbon nanotube hybrid architectures for flexible conductors and beyond," *ACS Appl. Mater. Interfaces*, vol. 7, no. 12, pp. 6716–6723, 2015.

[139] G. D. Cha, D. Kang, J. Lee, and D. Kim, "Bioresorbable Electronic Implants: History, Materials, Fabrication, Devices, and Clinical Applications," *Adv. Healthc. Mater.*, vol. 8, no. 11, p. 1801660–1801680, 2019.

[140] W. Huang *et al.*, "Highly electrically conductive and stretchable copper nanowires-based composite for flexible and printable electronics," *Compos. Sci. Technol.*, vol. 146, pp. 169–176, 2017.

[141] A. H. Najafabadi *et al.*, "Biodegradable nanofibrous polymeric substrates for generating elastic and flexible electronics," *Adv. Mater.*, vol. 26, no. 33, pp. 5823–5830, 2014.

[142] Y. Hu *et al.*, "Low cost and highly conductive elastic composites for flexible and printable electronics," *J. Mater. Chem. C*, vol. 4, no. 24, pp. 5839–5848, 2016.

[143] J. H. Kim *et al.*, "Simple and cost-effective method of highly conductive and elastic carbon nanotube/polydimethylsiloxane composite for wearable electronics," *Sci. Rep.*, vol. 8, no. 1, pp. 1–11, 2018.

[144] E. Ruiz-Hitzky *et al.*, "Clay-Graphene Nanoplatelets Functional Conducting Composites," *Adv. Funct. Mater.*, vol. 26, no. 41, pp. 7394–7405, 2016.

[145] S. M. Alhassan, S. Qutubuddin, and D. A. Schiraldi, “Graphene arrested in laponite-water colloidal glass,” *Langm.*, vol. 28, no. 8, pp. 4009–4015, 2012.

[146] A. Vashist *et al.*, “Advances in Carbon Nanotubes-Hydrogel Hybrids in Nanomedicine for Therapeutics,” *Adv. Healthc. Mater.*, vol. 7, no. 9, p. 1–43, 2018.

[147] X. Xu, J. Wang, Y. Wang, L. Zhao, Y. Li, and C. Liu, “Formation of graphene oxide-hybridized nanogels for combinative anticancer therapy,” *Nanomed. Nanotech., Biol. Med.*, vol. 14, no. 7, pp. 2387–2395, 2018.

[148] D. K. Chouhan *et al.*, “Graphene oxide-Laponite hybrid from highly stable aqueous dispersion,” *Appl. Clay Sci.*, vol. 132, no.1, pp. 105–113, 2016.

[149] J. Li, J. C. Cui, Z. Z. Yang, H. X. Qiu, Z. H. Tang, and J. H. Yang, “Stabilizing graphene layers by intercalating laponite between them,” *Xinxing Tan Cailiao/New Carbon Mater.*, vol. 33, no. 1, pp. 19–25, 2018.

[150] Y. Jin, C. Liu, W. Chai, A. Compaan, and Y. Huang, “Self-Supporting Nanoclay as Internal Scaffold Material for Direct Printing of Soft Hydrogel Composite Structures in Air,” *ACS Appl. Mater. Interfaces*, vol. 9, no. 20, pp. 17456–17465, 2017.

[151] C. Nethravathi, J. T. Rajamathi, N. Ravishankar, C. Shivakumara, and M. Rajamathi, “Graphite oxide-intercalated anionic clay and its decomposition to graphene-inorganic material nanocomposites,” *Langm.*, vol. 24, no. 15, pp. 8240–8244, 2008.

[152] P. I. Au, S. Hassan, J. Liu, and Y. K. Leong, “Behaviour of laponite gels: Rheology, ageing, pH effect and phase state in the presence of dispersant,” *Chem.*

Eng. Res. Des., vol. 101, no.1, pp. 65–73, 2015.

[153] H. Z. Cummins, "Liquid, glass, gel: The phases of colloidal Laponite," *J. Non. Cryst. Solids*, vol. 353, no. 41, pp. 3891–3905, 2007.

[154] J. L. Dávila and M. A. d'Ávila, "Rheological evaluation of Laponite/alginate inks for 3D extrusion-based printing," *Int. J. Adv. Manuf. Technol.*, vol. 101, no. 1–4, pp. 675–686, 2019.

[155] Y. Jin, W. Chai, and Y. Huang, "Printability study of hydrogel solution extrusion in nanoclay yield-stress bath during printing-then-gelation biofabrication," *Mater. Sci. Eng. C*, vol. 80, pp. 313–325, 2017.

[156] B. Liu *et al.*, "Cell-loaded injectable gelatin/alginate/LAPONITE® nanocomposite hydrogel promotes bone healing in a critical-size rat calvarial defect model," *RSC Adv.*, vol. 10, no. 43, pp. 25652–25661, 2020.

[157] J. Zhang, H. Eyisoylu, X.-H. Qin, M. Rubert, and R. Müller, "3D Bioprinting of Graphene Oxide-Incorporated Cell-laden Bone Mimicking Scaffolds for Promoting Scaffold Fidelity, Osteogenic Differentiation and Mineralization," *bioR.*, vol. 121, no. 2, pp. 637–652, 2020.

[158] S. Ye, Z. Yang, J. Xu, Z. Shang, and J. Xie, "Clay–graphene oxide liquid crystals and their aerogels: synthesis, characterization and properties," *R. Soc. Open Sci.*, vol. 6, no. 2, pp. 1–9, 2019.

[159] L. Liu *et al.*, "Preparation and characterization of chitosan/graphene oxide composites for the adsorption of Au(III) and Pd(II)," *Talanta*, vol. 93, pp. 350–357, 2012.

[160] J. Xu, K. Wang, S. Z. Zu, B. H. Han, and Z. Wei, "Hierarchical nanocomposites of

polyaniline nanowire arrays on graphene oxide sheets with synergistic effect for energy storage," *ACS Nano*, vol. 4, no. 9, pp. 5019–5026, 2010.

[161] Y. Pan, T. Wu, H. Bao, and L. Li, "Green fabrication of chitosan films reinforced with parallel aligned graphene oxide," *Carbohydr. Polym.*, vol. 83, no. 4, pp. 1908–1915, 2011.

[162] P. Li, Y. N. Dai, J. P. Zhang, A. Q. Wang, and Q. Wei, "Chitosan-alginate nanoparticles as a novel drug delivery system for nifedipine," *Int. J. Biomed. Sci.*, vol. 4, no. 3, pp. 221–228, 2008.

[163] N. M. Mahmoodi, "Magnetic ferrite nanoparticle-alginate composite: Synthesis, characterization and binary system dye removal," *J. Taiwan Inst. Chem. Eng.*, vol. 44, no. 2, pp. 322–330, 2013.

[164] L. Bippus, M. Jaber, and B. Lebeau, "Laponite and hybrid surfactant/laponite particles processed as spheres by spray-drying," *New J. Chem.*, vol. 33, no. 5, pp. 1116–1126, 2009.

[165] B. Brahimi, P. Labbe, and G. Reverdy, "Study of the Adsorption of Cationic Surfactants on Aqueous Laponite Clay Suspensions and Laponite Clay Modified Electrodes," *Langm.*, vol. 8, no. 8, pp. 1908–1918, 1992.

[166] T. U. Patro and H. D. Wagner, "Influence of graphene oxide incorporation and chemical cross-linking on structure and mechanical properties of layer-by-layer assembled poly(Vinyl alcohol)-Laponite free-standing films," *J. Polym. Sci. Part B Polym. Phys.*, vol. 54, no. 22, pp. 2377–2387, 2016.

[167] M. Fatnassi, C. H. Solterbeck, and M. Es-Souni, "Clay nanomaterial thin film electrodes for electrochemical energy storage applications," *RSC Adv.*, vol. 4, no.

87, pp. 46976–46979, 2014.

[168] M. Ionita, M. A. Pandele, and H. Iovu, “Sodium alginate/graphene oxide composite films with enhanced thermal and mechanical properties,” *Carbohydr. Polym.*, vol. 94, no. 1, pp. 339–344, 2013.

[169] D. K. Chouhan *et al.*, “Laponite-graphene oxide hybrid particulate filler enhances mechanical properties of cross-linked epoxy,” *J. Polym. Res.*, vol. 25, no. 2, pp. 1–12, 2018.

[170] R. Lapasin, M. Abrami, M. Grassi, and U. Šebenik, “Rheology of Laponite-scleroglucan hydrogels,” *Carbohydr. Polym.*, vol. 168, no. 1, pp. 290–300, 2017.

[171] S. R. Shin *et al.*, “Reduced Graphene Oxide-GelMA Hybrid Hydrogels as Scaffolds for Cardiac Tissue Engineering,” *Small*, vol. 12, no. 27, pp. 3677–3689, 2016.

[172] F. Yu, F. Zhang, T. Luan, Z. Zhang, and H. Zhang, “Rheological studies of hyaluronan solutions based on the scaling law and constitutive models,” *Polym. (Guildf).*, vol. 55, no. 1, pp. 295–301, 2014.

[173] R. K. Avery *et al.*, “An injectable shear-thinning biomaterial for endovascular embolization,” *Sci. Transl. Med.*, vol. 8, no. 365, pp. 1–13, 2016.

[174] J. Aalaie, “Rheological Behavior of Polyacrylamide/Laponite Nanoparticle Suspensions in Electrolyte Media,” *J. Macromol. Sci. Part B*, vol. 51, no. 6, pp. 1139–1147, 2012.

[175] Y. Zhou *et al.*, “Highly Stretchable, Elastic, and Ionic Conductive Hydrogel for Artificial Soft Electronics,” *Adv. Funct. Mater.*, vol. 29, no. 1, p. 1806220–1806228, 2019.

[176] A. Motealleh and N. S. Kehr, “Nanocomposite Hydrogels and Their Applications in Tissue Engineering,” *Adv. Healthc. Mater.*, vol. 6, no. 1, pp. 40–52, 2017.

[177] X. Ding, H. Liu, and Y. Fan, “Graphene-Based Materials in Regenerative Medicine,” *Adv. Healthc. Mater.*, vol. 4, no. 10, pp. 1451–1468, 2015.

[178] E. Y. Tyunina, V. N. Afanasiev, and M. D. Chekunova, “Electroconductivity of tetraethylammonium tetrafluoroborate in propylene carbonate at various temperatures,” *J. Chem. Eng. Data*, vol. 56, no. 7, pp. 3222–3226, 2011.

[179] M. Szekalska, A. Pucibowska, E. Szymanska, P. Ciosek, and K. Winnicka, “Alginate: Current Use and Future Perspectives in Pharmaceutical and Biomedical Applications,” *Inter. J. of Poly. Sci.*, p. 1–17, 2016.

[180] Z. Bao, C. Xian, Q. Yuan, G. Liu, and J. Wu, “Natural Polymer-Based Hydrogels with Enhanced Mechanical Performances: Preparation, Structure, and Property,” *Adv. Healthc. Mater.*, vol. 8, no. 17, p. 1900670–1900681, 2019.

[181] J. W. Jeong, et al., “Materials and Optimized Designs for HumanMachine Interfaces Via Epidermal Electronics,” *Adv. Mat.*, vol. 25, no. 67, pp.6839-6846, 2013.

[182] M. Guvendiren, H. D. Lu, and J. A. Burdick, “Shear-thinning hydrogels for biomedical applications,” *Soft Mat.*, vol. 8, no. 2, pp. 260–272, 2012.

[183] H. Jung, H.-M. Kim, Y. Bin Choy, S.-J. Hwang, and J.-H. Choy, “Laponite-based nanohybrid for enhanced solubility and controlled release of itraconazole,” *Int. J. Pharm.*, vol. 349, no. 1, pp. 283–290, 2008.

[184] K. Nagahama, D. Kawano, N. Oyama, A. Takemoto, T. Kumano, and J. Kawakami, “Self-Assembling Polymer Micelle/Clay Nanodisk/Doxorubicin

Hybrid Injectable Gels for Safe and Efficient Focal Treatment of Cancer," *Biomacro.*, vol. 16, no. 3, pp. 880–889, 2015.

[185] S. Xiao *et al.*, "Fine tuning of the pH-sensitivity of laponite-doxorubicin nanohybrids by polyelectrolyte multilayer coating," *Mater. Sci. Eng. C*, vol. 60, no. 1, pp. 348–356, 2016.

[186] M. Zhang *et al.*, "Ingenious pH-sensitive dextran/mesoporous silica nanoparticles based drug delivery systems for controlled intracellular drug release," *Int. J. Biol. Macromol.*, vol. 98, pp. 691–700, 2017.

[187] M. Gonçalves *et al.*, "PH-sensitive Laponite®/doxorubicin/alginate nanohybrids with improved anticancer efficacy," *Acta Biomater.*, vol. 10, no. 1, pp. 300–307, 2014.

[188] A. K. Gaharwar *et al.*, "Shear-Thinning Nanocomposite Hydrogels for the Treatment of Hemorrhage," *ACS Nano*, vol. 8, no. 10, pp. 9833–9842, 2014.

[189] R. K. Avery *et al.*, "An injectable shear-thinning biomaterial for endovascular embolization," *Sci. Transl. Med.*, vol. 8, no. 365, pp. 1–12, 2016.

[190] A. Sheikhi, S. Afewerki, R. Oklu, A. K. Gaharwar, and A. Khademhosseini, "Effect of ionic strength on shear-thinning nanoclay-polymer composite hydrogels," *Biomater. Sci.*, vol. 6, no. 8, pp. 2073–2083, 2018.

[191] T. N. Blanton and D. Majumdar, "Microstructure of Clay-Polymer Composites," *Adv. X-Ray Anal.*, vol. 42, no. C, pp. 562–568, 2000.

[192] S. Wang *et al.*, "Laponite nanodisks as an efficient platform for doxorubicin delivery to cancer cells," *Langm.*, vol. 29, no. 16, pp. 5030–5036, 2013.

[193] Y. Yang, J. Li, F. Chen, S. Qiao, Y. Li, and W. Pan, "Synthesis, Formulation, and

Characterization of Doxorubicin-Loaded Laponite/Oligomeric Hyaluronic Acid-Aminophenylboronic Acid Nanohybrids and Cytological Evaluation against MCF-7 Breast Cancer Cells," *AAPS Pharm. Sci. Tech.*, vol. 21, no. 1, pp. 1–10, 2020.

[194] G. Chen *et al.*, "Targeted doxorubicin delivery to hepatocarcinoma cells by lactobionic acid-modified laponite nanodisks," *New J. Chem.*, vol. 39, no. 4, pp. 2847–2855, 2015.

[195] S. Xiao *et al.*, "Fine tuning of the pH-sensitivity of laponite-doxorubicin nanohybrids by polyelectrolyte multilayer coating," *Mater. Sci. Eng. C*, vol. 60, pp. 348–356, 2016.